Effect of Morphology on Scalable Self-Assembling Robots –in Pursuit of Living Artificial Systems–

Dissertation

zur

Erlangung der naturwissenschaftlichen Doktorwürde

(Dr. sc. nat.)

vorgelegt der

Mathematisch-naturwissenschaftlichen Fakultät

der

Universität Zürich

von

Shuhei Miyashita

aus

Japan

Promotionskomitee

Prof. Dr. Rolf Pfeifer
Prof. Dr. Satoshi Murata
Prof. Dr. Rodney Douglas

Zürich, 2011

Abstract

One of the major features of biological systems is that the activities at the molecular level are realized in a decentralized fashion, namely, without any central control. The phenomena are termed self-assembly, defined as *the autonomous organization into patterns or structures without human intervention* (Whitesides *et al.*), and are expected to play a key role in the realization of life like machines (e.g. self-repairable machines).

In this thesis, aiming to investigate the potential for developing self-assembly systems that are applicable to different scales, we develop a series of cm-sized robotic components, which are capable of self-assembling on water. We tackle our objective mainly focusing on the role of morphology, with the belief that it is the key to understanding the phenomena.

Each robotic model across the series that we develop has an incremental level of complexity (from passive to logically reactive) and their evaluation is performed with respect to the level of autonomy of the systems. By observing the assembly processes that cause floating tiles to form a structure, we first elucidate how the difference of tiles' shape induces different aggregation patterns. The next model, in which we advance the floating tiles to self-propulsive modules, is built to examine the influence of dynamics of the system. The experimental and mathematical results reveal how dynamics affects the yield of targeted compounds. In following studies, as an attempt of electronically extended platforms, we present the achievements on self-assembly by introducing sensing and selective connection capabilities. Finally, as a conclusion of our ideas presented in the thesis, we describe the design of magnetic enzymes which can perform cascade conformation changes in a bottom-up manner. The method shown here opens up a new possibility for logical self-assembly.

We believe we have opened a possible path for the engineering of physically grounded high autonomous artificial self-assembly systems.

Zusammenfassung

Es ist eine wesentliche Eigenschaft biologischer Systeme, dass Vorgänge auf der molekularen Ebene dezentralisiert ablaufen, also ohne zentrale Steuerung. Dieses Phänomen namens "Selbstassemblierung" (self-assembly) ist definiert als *die autonome Organisation zu Mustern oder Strukturen ohne menschliche Intervention* (Whitesides *et al.*). Es wird vermutet, dass Selbstassemblierung bei der Realisierung von lebensähnlichen (z.B. sich selbst reparierenden) Maschinen eine Schlüsselrolle spielt.

Die vorliegende Dissertation zielt darauf ab, das Potential für die Entwicklung von selbstassemblierenden Systemen in verschiedenen Grössenskalen zu untersuchen. Wir entwickeln eine Reihe von zentimetergrossen robotischen Komponenten, die, auf einer Wasseroberfläche schwimmend, zur Selbstassemblierung fähig sind. Unser Hauptaugenmerk legen wir dabei auf die Morphologie, von der wir glauben, dass sie für das Verständnis dieses Phänomens von zentraler Bedeutung ist.

In jeder der von uns entwickelten Serien von Roboter-Modellen nimmt die Komplexität zu: von passiv bis hin zu logisch-reaktiv. Die Modelle werden in Abhängigkeit des Grads an Autonomie des Gesamtsystems evaluiert. Durch Beobachten des Assemblierungsprozesses, der die schwimmenden Segmente zu Strukturen zusammenfinden lässt, erläutern wir, wie verschiedene Segment-Formen zu unterschiedlichen Aggregationsmustern führen. Für die nächste Serie werden die schwimmenden Segmente zu sich selber antreibenden Modulen erweitert. Diese Serie dient dazu, den Einfluss der Dynamik auf das System zu untersuchen. Die experimentellen und mathematischen Resultate zeigen auf, in welcher Weise die Dynamik die Ausbeute gewünschter Aggregate beeinflusst. In den weiteren Serien wird die Fähigkeit zur Selbstassemblierung von elektronischen Modulen untersucht, die mit Sensoren und selektiver Verbindungsfähigkeit ausgestattet sind. Als Schlussfolgerung aus den in dieser Dissertation vorgestellten Ideen beschreiben wir am Ende das Design von magnetischen Enzymen, die kaskadierte Konformations-Änderungen in "bottom-up"-Manier durchführen können. Die vorgestellte Methode eröffnet neue Möglichkeiten für die logische Selbstassemblierung.

Wir hoffen, einen gangbaren Weg aufgezeigt zu haben für die Entwicklung von durch physikalische Prozesse kontrollierten, hochgradig autonomen künstlichen selbstassemblierenden Systemen.

Acknowledgments

First of all, I would like to thank my supervisor, Rolf Pfeifer, for providing me with the wonderful opportunity to explore my scientific interests in the environment of the Artificial Intelligence Laboratory. I wish to thank Peter Eggenberger, for initiating the project and for the sincere support given to me to start my life in this country. Special thanks go to Fumiya Iida, for giving me suggestions, and sharing the moments of Sunday afternoons in the office. I am further indebted to Satoshi Murata and Rodney Douglas for kindly reviewing this thesis and providing valuable comments. I would like to thank all my colleagues from the AI Lab for many productive discussions: Simon, Miriam, Gabriel, Raja, Matthias, Luis, Marc, Koji, Daisuke, Martin, Lukas, Thomas, Rico, Claudia, Pascal, Hanspeter, Mark, Alejandro, Jonas, Kojiro, Wenwei, Alex, Daniel B., Maik, Flurin, Matej, Lijin, Sarit, Nir, Hugo, Cristiano, Dorit, Maurice, Christof, Aubery, Saikat, Marco, Sladjana, Tobias, Thierry, Kostas, Atsushi, Jin, Hide, Daniel G., Hung, Naveen, Tao, Harold, Muku, Farrukh, Qian, Hassan, Sadeque, Naoki, Michael, Dominique, William, Dandolo, Kuri, and especially, I thank to the four people: Nathan, Max, Ruedi, JP, and Kohei, for the precious support of my project. It was wonderful time to be with you all. I would like to acknowledge all the people who have given their thoughtful and encouraging input to my work - Akio Ishiguro, Koh Hosoda, Zoltan Nagy, Hiroshi Yokoi, Henrik H. Lund, Erik Winfree, Kasper Stoy, Takashi Ikegami, Rodney Brooks, Daisuke Kurabayashi, Minoru Asada, Hiroshi Ishiguro, Radhika Nagpal, Peter Bentley, Metin Sitti, Roderich Gross, Alcherio Martinoli, Gregory Mermoud, John Reif, Masayuki Inaba, and Hajime Asama. Finally, I would like to express my gratitude to Dana, for the valuable shared time.

- **Chapter 1** and **Chapter 7** are based on [67] and I thank all the contributors, Maurice Göldi, Christof Audretsch, Rudolf Füchslin and Rolf Pfeifer. Especially I thank Ruedi for precious inputs and prudent guidance.

- **Chapter 2** is based on [70], and I thank Zoltán Nagy, Bradley J. Nelson, and Rolf Pfeifer. Also special thanks to Dana D. Damian and Damiano Lungarella for their assistance.

- **Chapter 3** is based on [69], and I thank Marco Kessler and Max Lungarella, for their valuable contributions. I appreciate Juan Pablo Carbajal's assistance for modeling the system.

- **Chapter 4** is based on [79], and I thank Zoltán Nagy, Simon Muntwyler, Ashish K. Cherukuri, Jake J. Abbott, Rolf Pfeifer and Bradley J. Nelson for the contributions.

- **Chapter 5** is based on [66] and I thank Flurin Casanova, Max Lungarella and Rolf Pfeifer for their contributions.
- **Chapter 6** was assisted by Christof Audretsch and Rudolf Füchslin. I greatly acknowledge helpful discussions in the chapter.

This research was mainly supported by the Swiss National Science Foundation. I appreciate and am very thankful for the support.

Contents

Chapter 1

Introduction

1.1 The Mystery of Life

Since the dawning era of human civilization, the origin of life has been one of the largest mysteries. The attempts to answer the question of how a high degree of order emerged from a molecular soup have produced some acceptable answers, but the fundamental truths remain obscure. The crystal structure shown in Figure 1.1 is approximately 50 cm tall and has a plant-like morphology. However, the structure is clearly dead even though we may know which the constitutive materials are. It seems we somehow possess a mean to identify living things out of non-living entities (objects).

Figure 1.1: The mystery of life: $CaCO_3$ crystal displayed in the Smithsonian National Museum of National History in Washington (photo taken by the author).

Inspection of the microscopic world of living systems often confronts us with the core mystery of its amazing capability. The invention of the microscope was a profound technical advancement, and the ground-breaking discovery of DNA by Watson and Crick led to enormous advances toward understanding the material basis of life. The discoveries in modern science present a new world and

provide an accurate view of microbiological systems. Living organisms form their own structures by metabolizing constituents simultaneously through an intricate web of molecular interactions. The scale varies from nanometers to meters; some of these organisms consist of a single cell, and others, of multicellular structures. Moreover, the components, which include a colony of cells that are annihilated and replaced, apparently lack a central coordinator, which complicates the mystery. These structures have evolved with increased complexity and continue to adapt with superb capabilities to severe environmental changes.

In contrast to the variety of sets of compounds so far revealed, however, discussions of the emergence of life from local interactions of components still gravitate around in-depth descriptions and modeling of interactions, e.g. through steady-state representations such as reaction pathways. Typically, to date, life has been thought of as a material-based physical phenomenon. While the intricate web of reaction networks provides us with the requisite level of complexity, the lack of a global picture suggests the importance of understanding the dynamics from the perspective of distributed systems [5]. Each molecule is governed by the laws of physics in its own environment, and the processes are autonomous and distributed without any centralized control. In other words, despite the progress, the emergence of life from the local interactions of components (such as molecules, proteins, and cells) remains one of the large mysteries of modern science. An in-depth examination of the micro-world produces evidence that warrants an even closer look as scientists attempt to define life [6, 28, 56, 99].

Recently, however, there is growing interest in the interactions among individual components that lead to the process of self-assembly. Such efforts are required to abstract higher-level design principles to clarify the actual dynamic processes underlying these interactions. The real challenges are just beginning, and they involve a thorough examination that treats life as a special "mode" of materials.

1.2 Self-assembly

In industry, as the difficulty of manufacturing small-sized machines starts to be a limiting factor, the concern with spontaneous assembly has been brought to attention. The term self-assembly, defined by Whitesides *et al.* as *the autonomous organization of components into patterns or structures without human intervention* [122][1], elicits images of dynamical components roving around the environment and spontaneously composing a targeted structure. Many researchers currently anticipate possibilities in self-assembly, such as machines (e.g. self-repairable machines), that will play a key role in the understanding of living systems that lead to the realization of life. We believe that examples of self-assembly, both natural and artificial, provide primal but engaging instances of systems that warrant further study.

Organizational phenomena that occur in nature demonstrate the principle of self-assembly. Such phenomena may be observed from the nano- to the celestial scale [122]. Figure 1.2 shows three different levels of natural entities that are resulted from self-assembly.

[1] Note the notion self-assembly does not only contain instance of decentralized functionality.

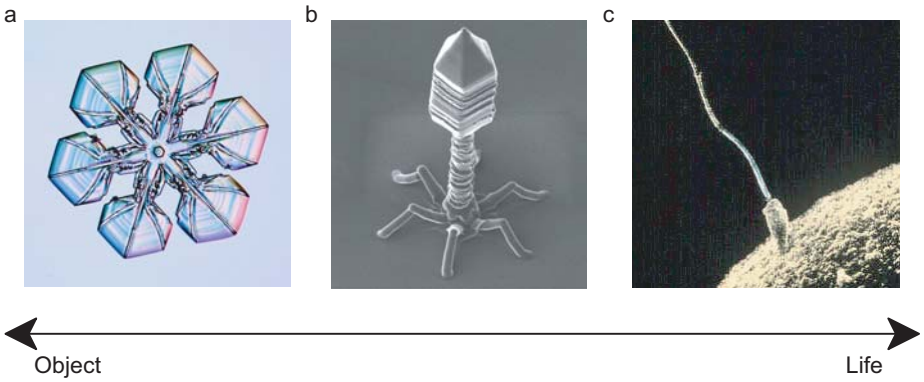

Figure 1.2: Crystal! Crystal? Crystal?? (a) snow flake [105], (b) artificial nano "T4 bacteriophage" [55], (c) flagellum (sperm) [1].

The molecules forming snowflakes are ordered lattices, the result of attraction/repulsion interaction that self-assembles in spontaneous crystallization. Such precise growth was first observed by U. Nakaya in a cloud-simulating chamber in the 1930s. Rabbit hair was used for the core of the crystal. The shapes are commonly hexagonal, but the details of the patterns vary depending on the environmental conditions, such as the humidity and temperature. Crystallization begins with a "core", often a speck of dust in the air, which allows other floating molecules to connect to the seed. Once molecules connect to the crystal, they change form, exposing other connection sites to which additional molecules attach. In other words, information of the connections is conveyed to external molecules though the formation process. The system is conservative in terms of energy dispersion; in other words, once an atom connects to the cluster and changes the form, it preserves the energy and sustains the formation by means of a hydrogen bond unless the temperature rises and breaks the bond.

The syntheses of viruses may offer a key to an understanding of the central issues of "living" systems[2]. The formation of complex symmetrical protein shells of spherical viruses is a well-studied example of self-assembly. The organism consists of about 70 different kinds of proteins and exploits the metabolism of a host cell (e.g., *E. coli*) to generate copies of itself. Moreover, it is truly remarkable that if the right kinds of proteins are mixed, the virus can be synthesized *in vitro* [59, 130]. The interactions at a local level are simple; the interactions of a large number of entities can lead to the emergence of complex structures through a process of self-assembly. Considering the fact that hundreds of protein molecules distinguish each other, the capability of selective binding is noteworthy.

One of the primitive forms of "living system" might be sperm (Figure 1.2). Sperm has a structure dedicated to one purpose; conveying the host DNA to an egg. Sperm has a head and a tail. The head contains inactivated DNA, and the tail propels the sperm toward an egg. The tail is a powerful flagellum, a hair-like organelle, which propels the organism. It does not contain any ribosome or endoplasm, which are unnecessary for its function. The dynamics of synthesis of a flagellum has been revealed recently. It is a well-ordered composition of

[2]Note that viruses are treated as non-living entities.

constitutive proteins, which grows from the base of the body.

Self-assembly is a common and arbitrary process in nature in which basic units come together and form a structure spontaneously. The information needed for the development of such a complex structure is often stored in the shape of the basic units, in their internal states, and in the rules of nature, which determine the precepts of their behavior and interaction [122]. The main advantage of self-assembly systems is that they are, to some extent, robust against malfunctioning because failure of one element does not have a great impact on the system as a whole. This suggests that self-assembly systems can repair themselves by replacing broken parts, as do many biological systems (self-repair).

Self-assembly needs to be distinguished from self-organization. While self-assembly is spontaneous aggregation of substances, self-organization has a more general meaning. It is the appearance of global patterns from uniform space, caused by local interactions. The patterns consist not only of substance but also, for example, of energy or a velocity field. Self-organization plays a crucial role in various disciplines, such as chemistry, biology, physics, and economics. The Bernard-convection or the Belousov-Zhabotinsky reaction (Turing patterns) and Hodgkin-Huxley equation are famous examples of self-organization. In this thesis, however, the main focus should be directed to self-assembly processes, not to self-organization.

According to Whitesides and Grzybowski, self-assembly can be classified into four categories [122]:

- **Static self-assembly:** this category contains all the systems that are at global or local equilibrium and do not dissipate energy (e.g., molecular crystals and most folded globular proteins). In this type of self-assembly, the formation of an ordered structure may require energy, but, once the structure is formed, it becomes stable. Most of the research in self-assembly is focused on this type. Many biological structures, such as actin and myosin fibers or ribosomes, are good examples of static self-assembly because they statically exist without dissipating energy to maintain their structures.

- **Dynamic self-assembly:** in dynamic self-assembly, interactions between different components that are responsible for the formation of structures or patterns only occur when the system dissipates energy (e.g., weather patterns or patterns formed by schools of fish, flocks of birds, solar systems, and galaxies). Dynamic self-assembly is the category with the closest relationship to self-organization, bridging both fields. The universe, which includes solar systems and galaxies, is a dynamic self-assembly system that started as unstructured matter after the Big Bang and has formed a complex figure over billions of years, in response to the laws of physics. Flocking is an example in which emerging formations can be observed as a result of interactions of relatively simple components. Birds and fish, for example, follow simple interaction rules and show astonishingly fertile schooling behaviors. It contributes optimally to oppose the individual against a predator or environmental conditions. These behaviors are the main contributors to birds' or fish' ability to withstand predators or negative environmental conditions.

- **Templated self-assembly:** this process is widely used in engineering, which is, in brief, a shape-matching process between the components and the features of the assembly environment. Epitaxy is one example in which colloids crystallize in directed optical fields. It involves the deposition of a monocrystalline film on a monocrystalline substrate. This category contains not only the process in which the template determines the global structure but also phenomena, such as crystallization, in which right materials grow from a seed under the proper environmental conditions.
- **Biological self-assembly:** nature is the effect of self-assembly, and biology is the effect of nature. This classification includes the characteristics of the three categories above. The exemplary feature of biological self-assembly is the variety and complexity of the functions that are produced. While the distinction between this category and the other three is unclear, it is the complexity of each that makes them unique. Examples of biological processes, such as metabolism, morphogenesis, and self-repair, among many, demonstrate the capacity for self-assembly. In general natural systems exhibit hybrid properties and cannot be easily categorized.

1.3 Research Trend in Artificial Self-Assembly

Despite nature's efficiency and precision in assembling supramolecular and mesoscopic structures, few attempts involving artificial self-assembly have been successful. Figure 1.3 classifies fields related to self-assembly. The X-axis represents the size of the component in each system, and the Y-axis represents the level of autonomy of the component. In general, the further right along the X-axis, the

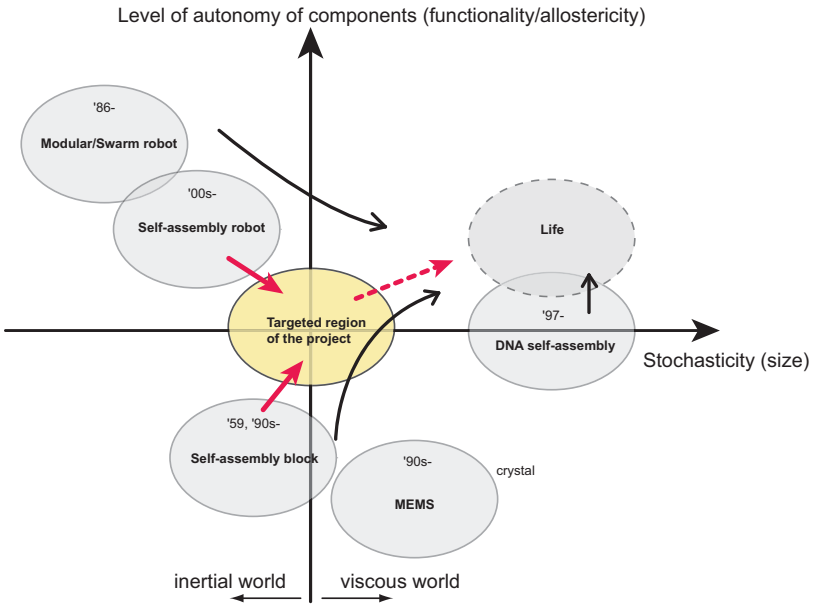

Figure 1.3: Road map toward living systems. In general, the further right along the X-axis, the more stochastic the system, and the further up the Y-axis, the more autonomous the component.

more stochastic the system, and the further up the Y-axis, the more autonomous the component. From a broad standpoint, two trends can be recognized: one originated from robotics, and the other, from synthetic molecular biology. Each field has its advantages and disadvantages, e.g., robotics is suitable for realizing a module with high autonomous components, such as microchips or memories, but it is not easy to downscale. On the other hand, it is challenging to realize a technologically interesting level of autonomy or computational capability with DNA tiles/strands. The targeted region of our project is shown in yellow in Figure 1.3. Our efforts will be primarily devoted to the investigation of the level of component autonomy and stochasticity, aiming at designing self-assembly robots (see further discussion in Section 1.5).

In this Section, we introduce various research related to artificial self-assembly following the trends described in Figure 1.3.

1.3.1 Modular Robots

Modular robots – autonomous machines consisting of typically homogeneous building blocks – promise a viable solution for the adaptation because they have the highly versatile ability — to re-configure their shape according to a given environment. The essential issues of how to develop cellular (modular) robotic systems were described already 20 years ago by Fukuda and his collaborators [30]. Followed by other early work, such as that proceeded similar idea and showed a modular robot in which components possessed different functionalities (e.g. vibration motor or battery) [81], or that achieves locomotion of a reconfigurable modular robot [126], several different types of modular robotic systems which could morph into desired target configurations [19,76], many different types of units that can rearrange the connectivity of their structural units to create new topologies to accomplish diverse tasks were proposed. Generally these self-contained modular systems include their own processor, power supply, communication system, sensors, and actuators, for example, such that can form aggregates by expanding and contracting its shape [93], aggregate as active three-dimensional structures that could move and change shape [57], employs Central Pattern Generator (CPG) for locomotion [71], physically self-reproduce itself [131], consists of joints and limbs that can elongate and contract [107]. These modules were designed to work in groups as part of a large configuration.

Among various approaches that have been mainly spotted on the design and construction of basic building blocks of a typically small repertoire, with docking interfaces, which allow transfer of mechanical forces and moments, and electrical power, and which can also be used for data communication [7,9,24,77,98,109], several successful models that resolved the dissociation of algorithm (software) and hardware [18,78].

A similar approach can be seen in the work presented by Jorgensen and Lund *et al.* [53], which consists of several fully self-contained robot modules. Because the units move or are directly manipulated into their target locations through deliberate active motion, the modular system is called "deterministically self-reconfigurable". The implication is that the exact location of the unit is known all the time, or needs to be calculated at run time. There are some robots that can be categorized in this section and have irregular properties, such as those in motion exploiting the friction to the ground or among modules [48,102], those use wheels and swarms [20,72]. The advancement of hardware takes off

a derivative field which focuses more on practical implementation, such as the approach for medical surgery/diagnosis [43, 79, 80]. Review papers of this field are [75] and [127].

1.3.2 Self-assembly Robots

Manufacturing technologies and industries heavily rely on robots. For macroscopic objects industrial robots are not only economical but are also reliable, fast, and accurate. They are widely used in production processes (i.e. pick-and-place car manufacturing robots) and other situations where their environment as well as their task are well defined and no unexpected situations occur. In contrast, as the assembled objects become more complex, conventional engineering technologies hit on a complexity barrier which entails lower yields and higher fabrication costs. Recent advances in robotics have pointed out the importance of self-assembly for building complex objects, aiming at exploiting the obvious advantages of living organisms.

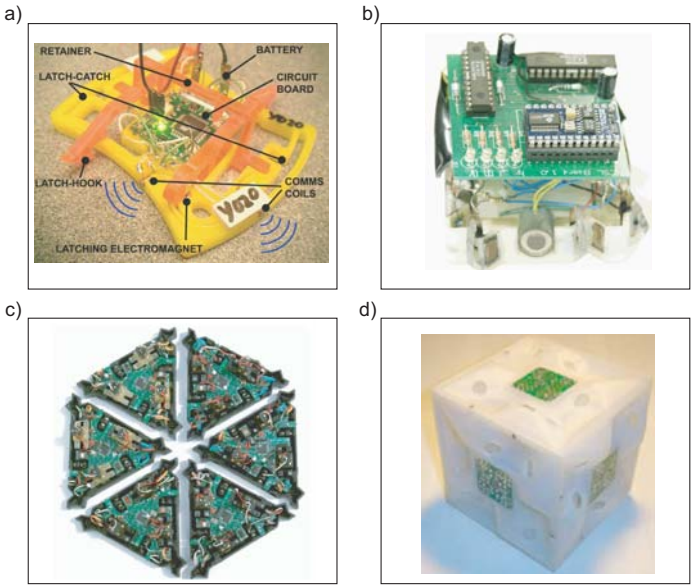

Figure 1.4: Self-assembling robots built by (a) Griffith *et al.* [38], (b) White *et al.* [119], (c) Klavins *et al.* [54], (d) White *et al.* [120]. The way of agitating varies; adding mechanical turbulence to the ground (b), air-jet turbulence (a, c), fluid turbulence (d).

Self-assembly systems are "stochastically self-reconfigurable" implying that (1) there are uncertainties in the knowledge of the modules' location (the exact location is known only when the unit docks to the main structure); and (2) the modules have only limited (or no) computational (deliberative) abilities. To date, a few robots that can self-assemble relying on stochastic environments have been built. These modules are either settled on a ground with low friction agitated for the achievement of locomotions. The way of agitating varies, such as adding mechanical turbulence to the ground (Figure 1.4 b) [119], air-jet turbulence (Figure 1.4 a c) [8, 38, 54]. Some have an unique environment, such

as one set in oil with fluid turbulence (Figure 1.4 d) [120]. Yokoi *et al.* took robotic and chemical approaches, in which he developed physically connected multi-robots system and a system that can control a drop of mercury [128]. A significant idea was proposed by Reynolds, who showed that a global behavior can emerge from local interactions [90]. A good review article surveying this field is addressed by Gross and Dorigo [39].

Although in all these systems the units interact asynchronously and concurrently, the work remains strong influences of reconfigurable modular robots relying on certain amount of state-based controls required for the modules to move, communicate, and dock (see Section 1.3.1). Moreover, the main difference from existing modular robotics shall be the way of supplying the modules. The robot or formed cluster waits for a supplemental module to be "delivered" from environment, instead of supplying it by itself. Although in all these systems the units interact asynchronously and concurrently, a certain amount of state-based control is still required for the modules to move, communicate, and dock. Generally the internal representations of the module's configurations, such as having a rewritable look up table, follow the same lines as conventional approaches.

1.3.3 Self-assembly Blocks

In contrast to those robotics approaches, there exists small but distinct another tide, which are more based on physics. Those trends, which exploits material properties for self-assembly can be categorized in two different types; pure passive types (Type I) and reactive types with some (internal) states (Type II).

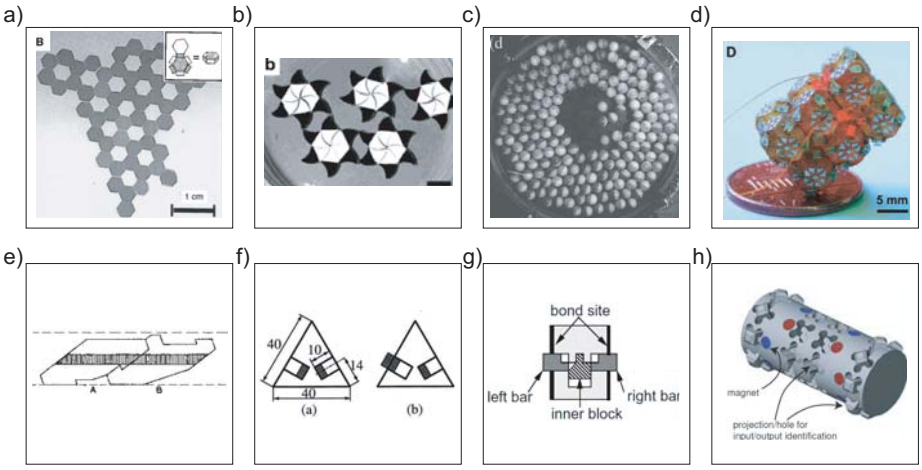

Figure 1.5: Self-assembly blocks designed by (a) Bowden *et al.* [15], (b) Mao *et al.* [62], (c) Breivik [17], (d) Gracias *et al.* [36], (e) Penrose *et al.* [87], (f) Tsutsumi *et al.* [113]. Due to their simplicity, these components have substantial capability to scale down and adopt to different environments. (a)-(d) are passive, while (e)-(h) have "states" and regulate their bindings. Yet few model attained "functionality" of the compound, such as an electric circuit (Figure 1.5 d).

Pioneering experiments on manual self-assembly were conducted half a century ago (Figure 1.5 e) [86, 87], where a provoking mechanical model of natural

self-replication in a stochastic environment was presented. He designed the implementation of internal states to a physical component, whose unit can move on a 2D plane. The work was followed by several studies on clustering patterns of passive elements, focusing on the role of shape on template and components matching [21]. A simple but elegant design was shown by Hosokawa, in which the components can react to an input and allow new bondings (Figure 1.5 f) [46]. Notable ideas about conformational switch were proposed by Saitou *et al.* (Figure 1.5 g) [94–97]. Although his work was rather conceptual demonstrations for theoretical justifications. A series of studies were conducted by the group of Whitesides; for the realization of positional coordinate of molecule-mimetic chemistry (Figure 1.5 a) [15, 16, 42, 124], circuit functionality (Figure 1.5 d) [12, 13, 36], reversible aggregation (Figure 1.5 b) [62], folding structure [10], rotation of magnets [41], and rotation of rotors [40]. Similarly, numerous research efforts have been devoted to the investigation of morphology [106]. Artificial chemicals that can form in several ways, such as polymers and dimers, depending on the temperature of the system were demonstrated in [17] (Figure1.5 c). Different aggregation patterns with various sizes of components were shown in [125]. An intelligent self-assembling block which can represent multiple states by the units' rotational angle was designed by [113] (Figure 1.5 h). The system can physically conduct XOR calculation on a 2D plane. These self-assembly blocks can be categorized into two types, namely those which are passive (such as (a)-(d) in Figure 1.5), or those which have "states" and regulate their bindings ((e)-(h) in Figure 1.5). What all these models are simple enough to be scaled down (realized in the physical level). Yet few model attained "functionality" of the compound, such as an electric circuit (Figure 1.5 d). Also these models presume environmental turbulence as the driving force of the reactions (not self-propulsive), which is a reasonable premise when the size of the modules is small enough.

It is remarkably fertile what Turing machine can express. Nature "carries out" computation not in the way as we achieve in computer, but in a more physically grounded way; sometimes in a self-assembly way[3]. The natural system often features disassembly (detachment) of components as well as assembly, and moreover, the components often express different functionalities by changing the internal states. In the case of crystal formation of snow flakes, the atoms change the shape and allow the next atom to attach. As for the cases with protein assemblies, a protein changes the configuration such that it exposes new bonding sites for a further reaction.

1.3.4 Self-assembly at Small Scales (MEMS, DNA self-assembly/origami)

By taking tools and methods from nature, many inroads have already been made to utilize self-assembly for the fabrication of structures at molecular scales. The early work at this scale ($\mu m \sim mm$) on self-assembly appeared in the '90s[4], such as the one which exploits hydro phobic/philic interactions [47], or the one that used capillary force [91]. Knowledge from molecular biology reminds us of the importance of the fertile encoding capability of molecular bonding; it is

[3] precisely, nature does not really carry out computation but we ca describe what nature does as computer

[4] unless we count work in chemistry

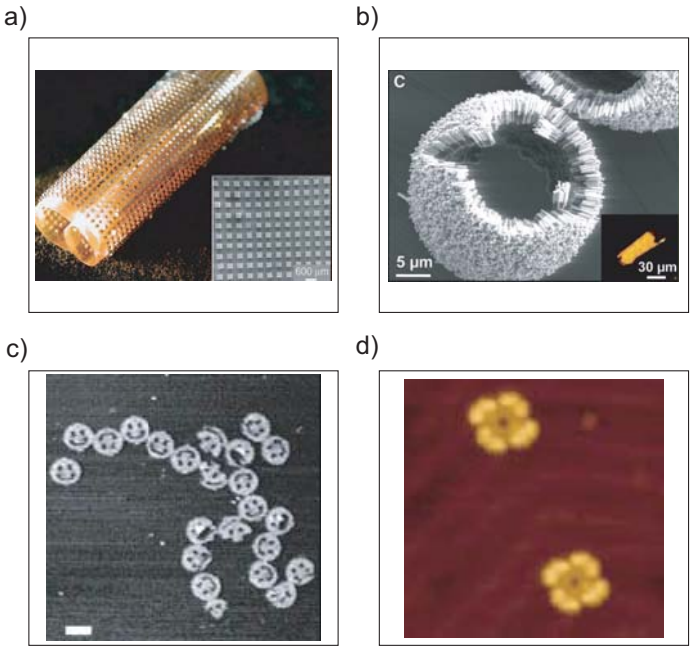

Figure 1.6: Examples of self-assembly at the micro a) fabrication of a Cylindrical Display by Patterned Assembly [51], b) self-Assembly of Mesoscopic Metal-Polymer Amphiphiles [83], and nano-scales c) folding DNA [92], d) selective assembly on a surface of supramolecular aggregates [129].

noteworthy that no matter how complicated the microscopic systems seem, they exploit non-covalent bonds (hydrogen bonds, ionic bonds, and van der Waals attractions) as interaction forces and somehow achieve an amazing specificity in docking with other selected molecules. An essentially analogous problem to the macroscopic approaches is investigated in the context of DNA folding where one of the objectives is to increase the yield rate of a self-assembly process (Figure 1.6 c) [61, 92, 100, 101, 104, 123]. While they are designing DNA for the elements, Yokoyama *et al.* assigned molecules for the assembly tasks (Figure 1.6 d) [129]. Their methods are powerful and effective, especially due to the exploitation of the advantages of the small scale, e.g. controlling the stochasticity through temperature in mass producing the assembled units.

Along with the progress on fabricating micro devices, some work from Micro Electro Mechanical Systems (MEMS) has shown noticeable outcomes, e.g. rod-like building blocks that form a series of single-layer superstructures consisting of bundles, tubes, and sheets (Figure 1.6 a, b) [51, 83]. The disadvantage is, if any, that the employable assembly parts are limited to what naturally exist or manufacturable at the scale. A review on small scale self-assembly is introduced in [11, 63].

It is plausible to assume that self-assembly can also lead to innovation in applications such as macro-scale multirobot coordination and manufacturing technologies for microscale devices. Concerning micro autonomous devices (robots), some pioneering work has been attempted. The main focuses were spotted on the actuation under externally added magnetic field environments [27, 84, 104],

some with corkscrew configuration [45, 49], or the other exploiting resonated frequency [97, 116]. Another attempt was carried out with chemistry for actuation [118]. Possibilities of microrobots' applications are described in [103].

1.3.5 Model Oriented Work

The eternal question of whether *Physical law is an abstraction of a real entity or the real entity is a figure of physical law* remains, reflecting the observer's frame of reference; however, wherever there is a phenomenon, there exists an effort to model it. In the middle of the last century, von Neumann tackled one of the problematic questions concerning the condition of self-reproduction. He developed a model that he demonstrated with a cellular automaton, in which 29 states were defined in each cell [114]. Langton continued with von Neumann's model; he simplified it by focusing exclusively on self-replication processes [58]. An elegant model with a graph structure was advocated by Tomita *et al.* [112]. Gillespie formalized a kinetic rate reaction of chemistry and established the basis of a self-assembly mathematical model [33–35]. Adleman, the developer of a DNA computing model, generalized self-assembly [3, 4]. Mermouod and Martinoli modeled a rate equation model, a Monte-Carlo model, and a physical simulation and compared the results [65]. Kumar *et al.* also used a rate equation model [64]. They focused on the so-called backward problem (see Section 1.4.1) and applied the method. These models make it possible to systematically analyze the critical paths of reactions in their targeted assembly processes.

1.4 Major Issues in Artificial Self-assembly

In this section, we systematize the problems of artificial self-assembling systems, and derive prerequisites for designing components.

1.4.1 The forward problem and the backward problem

In self-assembly, the problem to derive the final configuration from a given set of components/environments is called the *forward problem* [85][5].

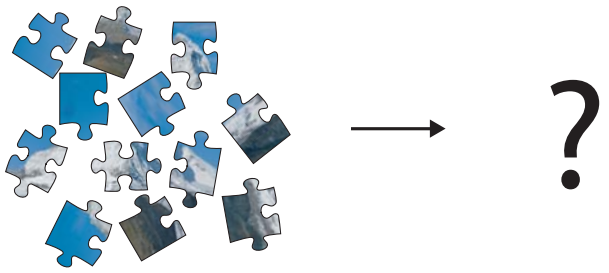

Figure 1.7: The *forward problem* – the problem to dissolve the net configuration from a given set of components.

[5]The game *Tetris*® is known as a NP-hard [23]. Also it may be useful to mention that some situations in self-assembly resemble the Knapsack problem, which is known as a NP-complete.

Conversely, the problem of designing components for a targeted configuration is called the *backward problem*. In this "reverse engineering" process, also known as one of the central problems in self-assembly, the designer has to start from the final structure and decompose it.

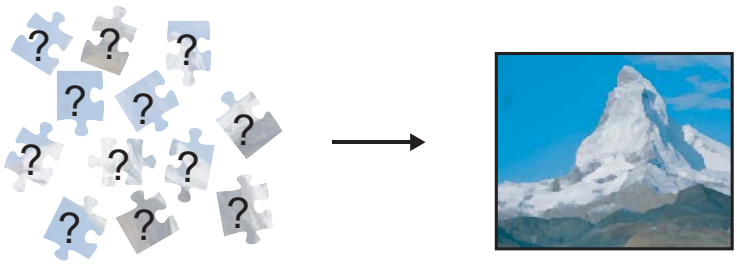

Figure 1.8: The *backward problem* – the problem of designing components for a targeted configuration.

Several aspects of both, the *forward* and the *backward problem*, show strong dependence on the length scale of the system. A necessary condition for the prediction of the result of a self-assembly process is detailed knowledge about the morphology of the components. And this knowledge is easier to get the larger the components are[6]. In contrast to cm-sized components, a molecule usually has many degrees of freedom and therefore the morphology and consequently the interaction between components are not always known with sufficient precision.

Similar considerations hold for the *backward problem*, and, from an engineering perspective, to an even higher degree. Given an object O for which one wants to design a self-assembly process. There are many possibilities to divide a large O into components. The smaller O, the more constraints with respect to the production of the components have to be considered: On the molecular scale, chemical synthesis set a limit to what can be accomplished.

We recognize three main problems centering around artificial self-assembly: namely, (A) the assembly issues, (B) the dynamics issues, and (C) the interactions issues (Figure 1.9). The explanations for each problem follow.

1.4.2 (A) Assembly Issues

The followings are the issues on assembling processes.

The mismatch problem (Addressing error)

In self-assembly, an assembly error (or undesired attachment) is induced when the system converges to an energetically local minimum through interactions between components, mainly due to the low addressing capability to attain the adequate bonding affinity level for connections (Figure 1.10).

There are two main strategies for solving the problem; increasing encoding accuracy of bond matching while regulating the agitation level of the system,

[6] This does not only refer to shape but also to other features of morphology, such as elasticity and degrees of freedom.

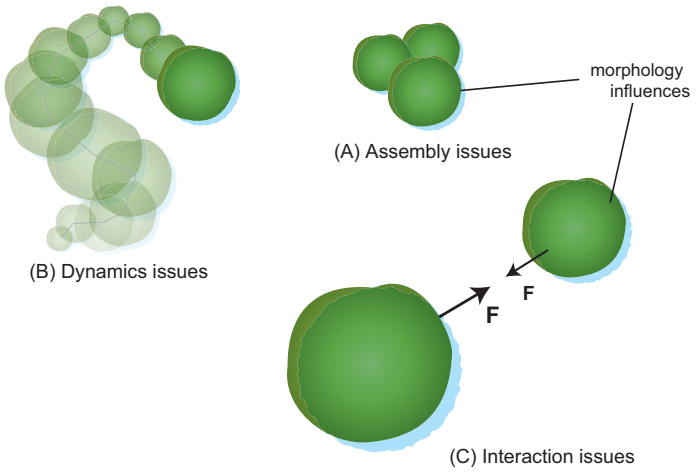

Figure 1.9: Three main issues centering around self-assembly. (A) assembly issues, (B) dynamics issues, and (C) interaction issues. The influence of morphology appears mainly in the assembly issues and interaction issues.

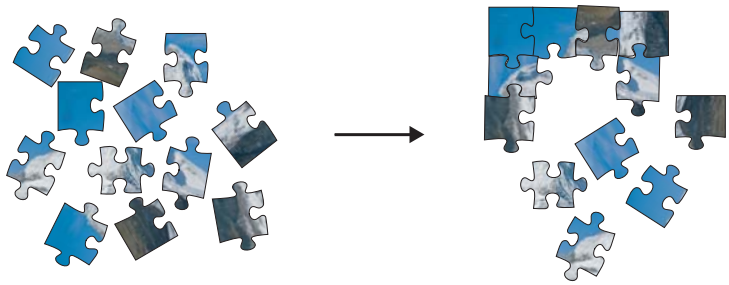

Figure 1.10: The *mismatch problem (adressing error)*. In this jigsaw puzzle example, an error is enhanced if the agitation level is low. It is always the comparison of the addressing accuracy and the environmental agitation.

and implementing internal states to components. Insights from molecular biology remind us of the importance of the fertile addressing capability to attain the adequate bonding affinity level for maintaining connections of molecular bonding; they exploit non-covalent bonds (hydrogen bonds, ionic bonds, and van der Waals attractions) as interaction forces and somehow achieve an amazing specificity in docking with other selected molecules[7]. The agitation level can be regulated by means of temperature or kinetic turbulence magnitudes. From an engineering perspective, the scaling behavior of the *mismatch problem* exhibits an interesting feature. The relative simplicity of the *backward problem* enables one to construct highly specific, literal plug-and-socket connection sites on the *cm* scale.

Molecules, on the other hand, may well be highly flexible (having many degrees of freedom) and, agitated by thermal motion, "sample" their configuration

[7]The trick of proteins distributing bonding sites around the body, and changes the morphology to pose another bonding site reminds us of the importance of internal states, which enables the component to feature different properties.

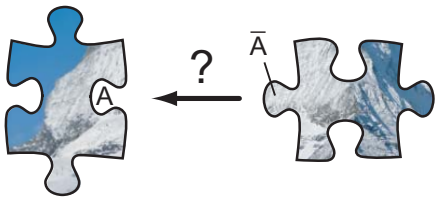

Figure 1.11: Addressing capability to attain the adequate bonding affinity level for maintaining connections. In jigsaw puzzle, only one piece has the "right" shape to connect to the complement piece (A to $\bar{A}$). This can be realized by differentiating the shapes of all the connection sites of pieces. In general, the strength of bonding can be calibrated by the implementation of bonding sites. In magnetic systems, the array of multiple magnets arranged at the bonding sites works equivalently.

space at a rapid pace. Because of this, e.g. two complementary DNA strands just have to be brought into close proximity: If they match, they will eventually bind. Such a "fast configuration sampling" is not possible above the molecular scale. One of the reasons for this is that whereas mechanical structures wear off, molecules don't: A molecular "joint" can be bent infinitely many times (as long as the bond doesn't break, it is in all respects as good as a newly formed one) [8] [9] [10].

⇒ **Prerequisite I: high addressing capability of bonding is required**

The topological dead end problem (Steric hindrance)

This problem occurs when components assemble in an undesired sequential order. The targeted structure is therefore unreachable, since some earlier assembled components block the way (Figure 1.12).

To solve this problem at scales where the benefits of molecular mechanical flexibility cannot anymore be harvested, the components should reflect the presence of its neighbors e.g. as the internal states, and logically order the assembly sequence. Yet in practice the amount of expressible internal states is limited due to the limited space in a component, leading to a risk of misrecognition by other components.

⇒ **Prerequisite II: the module should handle logical assembly**

[8] Note that there is an often overlooked difference between mechanical plug-and-socket structures and molecular binding sites: The former are designed to be inflexible, mechanically "hard", which implies that connecting plugs and sockets requires to bring them together on a trajectory with a rather narrowly defined tolerance.

[9] It is the micro-to (sub-)millimeter scale, at which molecular bonding (and corresponding recognition) is not strong enough anymore, whereas mechanical plug-and-socket connection mechanisms are still hard to produce.

[10] The *mismatch problem* is a fundamental problem in nature. The replication processes of DNA are greatly assisted by self-repair functionalities of enzymes.

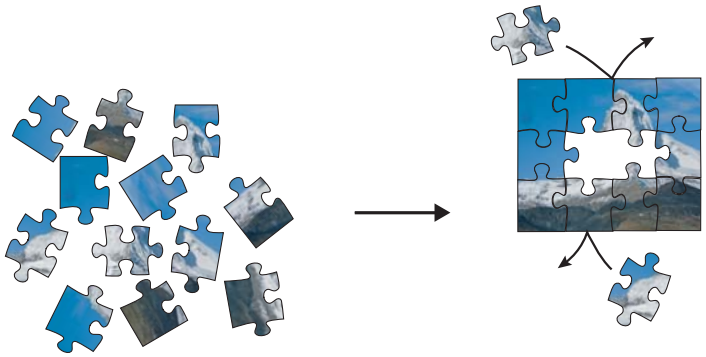

Figure 1.12: The *topological dead end problem (Steric hindrance)*. The components should reflect the presence of its neighbors e.g. as the internal states, and logically order the assembly sequence.

The parallel yield problem (Incompletion problem)

The problem of producing a desired configuration in large quantities (while avoiding incomplete assemblies) by homogeneous system is known as the *parallel yield problem* and has been studied in the context of biological and non-biological self-assembling systems [46][11]. Here, we term the problem that specifically occurs when components assemble in a right manner, however do not complete the targeted final structure, for combinatorial reasons (Figure 1.13; we assume the circular sector components connect side-by-side). This is because many assembly processes proceed in parallel and components are used in earlier more likely reactions of other assembly processes since reactions leading to the complement of the end product are more unlikely than the preceding reactions. This means that the self-assembly of many products is started but rarely fulfilled. In other

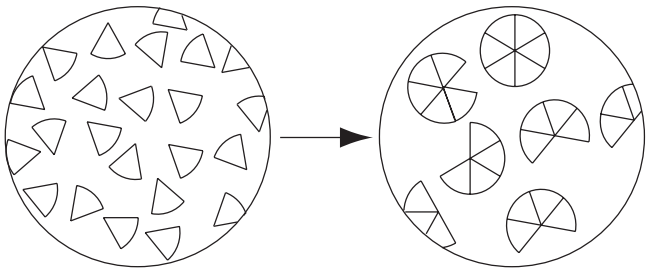

Figure 1.13: The *parallel yield problem (Incompletion problem)*. Here, we term the problem that specifically occurs when components assemble in a right manner, however do not complete the targeted final structure, for combinatorial reasons; we assume the circular sector components connect side-by-side).

words, the likelihood to accomplish the desired end product declines with the rise of the ratio between the likelihood of the earlier and the later reaction.

⇒ Prerequisite III: The system should cope with parallel assembly

[11] Hosokawa called it "yield problem". However, since it is often used for more general meaning, we termed it the *parallel yield problem* to avoid confusion.

2D vs. 3D

Self-assembly is probably the only practical way to manipulate and order nano- and micrometer-sized components into 3D structures (Boncheva *et al.*) [14]. The most of the developed platforms for the micro scale assembly have conducted the assembly process on 2D stages [84]. The distinction between a two dimensional model and a three dimensional model on self-assembly system is not as trivial as it may seem at first glance. Normally a component has six degree of freedoms (DOF) $(X, Y, Z, Roll(\phi), Yaw(\theta), Pitch(\psi))$ in 3D space. Here we distinct them into two types of 2D:

$$2\mathrm{D_I} \quad \mathrm{DOF} \quad = \quad (x, y, \phi, \theta, \psi) \tag{1.1}$$

$$2\mathrm{D_{II}} \quad \mathrm{DOF} \quad = \quad (x, y, \theta) \tag{1.2}$$

The $2\mathrm{D_I}$ allows a component to rotate in 3D on a 2D plane, while $2\mathrm{D_{II}}$ does not (the movement of components is restricted to a 2D plane).

Table 1.1 summarizes the difference of 2D and 3D in self-assembly.

Table 1.1: The difference between 2D vs. 3D in "3D" world

	component's supply	physical interaction	producible structure
$2\mathrm{D_I}$	*dead end problem*	**close to 3D**	**quasi-3D**
$2\mathrm{D_{II}}$	*dead end problem*	constrained	2D
3D	easier than 2D	3D	3D

1. **Difference on components supply** The difference is noticeable. The supply path is affected by the configuration of the structure in 2D models (*dead end problem*), while this has less influence on 3D structures.

2. **Difference on physical interaction** A component in $2\mathrm{D_I}$, can interact with another component on the plane as if it were in 3D[12]. Whereas in $2\mathrm{D_{II}}$, interactions among components is restricted to the 2D plane.

3. **Difference on product structure** Exceptions may be components which possess flexibility and fold (such as proteins).

⇒ Prerequisite IV: 2 dimensional model is minimum but sufficient

Targeted region

The increase of the level of similarity among components (or level of homogeneity of a system) is expected to improve the *mismatch problem*, while the risk to be affected by the *parallel yield problem* may rise. The implementation of internal states, on the other hand, is expected to improve the *parallel yield problem*, whereas it has little affects on the *mismatch problem*. Regarding the *dead end problem*, it is thought to ease the problem, due to the reusability of the components (Table 6.1). A possible approach that holds on different scales for a component can be: finding an adequate level of homogeneity of the system,

[12] for sufficiently large distances between the components

Table 1.2: expected effect of homogeneity and internal states on each problem

	mismatch	dead end	parallel yield
Homogeneity (morphology)	better	-	worse
Allostericity (internal states)	(-)	better	better

while increasing the level of autonomy by means of implementing internal states in each component. The challenging region lies in where the implementation of internal states keeping the heterogeneity level of systems is possible. Note that increasing the number of internal states may not always be an economic solution, thus the *mismatch problem* would become insuperable. Figure 1.14 shows the number of types of tiles in various self-assembly system against the number of states per tile that can be observed in each case (cited from [37]). The noteworthy characteristic is that few natural systems make use of internal states, but instead, quite a few of them feature various types of tiles. Griffith treated

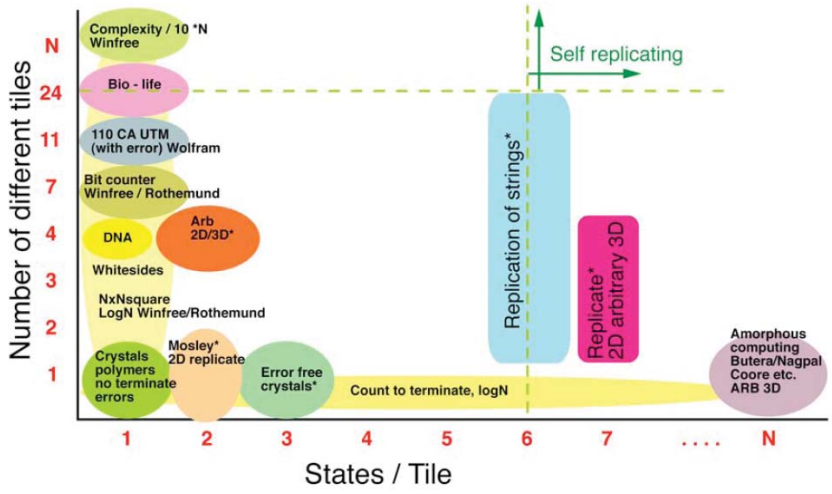

Figure 1.14: The number of (internal) states per tile (or component) against the number of different tiles (level of heterogeneity) in self-assembly systems (cited from [37]).

the most basic unit in biological systems as molecules, whereas it is controversial, since proteins change their state in multiple ways by folding. Normally, the possible number of internal state changes of a component seems to have a practical limitation. The problem of self-assembly is often finding the adequate level of component autonomy (capability of expressing different internal states) as well as the degree of heterogeneity, which are boty physically grounded[13][14].

⇒ **Prerequisite V: target allostericity and homogeneity**

[13]The state change is often captured as differentiation, which is beyond a frame of self-assembly.

[14]Like Rothemund's nanostructure with DNA string [92], a large degree of freedom may not be needed for all the components but for some template (relatively large scale) components.

1.4.3 (B) Dynamics Issues

Self-assembly is commonly believed to range from molecular to cosmological scales. However, it is also agreeable that few examples of self-assembly exist in our human living scales ($cm - m$). The second concern is about stochasticity, which varies to different scales.

Biological systems in the $nm - \mu m$ scale often show unique behaviors that cannot be observed in larger scales. This is mostly due to the influence of viscosity, which increasingly becomes dominant with decreasing length scales. The Reynolds number $\Re$ represents a ratio between viscous forces and inertial forces [89];

$$\Re \equiv \frac{\text{inertial forces}}{\text{viscous forces}} \approx \frac{av\rho}{\eta}. \tag{1.3}$$

where a is the radius of a particle, v is its speed, μ is fluid viscosity, and ρ is fluid density.

The size of $1\,cm$ is a critical size for self-assembling systems. For objects in water at the mm scale, viscosity is as important as inertia (the Reynolds number, that is, the ratio of inertial forces and viscous forces, is ≈ 1). It follows that objects smaller than that size are affected more by viscous forces whereas larger objects are affected more by inertial forces. For objects on the order of $1\,\mu\,m$ or less, such as bacteria, exploiting an environmental diffusion is a more effective way of locomotion than active propulsion (e.g., swimming bacteria are slower than diffusing molecules [74]). Good thought-provoking suggestions about the life at low Reynolds number are introduced in [89]. The author states the efficiency of creatures in small scale (μm) such as E. coli to use diffusion through their environment to change their position, rather than self-propelling. Whitesides implies the mechanical system in nanoscale would be different from that in micro scale, and one should learn more from biological systems [121].

Consider a particle that exists at $x = 0$ at $t = 0$. The positioning probability ($\rho(x,t)$) of x follows the diffusion equation:

$$\frac{\partial \rho}{\partial t} = D\frac{\partial^2 \rho}{\partial x^2} \tag{1.4}$$

where D is a diffusion coefficient.

Considering the initial condition $\rho(x,0) = \delta(x)$, and taking that the ρ satisfies the following normalized condition

$$\int_{-\infty}^{\infty} \rho(x,t)dx = 1, \tag{1.5}$$

we obtain

$$\rho(x,t) = \frac{1}{\sqrt{4\pi Dt}} \exp\Big(-\frac{x^2}{4Dt}\Big), \tag{1.6}$$

which obeys the Gaussian distribution.

The mean-square displacement $\langle x^2 \rangle$ can be derived as

$$\langle x^2 \rangle = \int_{-\infty}^{\infty} x^2 \rho(x,t)dx = 2Dt \propto t, \tag{1.7}$$

where $D = \frac{k_B T}{\zeta}$, k_B is the Boltzmann constant and ζ is a friction coefficient.

The time for transporting anything a distance l by stirring, is about l/v. Whereas, for transport by diffusion, it is l^2/D, where D is the diffusion coefficient in cm^2/sec [89]. Namely in the micro scale, and the ratio of these two

$$\begin{array}{rc} \text{time for transport by stirring:} & l/v \\ \text{time for transport by diffusion:} & l^2/D \end{array}$$

(termed stirring number; S) is

$$S \equiv \frac{\text{time for transport by stirring}}{\text{time for transport by diffusion}} = \frac{lv}{D} \approx 10^{-2} \tag{1.8}$$

which shows the efficiency of diffusion on a small scale [89].

If I have to push that animal to move it, and suddenly I stop pushing, how far will it coast before it slows down? The answer is, about 0.1 angstrom. And it takes it about 0.6 μsec to slow down. I think this makes it clear what low Reynolds number means. Inertial plays no role whatsoever (Purcell 1977 [89]).

At the scale of cm, where the viscosity is negligible, using agitation for travelling is a good tactic. Whereas at the molecular scale, Brownian motion enables the speedy spatial transitions. It is in the intermediate scale (μm), where those tactics lose validity because of the high viscosity and relatively small momentum.

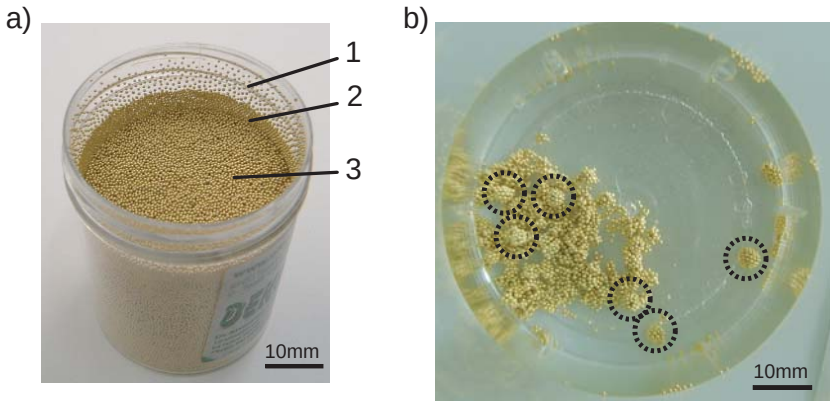

Figure 1.15: Self-assembly of mm scale particles. (a) $0.5\,mm$ beads in a cup. they tend to automatically form three layers which are dominantly affected by (1) static charge on the particles, (2) static charge on the wall, and (3) gravity. (b) Spherical clusters generated in water. We hypothesize that through the mixing and shaking, tiny air bubbles are created in the water. The air around each particle acts as a sticking connector producing attractive forces.

In Figure 1.15 a, $0.5\,mm$ size plastic particles are shown. When mixed with water and shaken, they tend to automatically form three layers which are dominantly affected by (1) static charge on the particles, (2) static charge on the wall, and (3) gravity. As can be seen in Fig. 1.15 b, several numbers of spherical clusters were generated. We hypothesize that through the mixing and shaking, tiny air bubbles are created in the water. The air around each particle acts as a sticking connector producing attractive forces. The implication is that we need

to be careful when relating our work to small scales. Principles of the scaling of physical effects can be found in [2, 22].

⇒ **Prerequisite VI: the component architecture should be scalable**

1.4.4 (C) Interaction Issues

The third issue is physical interactions among components. Here we briefly describe the basics of two conspicuous physical quantities that play a major role in self-assembly. We further view collision from the stand point of interaction, which is mostly affected by morphology of components.

Electrostatic interaction mechanisms

Given that an electric charge q_i exists. The electric field E created by this charge is

$$\vec{E} = \frac{q_i}{4\pi\epsilon_0}\frac{\hat{\vec{r}}}{|\vec{r}|^2}. \tag{1.9}$$

where ϵ_0 is the electric permittivity of free space.

The force F_{ji} that electric charge q_j receives is given by

$$\vec{F} = q_2\vec{E} \tag{1.10}$$

$$= \frac{q_1 q_2}{4\pi\epsilon_0}\frac{\hat{\vec{r}}}{|\vec{r}|^2}. \tag{1.11}$$

Therefore the decay of force over space is identical regardless of the scales.

Magnetic interaction mechanisms

We consider the magnets as dipoles with a magnetic moment $\vec{m}$. The magnetic potential $\phi_j(\vec{r})$ at a position $\vec{r}$ due to the magnetic moment $\vec{m}_j$ is given by

$$\phi_j(\vec{r}) = \frac{\mu_0}{4\pi}\frac{\vec{m}_j \cdot \hat{\vec{r}}}{r^2} \tag{1.12}$$

where $\mu_0 = 4\pi \times 10^{-7} Tm/A$ is the permeability of free space, and $\hat{\vec{r}} \equiv \vec{r}/|\vec{r}|$ assuming that $|\vec{r}| = r$ is much larger than the size of the magnet. The magnetic flux of the dipole is then given by

$$\vec{B}_j = -\nabla\,\phi_j \tag{1.13}$$

and the magnetic potential energy U_{ij} acquired by a second dipole $\vec{m}_i$ placed in the field of $\vec{m}_j$ is given by

$$U_{ij} = -\vec{m}_i \cdot \vec{B}_j. \tag{1.14}$$

Then, the force between the two dipoles is found by differentiating (6.5) with respect to $\vec{r}$.

$$\vec{F}_{ij} = (\vec{m}_i \cdot \nabla)\vec{B}_j \tag{1.15}$$

$$\vec{\tau}_{ij} = \vec{m}_i \times \vec{B}_j \tag{1.16}$$

We can determine the total potential energy of the system as

$$U_{total} = \frac{1}{2} \sum_{i,j\ i \neq j} U_{ij}. \tag{1.17}$$

The interaction force can not be limited to these two, but also such as fluid force (e.g. capillary force), which is not listed here. The scalability of physical interaction mechanisms – especially electrostatic and magnetic – are well examined in [2, 22]. Especially at the micro scale, magnetic force shows favorable scalability, behaving dominantly than other physical entities, such as electrostatic force or van der Waals force.

⇒ Prerequisite VII: employ magnetism

Collisions and Slides

The long range interaction described above is identical, regardless of the shape of components. However, the short range interaction – collision – is dominated by shape. The effect of collision in the context of self-assembly has not yet gathered so much attention. This is because collisions are not considered as main driving force in assembly, but rather a resistance factor. In our experience, the effect of morphology appears when components slide their relative positions and change their places. The issue contains some other factors, which may act an important role in molecular systems, such as a molecular diffusion driven by collisions.

1.5 Motivation

Engineering challenges

There has been a growing demand for the design of small artificial structures capable of performing useful tasks. For modular systems smaller than a few cm, there are three fundamental problems that still await a solution. These problems relate to actuator, battery (or power in general), and connector technology. When designing systems where a high quantity of components of small size is desired, solutions for these problems are of particular relevance. First, actuation endows the parts with the ability to move and re-configure. The second problem is concerned with providing power to the actuator(s). A typical solution is to use batteries. Batteries, however, are problematic, because they are only able to provide power for a limited amount of time. The third problem is the connection mechanism enabling the modular parts to realize sufficient degree of freedoms, by docking each other. Binding is crucial for reorganization and for a desired structure to hold. There is a strong interdependency between these issues. The requirements of the connection mechanism as well as the actuator are partly determined by the weight of each component. The heavier the components are, the more force needs to be applied to the binding location. In addition, the actuators have to apply larger torques to displace the components. The use of more powerful components in general leads to even heavier components. Also, the power consumption increases as a result of stronger connection mechanisms and actuators. Surprisingly, small size and weight reduction of modular parts is not a good way to solve this problem, because not only does the power/weight

ratio of the most common actuators decrease with a reduction in size, but so does the strength/weight ratio of common connectors. This implies that the most common ways of actuating, powering and connecting modular robots cannot be applied to small-sized entities. It follows that novel solutions to the *ABC bottlenecks* are necessary in order to make progress in small-scale self-assembly robotics.

Lack of focus on morphology

Figure 1.16 shows the scope of research in (a) engineering and (b) biology, depending on the different scale of their objectives (cited from [115]). It is

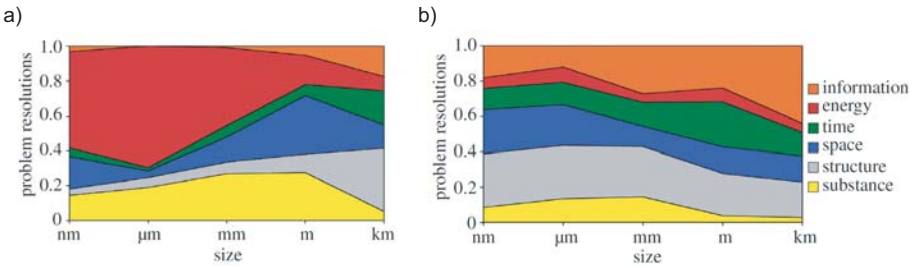

Figure 1.16: Scope of research in (a) engineering and (b) science depending on different scale lengths (cited from [115]).

noteworthy that, in engineering research from the *um* to the *cm* scale, most research focuses on energy, while, in scientific research, it is also devoted to structures. Unlike studies in biology, engineering deals with the entire structure on the material basis in good measure, which therefore enables to withdraw the energy states of their objectives. On the other hand, the difficulty in handling morphology ("structure" in the figure) in engineering remains the issue as a challenging work.

1.5.1 Objective and Prerequisites

The objective of this thesis is to investigate, from the technical viewpoint, the potential for developing self-assembly systems that are applicable to different scales. Using a novel architecture for artificial self-assembly systems, we examine the levels of autonomy within components with respect to performance achieved with each model. With regard to the components, we focus on morphology with the belief that it is the key to understanding the phenomena. In addition to the engineering aspect, another interest is the understanding of living systems in the abstract. With a closer examination of what constitutes life, premature functions of animated entities could be observed by means of molecular self-assembly[15]. To our knowledge, there have been few attempts to explore those perspectives.

Considering prerequisites I to VII (Figure 1.17), we manifest the following three prerequisites as the main objectives for designing modular architectures.

[15] A good example of successful productions of predefined complex structures can be seen in the region separating life from non-life, where one could observe premature functions of desired animated entities by means of molecular self-assembly.

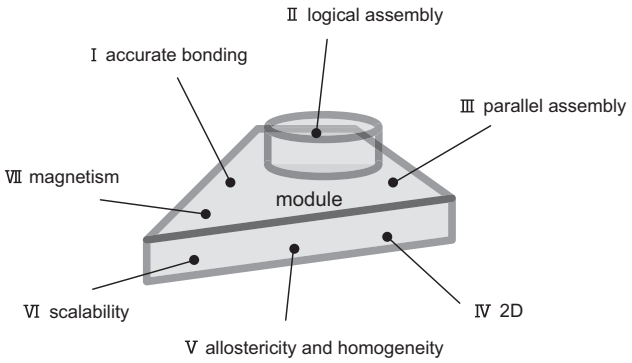

Figure 1.17: Prerequisites for designing modular architectures.

1. **The system should be distributed in a stochastic environment.** Once a set of experimental conditions is invoked, components are expected to act in parallel, following local causal rules imposed by the environment.
2. **The components should be sufficient to attain logical assembly.** The assembly sequence is intrinsically ordered by the components.
3. **The component architecture should be scalable.** The component design should be simple and scalable in order to minimize the inertial effect and exploit the environmental (thermal) agitation.

1.6 Overview of the thesis

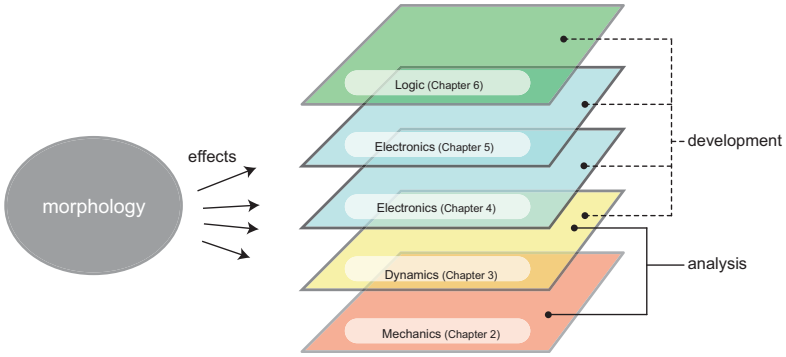

Figure 1.18: Overview of the thesis. Chapter 2, 3, and Appendix E are focusing on analysis, while Chapter 3, 4, 5, and 6 are on development. The effect of morphology are discussed in all the Chapters.

Chapter 2 of this thesis is focused on the mechanical aspects of self-assembly by using *cm*-sized magnetized floating tiles. By observing the processes that cause floating tiles to form a structure, we examine how the difference of tiles' shape induces different aggregation patterns.

Chapter 3 is focused on the dynamics of self-assembly. We advance the floating tiles to self-propulsive modules and discuss the dynamics of the acting modules and how they affect the yield of targeted compounds. The model shown in this chapter is the basis of what is used in subsequent chapters.

Chapter 4 is an introduction of electronically extended platforms, which feature Hall-effect sensors. The work shown here was carried out as an attempt to seek the possibilities of technical advancements of our system with conventional methods.

Chapter 5 is a description of a new connection method for a gate to logical self-assembly. Instead of mechanical or electromagnetical approaches, we assigned thermal means, that is, using Peltier elements that induce adhesion force between two modules by freezing the media (water) in between. The strong bonding force and various advantages are verified.

In Chapter 6, to summarize the ideas presented in the thesis, we describe the design of magnetic enzymes that can perform cascade conformation changes that opens up a new possibility for logical self-assembly.

Chapter 7 is a discussion of various concerns that are examined in this thesis. We mainly examine the role of the morphology of components with respect to the level of autonomy of the performed systems. Deriving the prerequisites proposed in Chapter 1, the summaries are presented. Finally, all of the parts are examined in the conclusion.

Some highly relevant materials are cited in the Appendices.

Chapter 2

How Components' Shape Influences the Assembly

Passive model

Self-assembly is a key phenomenon whereby vast numbers of individual components passively interact and form organized structures, as can be seen, for example, in the morphogenesis of a virus. Abstractly speaking, the process can be viewed as a spatial placement of attractive and repulsive components. In this paper, we report on an investigation of how morphology, i.e. the shape of components, affects a self-assembly process. The experiments were conducted with 3 differently shaped floating tiles equipped with magnets in an agitated water tank. We propose a novel measure, which qualifies the degree of parallelism of the assembly process. The results showed that the assembly processes were affected by the aggregation sequence in their early stages, where shape induces different behaviors and thus results in variations in aggregation speeds.

keywords
passive tile self-assembly; degree of parallelism; morphology; distributed system.

[1]Parts of the material in this chapter previously appeared in; S. Miyashita, Z. Nagy, B. J. Nelson and R. Pfeifer (2009) "The Influence of Shape on Parallel Self-Assembly", *Entropy*, Vol. 11(4), pp. 643-666.

2.1 Related Work

There have numerous attempts undertaken in various fields. A pioneering approach was taken by Penrose about 50 years ago [87]. He developed a mechanical self-replication model, which operated in a stochastic manner. Aggregation patterns of passive self-assembly were raised into prominence and employed by Hosokawa *et al.* [46, 47]. He examined the effect of *active* elements on the aggregation. Whitesides and his group investigated many self-assembling and self-organizing phenomena at different scales [15, 40–42] and categorized them into static, dynamic, templated, and biological self-assemblies, depending on the energy dissipation. Seminal ideas about conformational switching were proposed by Saitou [94]. He proposed a *reactive* mechanism for 1D self-assembly and assessed the functionality with kinetic rate equations. The units he designed feature mechanical internal states, such that the units react differently to their inputs, whereas the system is purely passive with respect to physical causation.

By mimicking tools and methods from nature, many advances have been made in utilizing self-assembly for the fabrication of structures at molecular scales [61, 92, 100, 101, 123, 129]. An important fact to stress here is that the models are grounded in real entities; thus they provide us with effective ideas. Also, the capacity level of the number of components that can be treated in each experiment is a certain advantage. Concerns that we have to confront include the difficulty of controllability, that is, the lack of a capability to directly adjust the level of activity.

To date, few stochastic self-assembling robots have been developed in the field of modular robotics (White *et al.* [119, 120]; Shimizu *et al.* [102]; Bishop *et al.* [8]; Griffith *et al.* [38]; Nagy *et al.* [80]; Miyashita *et al.* [66, 69]). In contrast to the advantage of such an approach - the possibility of its controllability - technological constraints such as heavy and big motors or large power consumption prevent the systems from being highly functional. Also, a certain amount of state-based control is required for the assembly process, which results in systems less suited to their complex environments.

In this paper, we use a simple yet effective model for the analysis of self-assembly — tiles with magnets in a stochastic environment — and examine the aggregation patterns as a function of the shapes of tiles. We characterize the diverse figures of molecules by the combination of shapes and magnetic forces. Besides we introduce a novel notion, the *Degree of parallelism* (DOP) as a measure of self-assembly and experimentally confirm its validity.

The paper is organized as follows. In Section 2.2, we describe the tiles and the experimental setup. Then, in Section 2.3, we describe the interaction mechanism, in particular the magnetic interaction, and introduce measures to quantify the self-assembly process. In Section 2.4, we present experimental results and a detailed analysis. This is followed by a discussion in Section 2.5 and Section 2.6 concludes the paper.

2.2 The Experimental Self-Assembly Platform

In order to evaluate the role of morphology in the self-assembly process, we constructed an experimental platform, which consisted of floating tiles equipped

with magnets, and a water tank with two vibrators (4 Hz, 6.5 V, 0.5 A) that induced turbulence on the water surface and thus provided randomness (Figure 2.1 b, total weight:1.3kg). We developed tiles with three different shapes (Figure 2.1 a): circles, squares, and squares with rounded corners. They were of identical weight ($0.2g$), surface area ($484mm^2$) and thickness ($2mm$). These shapes were selected after noting that a change in one variable coding the morphology, e.g. surface area, tended to affect the other dependent variables, e.g. diameter, shortest distance between edges and magnets. On each tile, one or

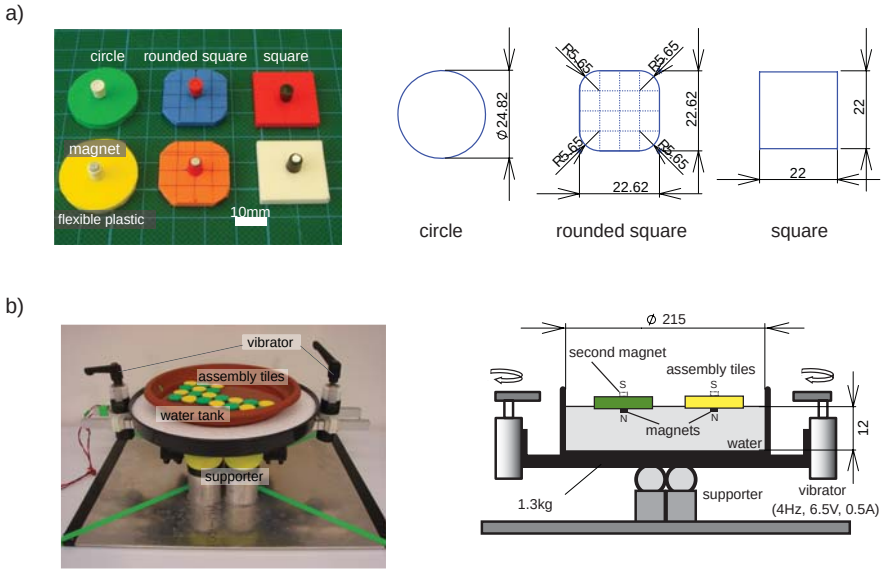

Figure 2.1: The experimental setup (unit: mm). a) 3 different tiles. b) Agitated water tank. Stirring the water generated random, fluctuating forces, providing the system with the energy necessary for assembly.

two (for the double magnet type) vertically oriented magnets were attached. The double magnet type was constructed to investigate the effects of magnetic strength (as depicted in Figure 2.1 b right, "second magnet"). On the water, a floating tile whose magnet pointed upwards attracted the other type whose magnet pointed downwards, whereas tiles with the same type of magnets repelled each other. Colors were introduced to distinguish between attracting and repelling tiles and to facilitate visual inspection of the self-assembly progress. For example, the magnet on the green circular tile in Figure 2.1 a is oriented opposed to the magnet on the yellow circular tile.

Exploiting these characteristics, we examined how such multiple tiles formed a structure through the interactions. For each trial, we initialized the positions of the tiles. Using a spacer, 10 tiles of the same color were placed in one side of the tank, and 10 tiles of the other color were placed at the opposite side. Then, the spacer was removed and the vibrators were turned on to agitate the water surface. Now the tiles with similarly oriented magnets (or of the same color) would repel, while opposing magnets (of different colors) would attract and thereby form a lattice structure. We defined the goal configuration as a single lattice formation, in which more than 90 % of the tiles touched opposing

tiles. The magnitude of the agitation was set such that it induced sufficient mobility in the tiles but also such that no two tiles overlapped on the water.

2.3 Interaction Mechanisms and Measures of the System

Long range interactions between two tiles are independent of their shapes and consist of the force between the magnets on the tiles. Because the magnets are oriented in parallel, there is no magnetic torque between the magnets. We consider the magnets as dipoles with a magnetic moment $\boldsymbol{m}$.

2.3.1 Magnetic potential energy

The magnetic potential $\phi_j(\boldsymbol{r})$ at a position $\boldsymbol{r}$ from the magnetic moment $\boldsymbol{m}_j$ is given by

$$\phi_j(\boldsymbol{r}) = \frac{\mu_0}{4\pi}\frac{\boldsymbol{m}_j \cdot \hat{\boldsymbol{r}}}{r^2} \tag{2.1}$$

where $\mu_0 = 4\pi \times 10^{-7} Tm/A$ is the permeability of free space, and $\hat{\boldsymbol{r}} \equiv \boldsymbol{r}/|\boldsymbol{r}|$ assuming that $|\boldsymbol{r}| = r$ is much larger than the size of the magnet. The magnetic flux of the dipole is then found as

$$\boldsymbol{B}_j = -\nabla\, \phi_j \tag{2.2}$$

and the magnetic potential energy U_{ij} acquired by a second dipole $\boldsymbol{m}_i$ placed in the field of $\boldsymbol{m}_j$ is given by

$$U_{ij} = -\boldsymbol{m}_i \cdot \boldsymbol{B}_j. \tag{2.3}$$

Then, the force between the two dipoles is found by differentiating (6.5) with respect to $\boldsymbol{r}$.

Since in our case the magnets are identical, we have $|m_i| = |m_j| = m$, and because they are parallel, the energy and the force expressions simplify to:

$$U_{ij} = -\frac{\mu_0}{4\pi}\frac{m^2}{r_{ij}^3} \tag{2.4}$$

$$F_{ij} = -\frac{dU_{ij}}{dr} = \frac{3\mu_0}{4\pi}\frac{m^2}{r_{ij}^4}, \tag{2.5}$$

and we can determine the total potential energy of the system as

$$U_{total} = \frac{1}{2}\sum_{i,j\ i\neq j}\{-\sigma_{ij}\ \frac{\mu_0}{4\pi}\frac{m^2}{r_{ij}^3}\}, \qquad \sigma_{ij} = \frac{\boldsymbol{m_i}\cdot\boldsymbol{m}_j}{|\boldsymbol{m}_i||\boldsymbol{m}_j|}. \tag{2.6}$$

Finally, we normalize the energy as $U'_{total} \equiv U_{total}/(\frac{\mu_0}{4\pi}m^2)$. Note that normalizing by this positive number, will make the self-assembly system tend towards a maximum of U'_{total} instead of a minimum.

The long range interaction described above is identical for each type of tile, independently of its shape, because identical magnets were used. Also, because the size of the tiles is comparable, so is their inertia, and consequently their dynamic behavior. However, the short range interaction, i.e. the final alignment, is dominated by shape and this was experimentally investigated.

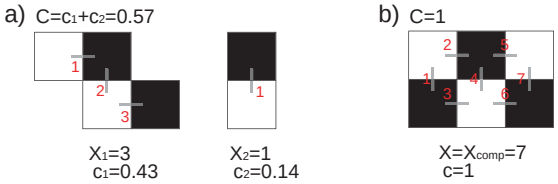

Figure 2.2: Example of clustering degrees where $X_{comp} = 7$. a) configuration with two clusters where $x_1 = 3$ (left) and $x_2 = 1$ (right). b) configuration with $x = X_{comp} = 7$. The two local clustering degrees are $c_1 = \frac{3}{7} = 0.43$ (left) and $c_2 = \frac{1}{7} = 0.14$ (right) in (a), while $C = c = \frac{7}{7} = 1$ in (b).

2.3.2 Degree of parallelism (DOP)

In self-assembly processes, a cluster consists of different components. In addition, components often exhibit different characters and behave differently by linking up together: e.g. proteins open/close their bonding sites flexibly. Systems that contain such multi-states have to be considered together with their initial conditions or physical boundaries, which makes an analytical derivation difficult.

For an answer, one useful insight can be derived from network theory. The idea is to focus only on connections between components (neglecting the identity of each component), and acquiring information about the compounds. To measure the geometrical connections of the tiles, we define the clustering degree. Let c_i be the clustering degree of a cluster i. We refer to it as a local clustering degree and define it as:

$$c_i = \frac{\text{number of connections within the } i\text{-th cluster}}{\text{number of connections within the complete configuration}} \equiv \frac{x_i}{X_{comp}} \quad (2.7)$$

X denotes the total number of connections in the system ($X \equiv \sum_i x_i$). We defined the global clustering degree C as the sum of the local clustering degrees ($C \equiv \sum_i c_i$).

Figure 3.13 shows examples of clustering degrees with 6 tiles ($X_{comp} = 7$). The two local clustering degrees are $c_1 = \frac{3}{7} = 0.43$ (left) and $c_2 = \frac{1}{7} = 0.14$ (right) in (a), while $C = c = \frac{7}{7} = 1$ in (b). Note that by defining X_{comp} we focus only on the "targeted" connections between the tiles, that can be recognized in the complete configuration. The concept can be extended and applied to assembly processes in general. In particular, in our experiments with 20 tiles, we assumed that the complete configuration was a lattice structure that was an alignment of 4×5 layers of tiles and had $X_{comp} = 31$.

Entropy is the common term to express the level of disorder, which is applied in information theory and thermal physics. Adleman [3] described the information-theoretic entropy of a discrete random variable that draws its values from a countable universe. Similar to the entropy concept, we defined the *degree of parallelism* (DOP) H as a function of the local clustering degrees (c_i), and taking a value between 0 to 1, namely:

$$H = -\sum_{i=1}^{N} c_i \ln c_i. \quad (2.8)$$

As an illustration of the DOP, consider the situation with an assembly of six tiles, depicted in Figure 3.14. In the figure, we classify and depict different

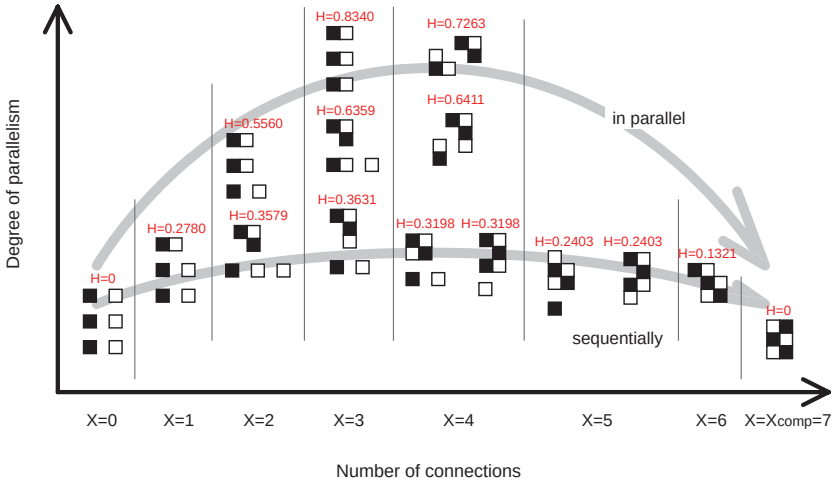

Figure 2.3: Example of the proposed *degree of parallelism* H where $X_{comp} = 7$. It shows the tendency that the more assembly proceeds in parallel, the larger the value becomes.

configurational clusters, according to the number of total connections X. We show each possibility among similar topological clusters, and align considering the number of formed clusters. The figure tells that as X increases, the DOP H increases, attaining a maximum for $X = 3$ or $X = 4$, and then decreasing to 0 for $X = Xcomp = 7$. Also, in each column (that is, within a group having the same number of connections), the more equally clustered, the higher the DOP. In other words, high values are derived from states in which the connections are equally distributed.

Suppose that there exist a number N of clusters. From Shannon's lemma, it follows that the value H becomes a maximum when N clusters are equally formed, namely;

$$\begin{aligned} H(X) &= -\sum_{i=1}^{N} c_i \ln c_i \\ &\leq -\sum_{i=1}^{N} \{\frac{X}{X_{comp}} \cdot \frac{1}{N}\} \ln\{\frac{X}{X_{comp}} \cdot \frac{1}{N}\} \\ &= -\frac{X}{X_{comp}} \ln\{\frac{X}{X_{comp}} \cdot \frac{1}{N}\} \end{aligned} \tag{2.9}$$

The upper limit in Eq. (3.23), i.e. the maximal value for H, is obtained when $c_i = \{\frac{X}{X_{comp}} \cdot \frac{1}{N}\}$ for $\forall i$, that is, when there are equal numbers of clusters of the same size. This characteristic can be extended to general assembly processes, irrespective of the number of tiles or clusters.

2.4 The Experimental Results

We carried out 15 iterative trials for each of 4 different combinations; square tiles and square tiles ($\mathcal{S}\cdot$ hereafter, $\cdot$ is either $\mathbf{s}$: with a single magnet or $\mathbf{d}$: with double magnets), circle tiles and circle tiles ($\mathcal{C}\cdot$), rounded-square tiles and rounded-square tiles ($\mathcal{R}\cdot$), and square tiles and circle tiles ($\mathcal{M}\cdot$).

2.4.1 Assembly completion time

The assembly completion time (completion of over 80% in (a) and 90% in (b)) of all trials are displayed in Figure 2.4 as a box plot. All the measured data are listed in the Appendix. The boxes on the left side of each column show assembly completion times for single magnet tiles, and on the right side show the times for double magnet tiles. We show the lower quartile (Q1), median (Q2), upper quartile (Q3), and the average of each combination in Table 2.1. The trials for which we did not observe convergence in a certain amount of time (>300s), are included as 300s (2 trials in $\mathcal{S}_\mathbf{s}$ 80% completion, 5 trials in $\mathcal{S}_\mathbf{d}$ 90% completion, 1 trial in each of $\mathcal{R}_\mathbf{d}$ 90% and $\mathcal{M}_\mathbf{d}$ 90% completion).

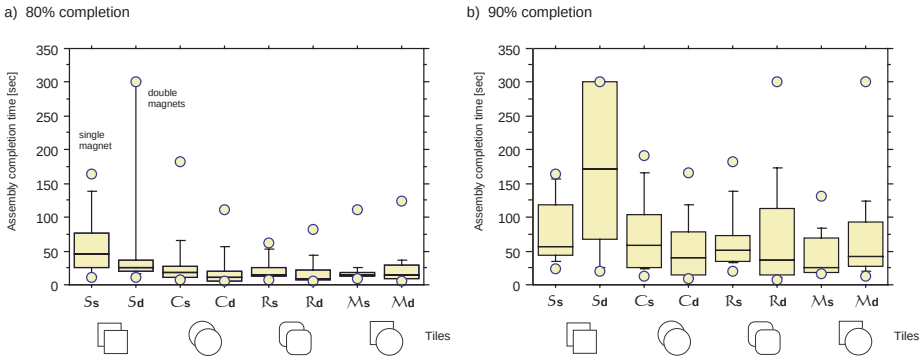

Figure 2.4: Comparison of assembly completion times. a) more than 80% completion. b) more than 90% completion. ($\mathcal{S}$: square, $\mathcal{C}$: circle, $\mathcal{R}$: rounded-square, $\mathcal{M}$: mixed). The boxes on the left side of each column show the assembly completion times for single magnet tiles, and on the right side show the times for double magnet tiles.

Comparison between different shapes

Regarding the difference in assembly speed from the perspective of the shapes, it is seen that on average, square tiles took the longest time to aggregate compared to the other shaped tiles. However, it should be noted that the shortest completion time of $\mathcal{S}_\mathbf{s}$ and $\mathcal{S}_\mathbf{d}$ were as fast as for the other conditions. This is because the minimum distance between the magnets of two connecting tiles was the shortest among all the combinations. Considering the changes in the magnetic attractive force, which is inversely proportional to the distance with a power of 4 (Eq. 6.7), small differences were dominant and induced strong attractive forces. As a factor which hindered the aggregation speed in $\mathcal{S}_\mathbf{d}$, we observed that frequently the connected tiles were aligned linearly and so prevented other tiles from connecting (*magnetic shielding effect*, see Figure 2.5 and Section 2.5). Once an isolated tile was surrounded by other similarly magnetized

Table 2.1: The lower quartile Q1, median, upper quartile Q3, and the averages of 80% and 90% completion level over all of the trials (unit:sec).

	$\mathcal{S}_\mathbf{s}$			$\mathcal{S}_\mathbf{d}$		
	80%	90%	increase rate	80%	90%	increase rate
Q1	26	43		19	69	
median	45	56		26	172	
Q3	83	129		38	300	
average[1]	56.5	76.6	136%	>68.5	>184.2	>269%
	$\mathcal{C}_\mathbf{s}$			$\mathcal{C}_\mathbf{d}$		
	80%	90%	increase rate	80%	90%	increase rate
Q1	10	26		6	13	
median	18	59		10	41	
Q3	29	105		22	80	
average	31.2	71.0	228%	20.9	54.2	259%
	$\mathcal{R}_\mathbf{s}$			$\mathcal{R}_\mathbf{d}$		
	80%	90%	increase rate	80%	90%	increase rate
Q1	12	33		5	14	
median	15	51		9	37	
Q3	26	76		19	117	
average[1]	21.5	67.8	315%	18.3	>71.0	>394%
	$\mathcal{M}_\mathbf{s}$			$\mathcal{M}_\mathbf{d}$		
	80%	90%	increase rate	80%	90%	increase rate
Q1	12	17		7	25	
median	15	26		13	42	
Q3	18	77		33	96	
average[1]	21.5	42.7	199%	23.8	>71.4	>300%

[1] The trials for which we did not observe convergence in a certain amount of time (>300s), are included as 300s (2 trials in $\mathcal{S}_\mathbf{s}$ 80% completion, 5 trials in $\mathcal{S}_\mathbf{d}$ 90% completion, 1 trial in each of $\mathcal{R}_\mathbf{d}$ 90% and $\mathcal{M}_\mathbf{d}$ 90% completion). All the measured data are listed in the Appendix.

tiles connecting each other, the single tile was trapped in the local region and difficult to transfer to a suitable position. This made it difficult for the system to converge and was the main source of such diverse variances. As for the other cases, $\mathcal{C}$, $\mathcal{R}$, and $\mathcal{M}$ showed better assembly than $\mathcal{S}$. $\mathcal{R}$ showed a slightly better assembly capability in speed compared to $\mathcal{C}$ ($\mathcal{C}_\mathbf{s}$ 80% vs. $\mathcal{R}_\mathbf{s}$ 80%, $\mathcal{C}_\mathbf{s}$ 90% vs. $\mathcal{R}_\mathbf{s}$ 90%, and $\mathcal{C}_\mathbf{d}$ 80% vs. $\mathcal{R}_\mathbf{d}$ 80%). Here we also saw the effect of the shortest distance between two magnets. $\mathcal{M}$ also showed good assembly speed, mainly due to rotational movement which facilitated reconfiguration in the local region.

Comparison between differently magnetized tiles

We observed two prominent tendencies when comparing conditions with/without a second magnet. Firstly, square tiles with second magnets had an increased assembly completion time, while in the other cases, we saw reductions in their assembly completion time. Secondly, the comparison of percentage rises between 80% completion and 90% completion in Table 2.1 indicates the difficulty

of the last stages' assembly in each combination, where we observed the big rises in $\mathcal{R}_{\mathbf{d}}$ and $\mathcal{R}_{\mathbf{s}}$. Taking these two outcomes into account, we can conclude that square tiles and rounded-square tiles had stricter optimal magnetized levels in their assemblies. This originated in the differences in the characteristics of the dynamics; namely, due to the shape and the strong force between two magnets, an alignment of square tiles and rounded-square tiles prevent flexible bends and connection sites. Another noticeable characteristic is that while $\mathcal{R}$ didn't change the speed so much along with an increase in magnetic force, $\mathcal{M}$ decreased the speed. We think that this is because, whereas rounded-square tiles are able to rotate around neighboring tiles and change their relative positions, a mixed combination with square tiles prohibits this movement and acts as a restriction with a stronger magnetic force.

2.4.2 The formed structures

In this section, we evaluate the formed structures of each assembly that is shown in Figure 2.5. We selected the fastest 10 aggregations out of 15 trials in each combination in order to keep the distributions of the population the same. From top to bottom, the four different combinations are listed and, in each combination, the upper row depicts the case with one magnet and the lower row depicts the double magnet case. In each row, trials are sorted with respect to the increase in assembly completion time.

In Figure 2.6, we plotted the DOP of all final configurations versus the time they took to complete. Considering the wide time range that square tiles took to reach a complete assembly, we displayed the other combinations in small windows, whose corresponding area is shown as a dotted square. An increase of DOP was observed for $\mathcal{C}$ and a decrease was observed for $\mathcal{S}$. This suggests that the combination of circular shape with a strong interaction force works not only to accelerate the aggregation speed but also works to achieve a dense structure. Changes were rarely observed with $\mathcal{R}$ and $\mathcal{M}$. The addition of a magnet has several meanings depending on the perspective that is described. In this work, adding a magnet corresponds not only to enhancing the attractive forces among the tiles, which was considered to relatively decay the effect of morphology of the shapes, but also to enhance the effect of shape especially once they connect. That is, it positively influences both the long range interaction due to magnetic forces and the short range interaction through the local shapes.

In some trials, we observed that tiles created gaps within the cluster, such as we can see in Figure 2.5 $\mathcal{C}_{\mathbf{d}}15$, $\mathcal{R}_{\mathbf{d}}11$, and $\mathcal{M}_{\mathbf{s}}9$. Unlikely to converge into a pure lattice cluster, they frequently created a hall ($\mathcal{S}_{\mathbf{s}}2$, $\mathcal{S}_{\mathbf{d}}19$), or a small gap ($\mathcal{R}_{\mathbf{s}}8$, $\mathcal{M}_{\mathbf{s}}10$). We quantified this tendency by comparing clusters' surface areas with their perimeters. Note here that the surface area means the entire area inside the cluster, including the gaps. We visually processed the image with Matlab, neglecting stand alone tiles and measured the surface area and the perimeter simply by counting the number of corresponding pixels (Figure 2.7).

In Figure 2.8, we display perimeters of $\mathcal{S}$ and $\mathcal{C}$ in (a), and $\mathcal{R}$ and $\mathcal{M}$ in (b) compared with the surface areas. Both variables are normalized by the mean values over all combinations and represented as percentages. In general, the further right along the x-axis, the more branched configurations were observed, and the further left, the more rounded were the configurations. The further up the y-axis, the more gaps are observed. We surmised that the normalized

populations followed Gaussian distributions and calculated the correlations of each combination. A large negative correlation was observed for $\mathcal{C}$ (-0.573), and a moderate negative correlation was observed in $\mathcal{R}$ (-0.322). Linearly fitted curves of $\mathcal{C}$ and $\mathcal{R}$ are shown in the figures as dotted lines. Almost no correlation could be seen in $\mathcal{S} = -0.021$ and $\mathcal{M} - 0.036$.

These two fitting lines clearly show reductions in the values of $\mathcal{C}$ and $\mathcal{R}$. This suggests that gaps remained for $\mathcal{C}$ and $\mathcal{R}$ as they formed relatively rounded clusters, whereas in the case of $\mathcal{S}$ and $\mathcal{M}$, gaps were rarely created between tiles, as we see in Figure 2.8. This is due largely to the characteristics of square tiles.

Figure 2.5: The formed structures of each assembly of the four different combinations. In each combination, the upper row depicts the case with one magnet and the lower row depicts the double magnet case. The trials are sorted with respect to the increase in assembly completion time. Tiles trapped by the *magnetic shielding effect* are marked with dotted circles.

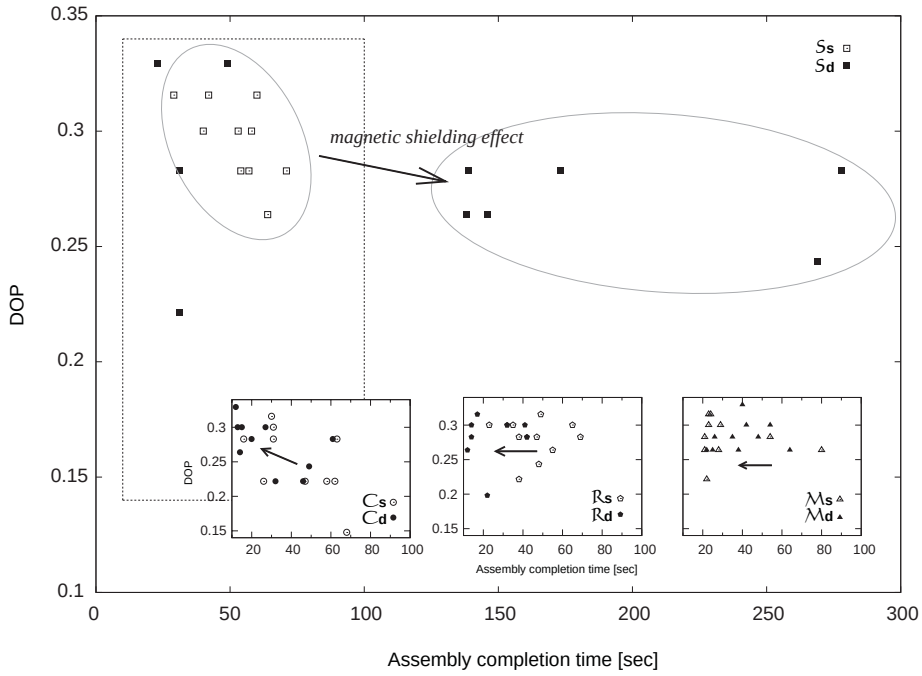

Figure 2.6: Comparison of DOP against the assembly completion time. Considering the wide time range that square tiles took to complete, we displayed the other combinations in small windows, whose corresponding area is shown as a dotted square.

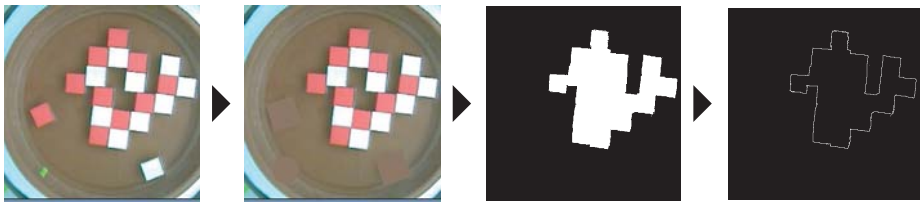

Figure 2.7: Image processing for the measurement of surface areas and perimeters of clusters. Note here the surface area means the entire area inside the cluster including the gaps.

The sharp corners induced a big difference in magnetic force, forcing a strong constraint on the next tiles. For the case of $\mathcal{R}$, they sometimes formed with a 45 degrees rotated formation, resulting in the outcome above.

2.4.3 Time evolution

In Figure 2.9, we selected one of the representative aggregations in which more than 95% of tiles were aggregated from each combination and displayed (the respective final configurations can be seen in Figure 2.5 $\mathcal{S}_{\mathbf{d}}13$, $\mathcal{C}_{\mathbf{d}}16$, $\mathcal{R}_{\mathbf{d}}15$, and $\mathcal{M}_{\mathbf{d}}11$). For each case of the raw data, we present the time sequence of trials listed from the left top to the right bottom (with an illustration of the most discriminative movement of the set on the left side). On the right side, we show

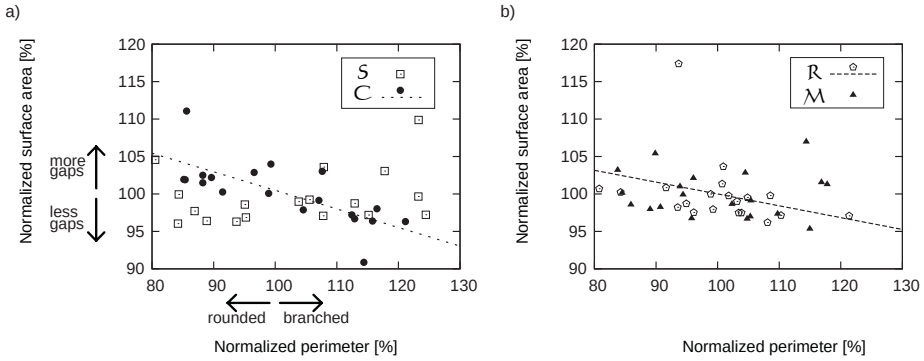

Figure 2.8: Comparison of surface areas against perimeters. Both variables are normalized and represented as percentages from mean values. A large negative correlation was observed in $\mathcal{C}$ (-0.573), and a moderate negative correlation was observed in $\mathcal{R}$ (-0.322). Linearly fitted curves of $\mathcal{C}$ and $\mathcal{R}$ are shown in the figures.

the transitions of the magnetic potential energy and the clustering degrees. We discuss each case individually:

- $\mathcal{S}_\mathbf{d}$**:** After the spacer was removed, the tiles moved randomly by changing their relative positions (1-3). The increase in potential energy and the clustering degrees can be seen in the right figure. Once two tiles were attached (often adjusting their relative positions by sliding), the relatively strong connection force kept the connection tight (2, 7). Note that this results in a large value of the potential energy. This caused the tiles to stay in the same configuration, that is to say, reconfiguration was made more difficult (e.g. 8). As a result, the system produced an irregular shape (8). In this transition, the tiles first formed two small clusters (3-6) and subsequently they bonded together (7). It is worth noting that this large scale docking did not cause a big stored energy jump as expected (reflected in the right figure). This suggests that a major dominance of the energy is induced by locally connecting two tiles but among tiles that are apart. In addition to that, we observed that a white tile highlighted with a dotted circle was assisted to attach to the cluster by a red tile in the transformation from (3) to (5) (*magnetic shielding effect*, see Section 2.5).

- $\mathcal{C}_\mathbf{d}$**:** In the beginning, several small groups were formed (1-2). The speed of aggregation was fast, whereas connections between two tiles were relatively weak and the tiles changed their relative positions smoothly (3-4 and 6-8). In particular, the transformation highlighted with a dotted circle that can be seen from (7) to (8) is supposed to be rarely observed in the square tile combinations (see Section 2.5). The increase in potential energy is lower than in the case of square tiles, especially since the closest distance between two magnets is greater (recall that we set the surface area of the tiles to be the same). The transition took 22s for 90% aggregation, and took 79s for the further global configuration (7-8).

- $\mathcal{R}_\mathbf{d}$**:** The characteristic of these tiles was that they frequently rotated and changed directions according to the landscape of potential energy (2-

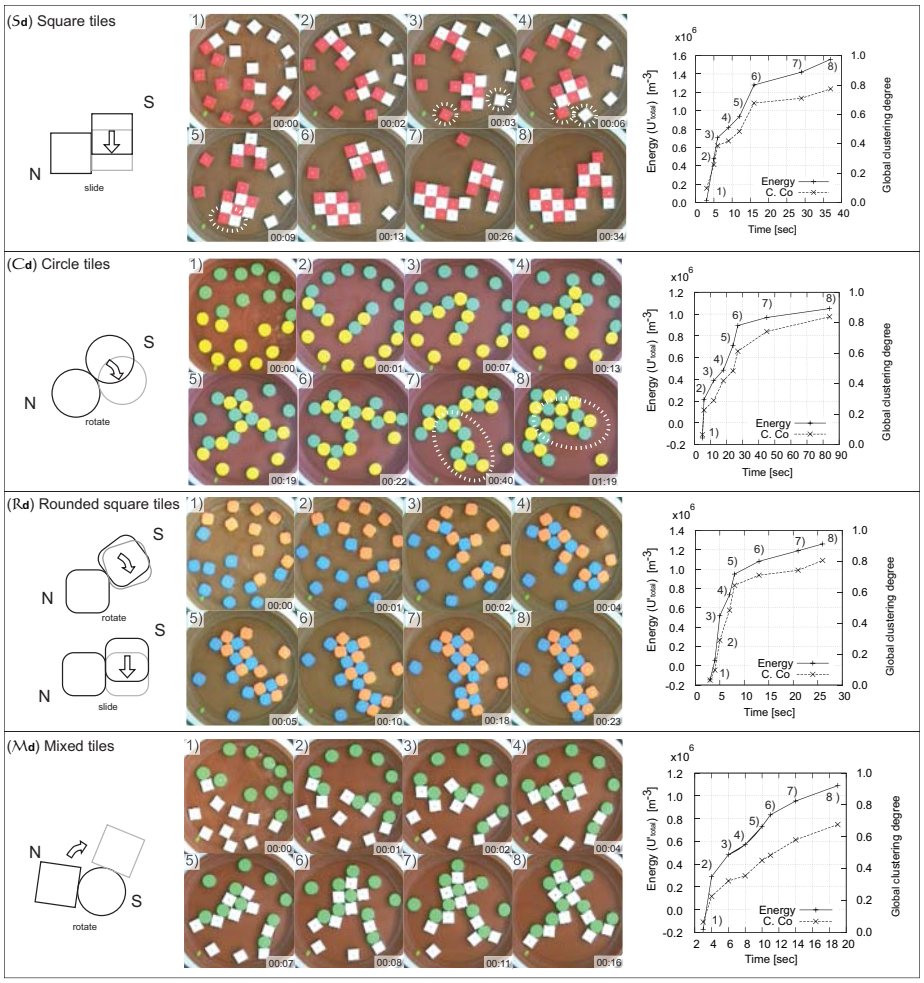

Figure 2.9: Representative aggregations of 4 combinations in which more than 95 % of tiles aggregated. For each case of raw data, we present the time sequence of trials listed from the left top to the right bottom (with an illustration of the most discriminative movement of the set on the left side). On the right side, we show the transitions of the magnetic potential energy and the clustering degrees.

4). These tiles possessed positive characteristics of both square and circle tiles, namely, a flexible reconfigurability and a stable lattice formation. The lattice structure was reached rapidly (23s) and was sufficiently stable to resist agitation (8). The potential energy converged to a value between those for the cases of square tiles and circle tiles (shown on the right).

- $\mathcal{M}_{\mathbf{d}}$**:** This was the only heterogeneous combination in terms of shape. Rotation was also observed. The circle tiles acted as a "hinge", carrying a connected square tile to another position (2-3, 6). Structured lattice regions were stabilized by square tiles fixing the relative positions (8), while due to the flexibility of such combinations, the system often produced branching shapes, which were characterized by lowest clustering degrees

(see Figure 2.5 $\mathcal{M}_\mathbf{d}$).

Figure 2.10 shows the 4 transitions (which are shown in Figure 2.9) of global clustering degrees plotted against (a) magnetic potential energies (U'_{total}), and (b) averaged potential energies (U'_{total}/U'_{comp}). In Figure 2.10 a, a linear in-

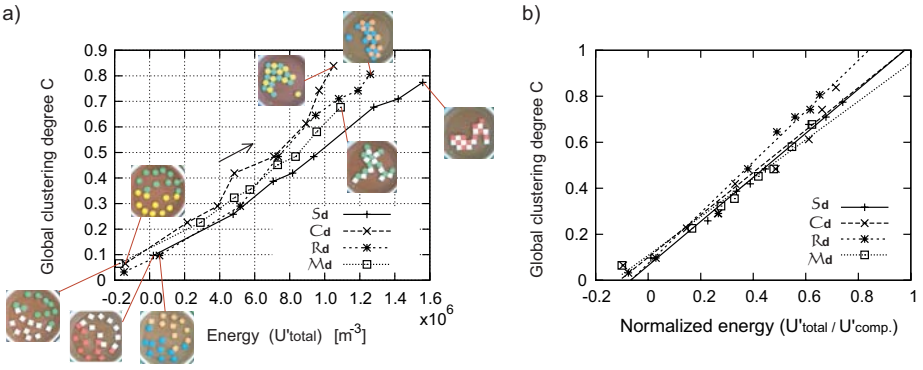

Figure 2.10: Comparisons of the 4 transitions of clustering degrees plotted against (a) potential energy, and (b) normalized potential energy.

crease in global clustering degrees was observed (note that $\mathcal{C}_\mathbf{d}$ took longer time than the others). The linear increase in the number of connections led to an increase in potential energy, showing that the systems were following the terrain of their potential energy to their stable minima. Note that we expect to observe small fluctuations in their energy transitions on the micro scale. Due to the fact that the closest distance between two magnets is the shortest in $\mathcal{S}$ (*shape parameter consistency problem*, see Section 2.5), in that situation the largest value of the potential energy existed among the 4 combinations, irrespective of the branched configuration. The gradient of the transition represents the tendency of potential aggregation; here the steeper gradient represents the efficacy of the tiles with respect to aggregation, in contrast to the potential energy. Therefore, for the circle tiles ($\mathcal{C}_\mathbf{d}$), the clusters sustained a tendency to keep reconfiguring, as further agitation occurred. Here, the square tiles ($\mathcal{S}_\mathbf{d}$) seemed to have less probability for reconfiguration (see Section 2.5 for further discussion). In Figure 2.10 b, linearly fit curves are displayed, along with the plots. Given that the numbers of tiles contained in a cluster were the same, the clustering degree tended to be higher, if the cluster had a rounded shape. The inclinations of each plot are 0.958 ($\mathcal{S}_\mathbf{d}$), 0.922 ($\mathcal{C}_\mathbf{d}$), 1.10 ($\mathcal{R}_\mathbf{d}$), and 0.837 ($\mathcal{M}_\mathbf{d}$), respectively, showing that combinations for $\mathcal{R}$ exhibited good aggregation behavior, whereas this was not the case for $\mathcal{M}$.

Figure 2.11 shows the transitions of DOP, where the x-axis represents the magnetic potential energy normalized by the energy of their complete structures (U'_{total}/U'_{comp}). It can be seen that $\mathcal{C}_\mathbf{d}$ traces out relatively low values representing a rather sequential aggregation. Note that a large decrease in the value for the last transition of $\mathcal{S}_\mathbf{d}$ can be observed, where two large clusters combined and eventually resulted in a configuration of one cluster. Considering that both aggregations achieved a quick assembly (27 s in $\mathcal{C}_\mathbf{d}$ and 34 s in $\mathcal{S}_\mathbf{d}$), it can be observed that $\mathcal{C}$ proceeds to aggregation at a good pace, irrespective of the aggregation sequence, whereas $\mathcal{S}$ is affected by the sequence (we

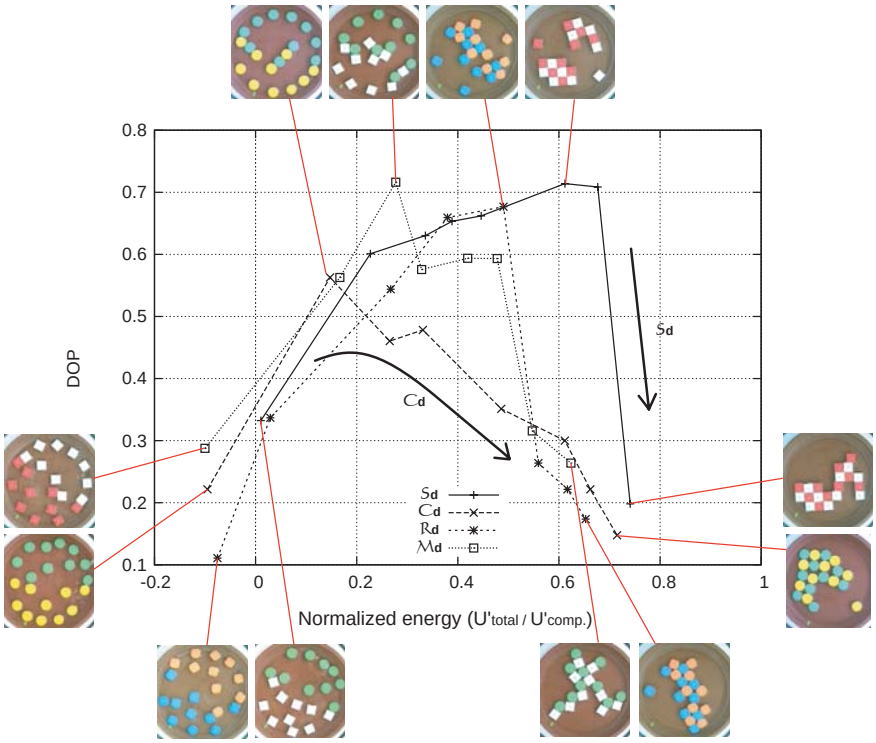

Figure 2.11: Measured clustering degrees and the DOP plotted against normalized energy.

show this tendency in Figure 2.14). The attained points for the 4 transitions tell the complete story of their formed structures, suggesting that the reactions were still in a state of local minima. Although it is natural to consider that an increase of the agitation level is needed to overcome this convergence, such a change often leads to the destruction of some appropriate connections as well. This is known to happen, especially when the formed structure has isometry — different configurations with identical connection topologies [29].

2.5 Discussion

Toward the aim of general self-assembly principles, we discuss two issues that we encountered during the experiments.

2.5.1 Shape parameter consistency problem

This problem arose when we simply tried to compare different shapes in the context of self-assembly; i.e. setting the surface area of different shapes to be the same resulted in a variation in diameters. In other words, this variation can be exploited for the desired behaviors in self-assembly. As a consequence, the magnetic force that a square tile can generate on its neighbor is 1.62 times as large as that of circle tiles. Hence the inducible maximum magnetic force

between two tiles could not be made consistent, and thus variation resulted in their stored potential energies.

2.5.2 Magnetic shielding effect and the influence of shape on self-assembly

The magnetic shielding effect is the effect where the long range magnetic interaction force is effectively canceled by another magnet. This effect was frequently observed with square tiles, which were not flexible with respect to changing their relative positions. This can be illustrated with a simple superposition argument, examining Eq. (4) or (5). For example, the total energy in x-y space can be shown in Figure 2.12 a, where the three aligned tiles expect another tile (marked as A) to attach (we show $-U'_{total}$, for intuitive visualization). Here we see that

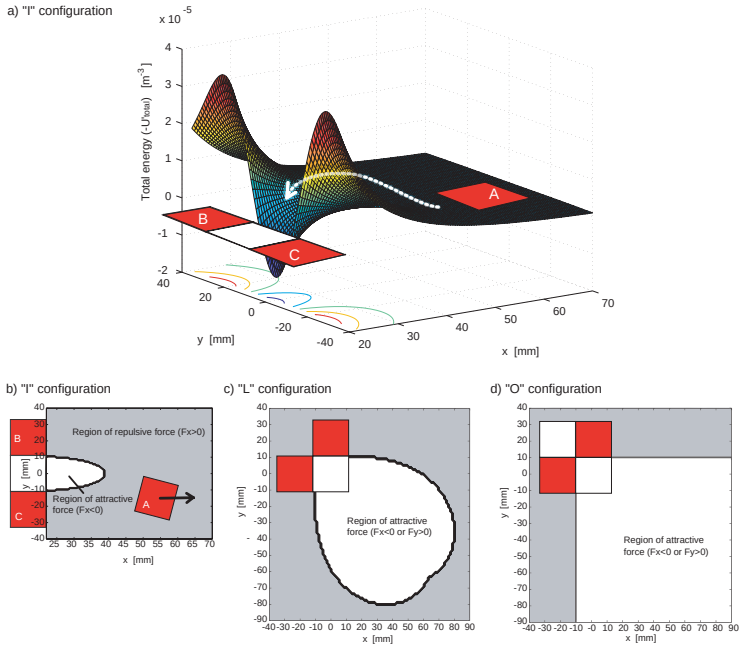

Figure 2.12: *Magnetic shielding effect.* a) The positive energy from two red tiles (B, C) acts as a shield, preventing the red tile (A) from connecting to the white tile. b) The small attractive region is displayed. The tile A is repelled from the cluster in the grey region. c) If the first two attachments are made with an "L" configuration instead of a straight one, a wider attractive region is kept open for the third red tile. d) An additional white tile can expand the attractive region even farther ("O" configuration).

the positive energy from the two red tiles acts as a shield, preventing the red tile (A) from connecting to the white tile. The force exerted on a fourth tile, marked by A, is the sum of the three forces —two repulsive and one attractive— from the three connected tiles. If A is at a sufficiently large distance, the repulsive force acts effectively on A, which makes the attachment of A to the rest of the cluster almost impossible (Figure 2.12 b). The tile A needs turbulence which would enable it to overcome the repulsive force and jump into the attractive region of the cluster. What has to be noticed is that this problem can be avoided

with a different aggregation sequence. Here, if the first two attachments are made in an "L" instead of a straight configuration, a wider attractive region is kept open for the third red tile (Figure 2.12 c). Furthermore, an additional white tile can expand the attractive region even farther (Figure 2.12 d, "O" configuration). Several fundamental issues can be observed in this phenomenon: the existence of appropriate sets of complementary tiles, the potential role of the aggregation pattern, an adequate agitation level, and the necessity of a physical boundary.

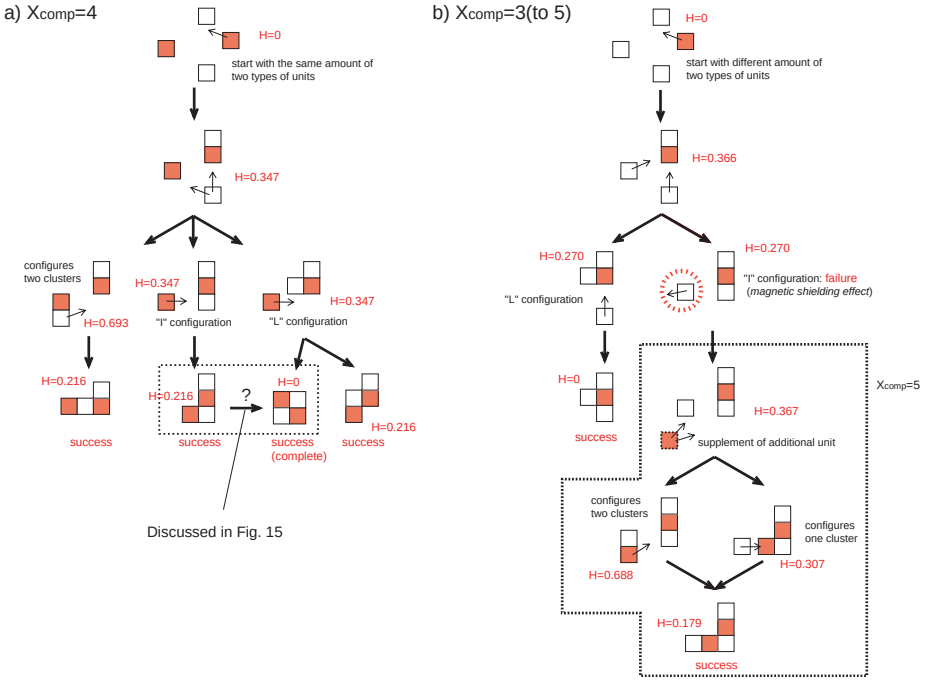

Figure 2.13: Two examples of square tile assembly. a) Starting with two identical sets of opponent tiles. b) Starting with one red tile and three white tiles.

For further investigation, we show two representative convergence paths with 4 square tiles in Figure 2.13; starting with 2 red and 2 white tiles in (a), and 1 red and 3 white tiles in (b). Here the orders of the paths are expressed with arrows. Each DOP H is also shown for the formed cluster. Surprisingly, in Figure 2.13 a, all the paths allow the system to converge. That is, the system has little influence of the *magnetic shielding effect*, and always completes the aggregation process. However, in Figure 2.13 b, the system has the possibility to be trapped by the problem and doesn't manage to converge to a single cluster (i.e. a white square tile highlighted with red dotted circle). However, this occasion can be avoided if there is another opponent tile in the system (the dotted red square tile; "supplement of additional unit"). Once this tile is added to the system, no matter to which direction that the system proceeds to assembly, it never encounters the problem. This indicates that having a similar number of sets of opponents on a regular basis helps a system from falling into a local minimum. It also explains why systems proceeded with a fast aggregation in the early stages in the experiments.

In Figure 2.14, we plot the DOP transitions of square tiles (shown in Figure 2.5 $\mathcal{S}_\mathbf{d}$) vs. the change in the global clustering degrees. We divide the transitions into two groups, namely, a fast aggregation group (Figure 2.5 $\mathcal{S}_\mathbf{d}$ 11 - 14, $<$ 1 min) and a slow aggregation group (Figure 2.5 $\mathcal{S}_\mathbf{d}$ 15 - 20, $>$ 2 min), and show the transitions in Figure 2.14 a and Figure 2.14 b, respectively. As a reference, we plot mathematically derived DOP curves in which the tiles aggregate in the most sequential way. Note that these curves are the lowest values that the system can take. The figure indicates that, in the case of rapid

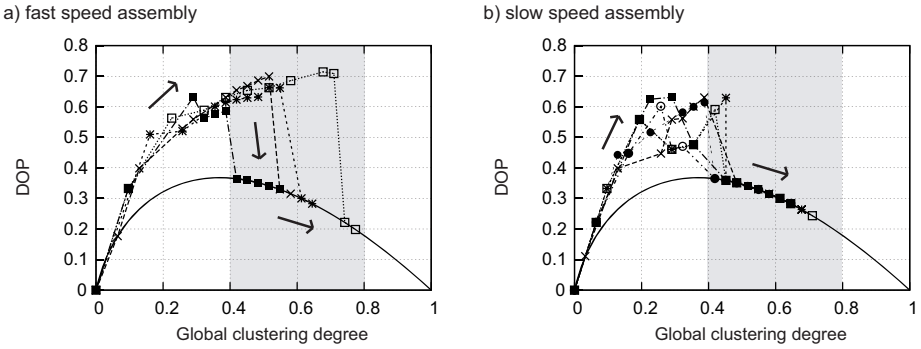

Figure 2.14: The DOP transitions of square tiles (Figure 2.5 $\mathcal{S}_\mathbf{d}$) vs. the change in global clustering degrees. a) Transitions whose assembly completion times (90%) are less than one minute (Figure 2.5 $\mathcal{S}_\mathbf{d}$ 11 - 14). b) Transitions which took more than two minutes (Figure 2.5 $\mathcal{S}_\mathbf{d}$ 15 - 20). In the case of rapid transitions, the tiles tended to form two clusters and subsequently aggregated and configured a cluster. This tendency can be observed as large DOP reductions in the second half stages of their transitions, where the global clustering degrees are between 0.4 and 0.8 (highlighted with a gray colored background).

transitions, the tiles tended to form two clusters and subsequently aggregated and configured a cluster. This tendency can be seen as large DOP reductions in the second half stages of their transitions, where the global clustering degrees are between 0.4 and 0.8 (highlighted with a gray colored background). This aggregation pattern can be characterized as parallel growth, where the system proceeds with its assembly utilizing a high degree of parallelism. However, transitions that took a relatively long time (more than 2 minutes) show a tendency to form one large cluster in their early stages, preventing single surrounding tiles from assuming appropriate positions. This comparison clearly shows that the method of aggregation affects the efficiency of self-assembly.

In Figure 2.15, we investigate the possibility of the transformation which we see in Figure 2.13 (dotted square in (a)). We measured the transitions in magnetic potential energy of square tiles and circle tiles. The energy is normalized by dividing by the absolute initial values ($-U'_{total}/|U'_{total}\big|_{\theta=90}|$). Each tile is supposed to move from position A(C) to B(D). The figure indicates that, in the case of square tiles, a potential barrier has to be overcome to arrive at a stable position, whereas in the case of circle tiles, the tile is supposed to roll down to the position D without any assistance (we don't consider friction). The effect of shape can be clearly recognized here.

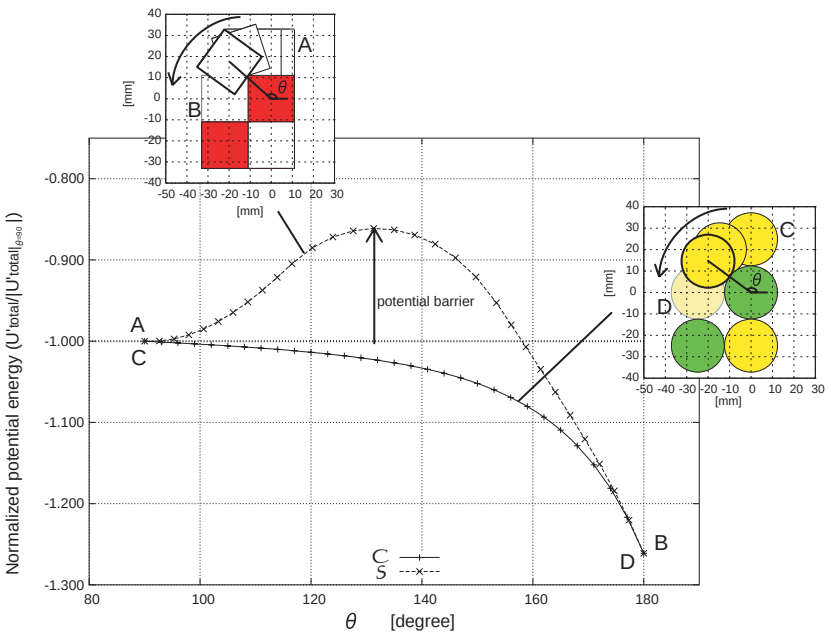

Figure 2.15: Normalized potential energy ($-U'_{total}/|U'_{total}\big|_{\theta=90}|$) vs. the rotational angle θ. In the case of square tiles, a potential barrier has to be overcome to arrive at a stable position (B), whereas in the case of circle tiles, the tile can roll down to the position D without any assistance.

2.6 Conclusion

In this paper, we have shown how the morphology of components affects the self-assembly process. We have proposed a new measure, the *degree of parallelism* (DOP), to quantify the aggregation characteristics. The DOP captures how the system allocates connections into different clusters. The results acquired using this measure showed that the early stages of the aggregation pattern are crucially influential to the rest of the entire assembly process. It was observed that a shape which has rounded corners, such as a circle or a rounded-square eases the problem — the *Magnetic shielding effect* — and facilitates efficient assembly at an appropriate magnetized level. We clearly show that a change in the morphology of components can induce different aggregation patterns, affecting the completed structure of their final configurations.

Appendix 2A

The assembly completion time [sec] (80% and 90% completion) of all combinations.

	$\mathcal{S}_\mathbf{s}$		$\mathcal{S}_\mathbf{d}$		$\mathcal{C}_\mathbf{s}$		$\mathcal{C}_\mathbf{d}$	
trials	80%	90%	80%	90%	80%	90%	80%	90%
1	12	34	19	136	9	26	16	56
2	45	45	142	162	8	27	6	10
3	51	56	33	46	19	54	13	29
4	19	129	19	20	18	109	22	24
5	26	53	17	172	29	59	7	13
6	11	24	38	266	18	26	56	119
7	46	55	27	27	10	23	26	117
8	58	58	26	>300	23	166	6	11
9	90	90	>300	>300	29	97	11	80
10	83	157	26	26	182	192	11	46
11	36	67	20	>300	12	13	10	41
12	138	138	21	135	25	105	7	11
13	164	164	29	273	14	59	6	17
14	26	36	11	>300	65	65	5	73
15	43	43	>300	>300	16	44	111	166
average[1]	56.5	76.6	>68.5	>184.2	31.2	71.0	20.9	54.2
	$\mathcal{R}_\mathbf{s}$		$\mathcal{R}_\mathbf{d}$		$\mathcal{M}_\mathbf{s}$		$\mathcal{M}_\mathbf{d}$	
trials	80%	90%	80%	90%	80%	90%	80%	90%
1	14	183	82	139	10	17	20	38
2	18	138	8	14	13	77	7	20
3	13	43	10	28	12	17	36	96
4	26	65	10	174	12	36	5	81
5	8	20	19	39	18	84	124	124
6	12	46	5	11	17	26	14	25
7	24	32	9	11	14	26	10	106
8	27	76	5	8	26	48	13	42
9	15	45	8	17	20	23	34	50
10	13	130	22	37	15	81	15	34
11	12	51	5	37	17	17	8	12
12	15	33	9	>300	10	17	33	37
13	62	62	43	104	12	21	19	>300
14	12	33	11	117	112	132	13	21
15	52	60	29	29	15	19	6	65
average[2]	21.5	67.8	18.3	>71.0	21.5	42.7	23.8	>71.4

[2] The trials which took longer than 300s are included as 300s (listed with ">").

Chapter 3

How Dynamics Influences the Yield of Self-assembly Robots

Self-propulsive model

Self-assembly is considered to be a key to understanding the nature of life. It is through autonomous and spontaneous self-aggregation that a truly vast number of organized structures form from simple parts. In this paper, based on a novel self-assembly platform consisting of self-propulsive cm-sized modules capable of aggregation on the surface of water, we study the effect of stochasticity and morphology with respect to the yield rate of targeted formations in self-assembly processes. Specifically, we focused on a unique phenomenon that a number of modules instantly compose a targeted product, while they avoid some undesired states of certain geometrical formations (termed one-shot aggregation). Together with a focus on the role that the morphology (shape) of the modules plays, we validate the effect of one-shot aggregation with a kinetic rate mathematical model. Moreover, we examined the degree of parallelism of the assembly process, which is an essential factor in self-assembly, but is not systematically taken into account by existing frameworks.

keywords
dynamics; stochasticity; reverse reaction; one-shot aggregation; yield problem; degree of parallelism; morphology; distributed system; emergent behavior.

[1]Parts of the material in this chapter previously appeared in; S. Miyashita, M. Kessler and M. Lungarella (2008) "How Morphology Affects Self-Assembly in a Stochastic Modular Robot", *IEEE International Conference on Robotics and Automation (ICRA)*, pp. 3533-3538.

3.1 Introduction

Manufacturing technologies and industries heavily rely on robots. For macroscopic objects industrial robots are not only economical but are also reliable, fast, and accurate. Such robots, however, hit a barrier – entailing lower yields and higher fabrication costs – as the assembled objects become smaller and more complex. One potential solution to this problem is to exploit processes of self-assembly, that is, processes in which the interaction of pre-existing components leads to organized structures without human intervention. Such components could be, for instance, identical mechanical units (modules).

Self-assembly is known of crucial importance in the biological realm at all scales. For instance, the formation of the complex symmetrical protein shells of spherical viruses is a well-studied example of self-assembly. The shell of the T4 bacteriophage (so-called because it infects bacteria) is composed of hundreds of parts and it is not plausible to assume that the instructions for its construction are contained only in the genetic material of the virus. The organism consists of about 70 different kinds of proteins and exploits the metabolism of the host cell (e.g. E. Coli) to generate the copies of itself [59, 130]. Moreover, it is truly remarkable that if the right kinds of proteins are mixed, the virus can be synthesized *in vitro*. Although the discussion of whether or not viruses are living things has been controversial ever since they were first discovered, they are generally considered to be non-living entities because they cannot reproduce without the help of a host organism. As the research outlined above shows, the rules that govern interactions at a local level are simple; the interactions of a large number of entities can lead to the emergence of complex structures through a process of self-assembly.

In order to develop a better formal understanding of the general principles underlying self-assembly, many attempts have been made to create descriptive models. Pioneering experiments on artificial self-replication were conducted by Lionel and Roger Penrose almost 50 years ago [87]. They presented a mechanical model of natural self-replication in a stochastic environment. Hosokawa's work [46, 47] in the 1990's followed this stream, examining the clustering pattern of passive elements. The group of Whitesides revealed different types of self-assembly at small scales [15, 40–42]. Notable ideas about conformational switch (physics based internal state of a component) were proposed by Saitou [94].

Recent advances in robotics have highlighted the importance of self-assembly for building complex objects, aimed at exploiting the obvious advantages of living organisms. Modular robots – autonomous machines typically consisting of homogeneous building blocks – promise a viable solution because they have the ability to be highly versatile. For instance, at least ideally, they can re-configure and adapt their shape according to a given task-environment. Work has mainly been focused on the design and construction of the basic building blocks of a typically small repertoire, with docking interfaces, which allow transfer of mechanical forces, moments and electrical power, and which can also be used for data communication [18–20, 30, 53, 57, 72, 76–78, 81, 93, 126, 131].

To date, a few self-reconfigurable modular robots relying on stochastic self-assembly have been built [8, 38, 54, 102, 119, 120]. The main difference from existing modular robotics is the way in which the modules are supplied. The robot or formed cluster waits for a supplemental module to be "delivered" from the environment, rather than supplying it itself. Although in all these systems

the units interact asynchronously and concurrently, a certain amount of state-based control is still required for the modules to move, communicate, and dock. Generally, the internal representations of the module's configurations, such as rewritable look-up tables, follow the same lines as conventional approaches.

By taking tools and methods from nature, many inroads have already been made in utilizing self-assembly for the fabrication of structures at molecular scales [61,92,100,101,123,129]. These methods are powerful and effective, especially due to the exploitation of the advantages of small scales, e.g. the ability to control stochasticity through temperature during mass production of the assembled units. An essentially analogous problem to the macroscopic approaches has been investigated in the context of DNA folding where one of the objectives is to increase the yield of self-assembly processes [92]. Similarly, a lot of research effort is being devoted to the development of high-yield procedures for integration and mass manufacturing of heterogeneous systems via self-assembly of mesoscopic and macroscopic components [12, 36, 124]. The disadvantage of such an approach may be, if anything, that the assembly parts that can be employed are limited to what naturally exist or are manufacturable at the scale in question.

In this paper, motivated by the outstanding potential need for realizing effective self-assembly system, we set the goal of this study is to investigate the role of stochasticity and morphology on self-assembly from the perspective of necessary condition and propose the novel approach that can be used in versatile scales. We made the following set of prerequisites for establishing the experimental conditions.

1. **The system should be "stochastic" and "distributed" with all components being autonomously assembled in parallel.** Small-scale self-assembly systems that appear in nature, such as molecular reactions, are considered to be distributed systems in stochastic environment, implying that there are uncertainties in the global information concerning the components, e.g. locations and total number of modules. Therefore, the model should be compatible with molecular systems to some degree.

2. **The components should have only limited (or no) computational (decisive) abilities but be self-sufficient.** Once a set of experimental conditions is invoked, modules are expected to act independently (be untethered), following local causal rules imposed by the environment, in terms of actuation (self-propulsion) and power.

3. **The module architecture should be scalable.** Based on the fact that self-assembly must take place on a small scale in order to achieve environmental stochasticity, the module design should be scalable and simple.

In the following Section 2, we introduce the proposed model and describe its behavior. In Section 3, we estimate the convergence of the model based on kinetic rate calculations. We further examine the observed aggregation pattern employing the notion of *degree of parallelism* in Section 4. In Section 5 we present our conclusions.

3.2 The model: self-propulsive modules

3.2.1 Modules and experimental setup

The term "self-assembly" implies that the elements or parts involved assemble in a spontaneous manner without external intervention or control. Such behavior is typical of dissipative systems. Taking this into account, we chose to produce a set of modules with different shapes that swarm on water.

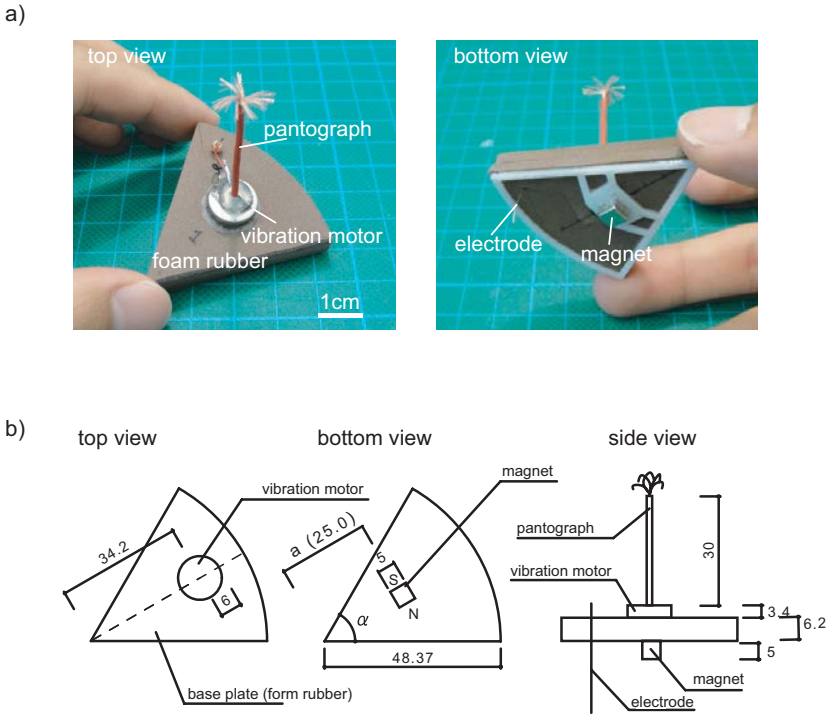

Figure 3.1: A self-propulsive module. (a) Photographs of an individual module. (b) Schematic representation of the module (units: $[mm]$). Each module weighs $2.8\,g$ and has a footprint of $12.25\,cm^2$.

The modules, which we call *Tribolon*[2], are equipped with a flat coreless vibration motor (T.P.C DC MOTOR FM34F, $12000 \sim 14000\,rpm\,(2.5 - 3.5\,Volts)$) on the top of the base plate to allow self-propulsion, and a single permanent magnet (flux density $1.3\,T$, $5 \times 5 \times 5\,mm^3$, we decided that a single module should contain only one magnet) at the bottom for attractive/repulsive interactions (Figure 3.2). This allowed the modules to jiggle and move around in their environment. The "shape" of the modules can be characterized by a set of angles and lengths. However, an inevitable problem which arises is that a change in one parameter can lead to changes in other parameters, which makes it difficult to discuss the implications of a single parameter change. Here, in order to minimize this problem, we chose a circular-sector-shaped tiles spanning an angle α ($\alpha = 60°$ in Figure 3.1).

[2]derived from Tribology

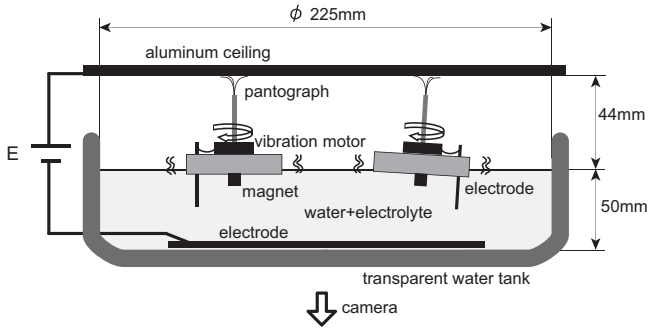

Figure 3.2: Illustration of the experimental environment with two modules.

As a power supply, rather than using batteries for each module, we opted to supply electricity through a pantograph that draws current from a metallic ceiling (Figure 3.2). When an electrical potential is applied to the ceiling plate, current flows through the pantograph to the vibration motor, returning to ground via electrodes immersed in the conductive water (salt solution). Due to this setup, all modules receive the same constant power and they can be lightweight ($2.8\,g$ each), which would not be the case if batteries were used.

The salt solution ($83.3\,g/l$) can generate current flow by the chemical reactions in Eq. (3.1).

$$2\mathrm{NaCl} + \mathrm{H_2O} \rightarrow \mathrm{H_2} \uparrow + \mathrm{Cl_2} \uparrow + 2\mathrm{NaOH} \tag{3.1}$$

The concentration of the salt solution is sufficient to sustain current flow during the entire course of the experiment. In order to avoid chemical deposition onto the electrodes, we used platinum for the electrode material. The base plate is made of foam rubber to produce a certain amount of friction. We set a camera below the tank and observed the modules through the transparent bottom.

3.2.2 Magnetism

Given N as the number of hard magnets existing in the system, the force ($\boldsymbol{F}_{ij}$) and the torque ($\boldsymbol{\tau}_{ij}$) experienced by i-th magnet by interacting with j-th magnet ($i, j \in$N) can be expressed and simplified as:

$$\boldsymbol{F}_{ij} = \mu_0 \int_{vi} (\boldsymbol{M}_i \cdot \nabla)\, \boldsymbol{H}_j \, dv \approx \mu_0 v_i (\boldsymbol{M}_i \cdot \nabla) \boldsymbol{H}_j \tag{3.2}$$

$$\boldsymbol{\tau}_{ij} = \mu_0 \int_{vi} (\boldsymbol{M}_i \times \boldsymbol{H}_j)\, dv \approx \mu_0 v_i \boldsymbol{M}_i \times \boldsymbol{H}_j \tag{3.3}$$

where $\boldsymbol{H}_j$ is the magnetic field exerted by j-th magnet, $\mu_0 = 4\pi \times 10^{-7}$ (Tm/A) is the permeability of free space, v_i and $\boldsymbol{M}_i$ are the volume and the magnetization of i-th magnet, respectively.

The magnetic field created by j-th magnet with respect to the position $\boldsymbol{r}$ can be described as

$$\boldsymbol{H}_j(\boldsymbol{r}) = \frac{1}{4\pi|\boldsymbol{r}^3|}\Big(\frac{3(\boldsymbol{m_j} \cdot \boldsymbol{r})\boldsymbol{r}}{|\boldsymbol{r}|^2} - \boldsymbol{m_j}\Big) \tag{3.4}$$

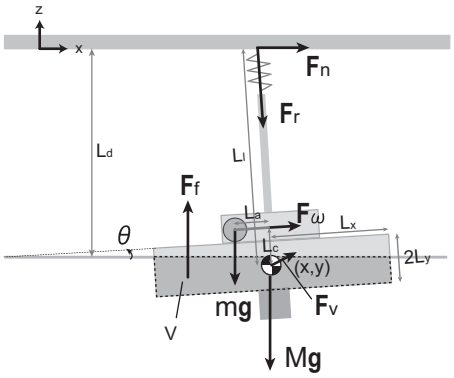

Figure 3.3: Schematic of a single module.

m	Mass of the eccentric weight
M	Mass of the module body
I	Moment of inertia around the center of mass
θ	Rotational angle of the module
$\boldsymbol{F}_\omega$	Centripetal force
$\boldsymbol{F}_n$	Frictional force
$\boldsymbol{F}_r$	Resistive force
$\boldsymbol{F}_f$	Buoyancy force
$\boldsymbol{F}_v$	Viscous force
$\boldsymbol{g}$	Gravitational acceleration vector
L_a	Amplitude of eccentric mass rotation
L_l	Natural length between center of mass and the ceiling
L_x	Radius of the module
L_y	Half of the height of the module
L_c	Distance between center of mass and center of vibration motor
L_d	Distance between the ceiling and water

where $\boldsymbol{m_j} = v_j \boldsymbol{M}_j$.

Utilizing $\boldsymbol{H}$, the total magnetic potential energy of the system (U_{total}) can be described as

$$U_{total} = -\frac{\mu_0}{2} \sum_{i,j\ i \neq j}^{N} \int_v \boldsymbol{M}_i \cdot \boldsymbol{H}_j \, dv \tag{3.5}$$

We normalize the energy as $U'_{total} \equiv U_{total}/(\frac{\mu_0}{4\pi} v^2 M^2)$ assuming all the magnets are equally magnetized.

3.2.3 Model of motion

The long range interaction described above is identical for each type of module, regardless of its shape, because identical magnets were used. However, the short range interaction, i.e. the final alignment, is dominated by shape and this was experimentally investigated. For the sake of simplicity, we consider the motion of a module in two dimensions (Figure 3.3). Note that the modules could tilt, inducing rather large fluctuations in the current flowing through the motors.

Let $\boldsymbol{x} = [x, z]^T$ be a position vector in a Cartesian coordinate system. Transitional and rotational motions can then be described by Eq. (3.6) and Eq. (3.7), respectively.

$$M\ddot{\boldsymbol{x}} = \boldsymbol{F}_\omega + \boldsymbol{F}_r + \boldsymbol{F}_f + \boldsymbol{F}_n + \boldsymbol{F}_v + (M+m)\boldsymbol{g} \tag{3.6}$$

$$I\ddot{\theta} = \boldsymbol{r}_\omega \times \boldsymbol{F}_\omega + \boldsymbol{r}_\omega \times m\boldsymbol{g} + \boldsymbol{r}_f \times \boldsymbol{F}_f + \boldsymbol{r}_n \times \boldsymbol{F}_n \tag{3.7}$$

where $\boldsymbol{r}_\omega$, $\boldsymbol{r}_f$, $\boldsymbol{r}_n$, and $\boldsymbol{r}_v$ are directional vectors from the center of mass of the module to the action points $\boldsymbol{F}_\omega$, $\boldsymbol{F}_f$, $\boldsymbol{F}_n$, and $\boldsymbol{F}_v$, respectively. Each force can

be simplified as:

$$F_\omega = mL_a\omega^2\cos(\omega t+\phi) \quad (3.8)$$

$$F_r \approx -k(\frac{y}{\cos\theta}-L_l) \quad (3.9)$$

$$F_n = \mu F_r\cos\theta \approx -\mu k(y-L_l\cos\theta) \quad (3.10)$$

$$F_f = -Vg \quad (3.11)$$

$$\boldsymbol{F}_v \approx -c\dot{\boldsymbol{x}} \quad (3.12)$$

where ϕ specifies the initial phase of the eccentric mass, V is the volume of foam rubber that is under water, k is the spring constant of the pantograph, μ is the kinetic frictional coefficient, and c is the coefficient of viscosity of the salt water. What is important here is that the rotational speed of the eccentric mass is quasi proportional to the voltage applied. As this speed increases, it leads to faster movement of the modules and stronger collisions between them.

Figure 3.4 shows snapshots of the characteristic trajectories of two modules during a 9-*sec* interval. Module 1 strikes module 2 while being attracted by the magnetic force between them. It should be noted that due to the rotation of the eccentric mass, each module repels other modules along a certain direction. Moreover, because the repulsion force varies, the modules change their relative positions frequently (illustrated on the right). This is because the repulsion force between two modules depends on the position of the rotating masses in each vibration motor as well as on the friction of the rubber foam.

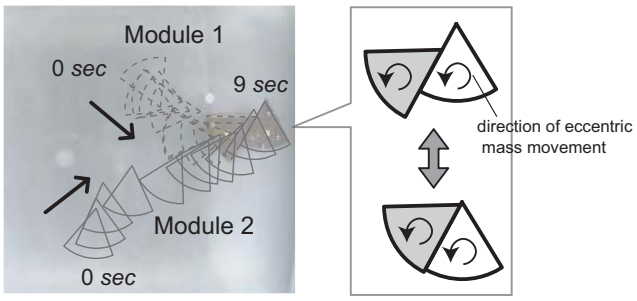

Figure 3.4: Trajectories of two modules during a 9-*sec* interval. Module 1 strikes module 2 while being attracted by the magnetic force between them. The illustration on the right shows that the relative positions of these two modules are unstable, depending strongly on the friction of the form rubber.

3.2.4 Aggregation behaviors

Snapshots taken during three experiments using 6 modules are shown in Figure 3.5 (see the attached movie.). In each experiment, a different electric potential was applied between the ceiling plate and the immersed electrode causing the modules to aggregate in different ways.

In the experiment shown in Figure 3.5 a, we applied a potential of $E = 7V$. The modules first moved along random paths in a manner vaguely reminiscent of Brownian motion. After some time ($\approx 9\,sec$), due to the magnetic attraction, some of the modules were pulled together forming 2-clusters (denoted by X_2; X_k designates a cluster consisting of k modules). These clusters further combined

to generate a 4-cluster (X_4), then a 5-cluster (X_5), and eventually a 6-cluster (X_6) (sequential aggregation). Once this final state was reached, the entire circular structure started to reform a propeller-like structure sliding the relative positions (see Figure 3.4). This is due to the stability of the configuration when all remaining spaces were occupied by modules, which induced constant repulsive forces among them (note that each module repels its neighbor in the same direction). Subsequently, this stable configuration causes synchronized contact of the pantographs to the ceiling, leading to a pulsed current flow. Consequently, the 6-cluster underwent a rotational movement.

In the snapshots reproduced in Figure 3.5 b, the potential was set to $E = 8V$. As a result of the higher potential, the motors vibrated at a higher frequency, increasing the likelihood of breakup of clusters. Most of the time, all cluster types disintegrated shortly after formation, except for the 6-cluster (X_6) which, due to its symmetry, proved to be a stable structure. It is important to note that the formation of the 6-cluster at $T = 98\,sec$ was accidental (here termed "one-shot aggregation"). This tendency of suppressing intermediate states is thought to be a potential solution to the yield problem (see Section 3.2.5). In Section 3.3, we focus on the characteristics of these two aggregation patterns and compare the results of numerical simulations.

The snapshots in Figure 3.5 c were obtained at a potential of $E = 9V$, which induced such rapid vibration that the formation of a 6-cluster became unlikely. In fact, even over prolonged experimental observation, no stable cluster was observed (random movements).

The experimental setup had a deficiency in keeping up the vibration motors speed at a high voltage ($8 - 9V$) for a long time because of self-generated heat. We confirmed these results by checking the stability of the circular configurations shown in (b) and (c) by performing 10 trials, each time initializing the experiment with 6 modules arranged in a circular configuration (the desired configuration). It was confirmed in all the cases that while at $8V$, the circular configuration remained stable, it broke up at $9V$. Considering that the tendency of segregations between two modules rises along with higher voltage supply, the described results seem probable. We further investigate this issue by modeling mathematical kinetic rate model in Section 3.3.

3.2.5 Yield problem

The problem of producing a desired configuration in large quantities (while avoiding incorrect assemblies) is known as the yield problem and has been studied in the context of biological and non-biological self-assembly systems [46, 47]. As an example, let us assume that the self-assembly process is initialized with 7 modules. In fact, the likelihood that the system actually settles into the desired configuration (e.g. a circle) is rather low due, and it is more likely that the kind of patterns shown in Figure 3.6 will occur. In this respect, suppressing the probability of producing stable intermediate states may help in reducing the occurrence of this problem, as is the case in Figure 3.5 b. We further investigate this issue in Section 3.3.

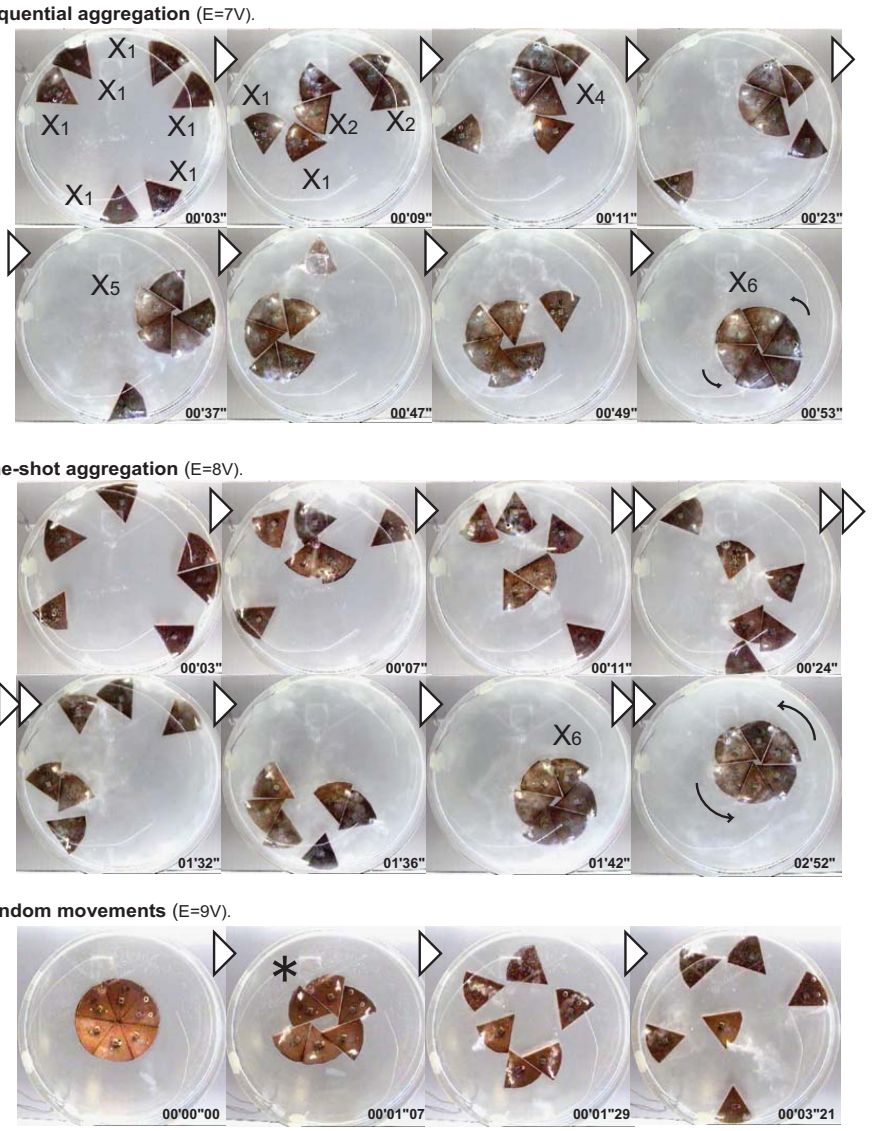

Figure 3.5: Experimental results. Self-assembly process as a function of applied electric potential E. (a) $E = 7V$, sequential aggregation. (b) $E = 8V$, "One-shot aggregation". (c) $E = 9V$, random movements. We checked the stability of the circular configurations shown in (b) and (c) by performing 10 trials beginning with circular configurations. It was observed that at $8V$, the circular configuration were stable, while it broke up at $9V$ (see the attached movie).

3.3 Chemical kinetics rate model

In order to quantitatively investigate the formation and stability of self-assembled circular-sector-shaped modules, a mathematical model was developed based on kinetic rate equations [35, 46, 64, 65]. In this section, we call the conditions which correspond to the phenomena observed in Figure 3.5 a, b, (voltages of $7V$

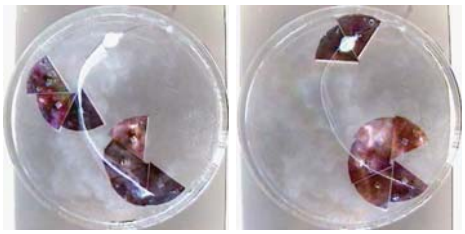

Figure 3.6: Yield problem and stable clusters. 7 circular sectors are placed in the arena. In most cases, however, the modules organize themselves in two clusters.

and $8V$) "sequential aggregation" and "one-shot aggregation". The difference between them is that in the sequential aggregation process, a module should maintain its connection to a neighboring module once it has attached to it, while in the one-shot aggregation process, a single module may also disaggregate from a cluster at a constant speed (except for the stable configuration X_6, shown in Figure 3.5).

For the analysis, the intermediate products are represented by state variables. One can express the state transitions of the clusters as:

$$\begin{array}{lll} 2\mathrm{X}_1 \rightleftharpoons \mathrm{X}_2, & \mathrm{X}_1 + \mathrm{X}_2 \rightleftharpoons \mathrm{X}_3, & \mathrm{X}_1 + \mathrm{X}_3 \rightleftharpoons \mathrm{X}_4, \\ \mathrm{X}_1 + \mathrm{X}_4 \rightleftharpoons \mathrm{X}_5, & \mathrm{X}_1 + \mathrm{X}_5 \rightarrow \mathrm{X}_6, & 2\mathrm{X}_2 \rightarrow \mathrm{X}_4, \\ \mathrm{X}_2 + \mathrm{X}_3 \rightarrow \mathrm{X}_5, & \mathrm{X}_2 + \mathrm{X}_4 \rightarrow \mathrm{X}_6, & 2\mathrm{X}_3 \rightarrow \mathrm{X}_6 \end{array} \tag{3.13}$$

where X_k stands for the state of a cluster consisting of $k(\in 1, ..., 6)$ modules (e.g. two single modules X_1 can merge to form one cluster X_2). Reversible reactions are only possible in case of the one-shot aggregation. Note that we defined the transitions $2X_2 \rightarrow X_4$ and $X_2 + X_3 \rightarrow X_5$ to be irreversible, and X_6 to be the final state, since we seldom observed such disassembly in the experiments. The robustness of these clusters is mainly due to the geometrical stability of these configurations.

The transition of the state vector $\boldsymbol{x} = (x_1, \ldots, x_6)$, in which x_k denotes the number of clusters consisting of k modules, obeys the following difference equation if x is large enough:

$$\boldsymbol{x}(t+1) = \boldsymbol{x}(t) + \boldsymbol{F}(\boldsymbol{x}(t)) \tag{3.14}$$

where t corresponds to the number of time steps, or more precisely, to the number of collisions between clusters. F_k is a transition function expressed as the sum of the products of (i) the collision probability P_{ij}^c $(i, j \in 1, ..., 6)$, the bonding probability P_{ij}^b, and the stoichiometric number ν_{ij} and (ii) the sum of the products of the disassembly probability $P_{i'}^d$ and stoichiometric number $\nu'_{i'}$, namely:

$$F_k(x) = \sum_{i,j} \nu_{ij} P_{ij}^c P_{ij}^b + \sum_{i'} \nu'_{i'} P_{i'}^d x_{i'} \tag{3.15}$$

where the stoichiometric numbers ν_{ij} (assembly) and $\nu'_{i'}$ (disassembly) are coefficients of the reaction seen in Eq. (3.13). The subscripts i and j in ν_{ij} denote

the size of the two clusters assembling, and in $\nu'_{i'}$ the size of the disassembling cluster. The stoichiometric numbers correspond to the number of modules that make up the colliding clusters, and they have a positive sign if X_k is a product, and a negative sign if X_k is a reactant. Note that we are only interested in individual collision events. The model ignores the specific positions of the modules, assuming a well-mixed system.

The collision probability P^c_{ij} can be represented by Eq. (3.16), assuming that two clusters X_i and X_j are picked randomly in each time step.

$$P^c_{ij} = \begin{cases} 2x_i x_j/(\sum_k x_k)^2 & (i \neq j) \\ x_i^2/(\sum_k x_k)^2 & (i = j). \end{cases} \tag{3.16}$$

In Figure 3.7, two configurations consisting of circular-sector modules are shown. Here, S_k and M_k represent regions of the plane, and α, β, and γ represent angles in radians.

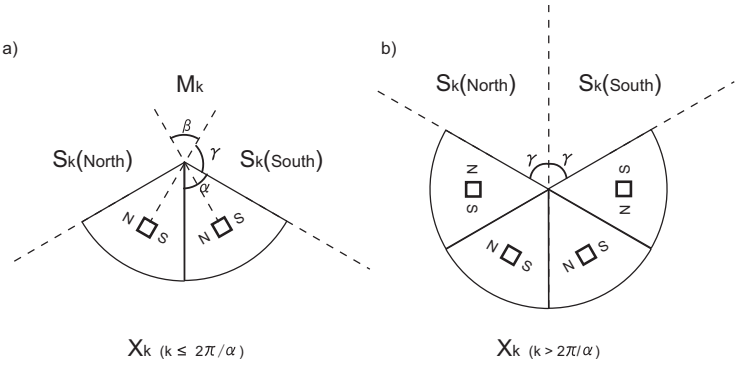

Figure 3.7: Two configurations consisting of circular-sector modules. α, β, and γ specify the corresponding angles, and $S_k(North), S_k(South)$, and M_k denote the specific regions referred to in Eq. (3.17). (a) The size of cluster is less than a half circle. (b) The size of cluster is more than a half circle.

Considering the geometric coordination, the conditional probability of bonding when two modules X_i and X_j collide is given by

$$\begin{aligned} P^b_{ij} &= P((X_j \; in \; S_i(South)) \cap (X_i \; in \; (S_j(North) \cup M_j))) \cdot 2 \\ &\quad + P((X_j \; in \; M_i) \cap (X_i \; in \; (S_j(North) \cup S_j(South) \cup M_j))) \\ &= \begin{cases} \frac{\gamma_i}{2\pi} \cdot \frac{\beta_j + \gamma_j}{2\pi} \cdot 2 \; + \; \frac{\beta_i}{2\pi} \cdot \frac{\beta_j + 2\gamma_j}{2\pi} & (i + j \leq \frac{2\pi}{\alpha}) \\ 0 & (i + j > \frac{2\pi}{\alpha}) \end{cases} \end{aligned}$$

where

$$\begin{aligned} \beta &= \begin{cases} \alpha + (k-2)\alpha & (k \leq \frac{\pi}{\alpha}) \\ 0 & (k > \frac{\pi}{\alpha}) \end{cases} \\ \gamma &= \begin{cases} \pi + (\frac{1}{2} - k)\alpha & (k \leq \frac{\pi}{\alpha}) \\ (2\pi - k\alpha)/2 & (k > \frac{\pi}{\alpha}) \end{cases} \end{aligned} \tag{3.17}$$

and k represents the number of modules contained in the cluster. We assume that these modules will bond if (i) X_i is in the region $S_j(South)$ of X_j, and (ii)

X_j is in the region $S_i(North)$ of X_i; i.e., if the magnetic north pole of module 2 (area N_2) faces the south pole of module 1 (area S_1) or vice versa.

P^d is set to zero for the case of sequential aggregation. In one-shot aggregation, we arrive at P^d using a model similar to the law of mass action used to describe chemical reactions. With the equilibrium constant K of the reaction $X_i + X_j \rightleftharpoons X_{i+j}$ being given by $K = k_+/k_-$, k_+ and k_- can be interpreted as the probability of bond formation and disassembly, respectively. With the bonding probability $\hat{P}^b$ set to the average of $\sum_j P^b_{1,j}$, K can be written as $K = \hat{P}^b/P^d = exp(\frac{-\Delta U'}{\rho v^2})$, where $\Delta U'$ is the energy of the bond formed between two modules. This means K grows exponentially with the bonding energy divided by the system's kinetic energy [65]. We set this bond strength to be the normalized magnetic potential energy of a 2-cluster X_2 calculated with Eq. (3.5). ρv^2 is the mean energy of all the modules in our system, which have a Brownian-like motion. Since we cannot derive the total kinetic energy of the system, we set ρ to be a constant with units of s^2/m^5 and v^2 to have a value proportional to the systems' agitation. This leads to the probability of disassembly of a bond in the next time step to be $P^d = \hat{P}^b exp(\frac{\Delta U'}{\rho v^2})$. For further calculations we set $\rho = 1\, s^2/m^5$ and $v = 0.0232\, m/s$ (the mean velocity of the modules in our system). The disaggregation is set to occur in proportion to the number of each cluster. Taking the geometric configurations of each cluster into account, we set $P^d_2 = P^d$, since there is only one bond that can be dissolved. We set $P^d_1 = P^d_6 = 0$, since the modules do not disassemble. For X_3 to X_5 clusters, we consider the leftmost or the rightmost module leaving the cluster (see Figure 3.7 (b)). Therefore we double the coefficient, namely setting $P^d_3 = P^d_4 = P^d_5 = 2P^d$.

Finally we obtain F_k as:

$$
\begin{aligned}
F_1(\boldsymbol{x}) &= \{-2P^b_{11}x_1^2 - 2P^b_{12}x_1x_2 - 2P^b_{13}x_1x_3 - 2P^b_{14}x_1x_4 - 2P^b_{15}x_1x_5 \\
&\quad +2P^d_2x_2 + P^d_3x_3 + P^d_4x_4 + P^d_5x_5\}/(\sum_k x_k)^2 \\
F_2(\boldsymbol{x}) &= \{P^b_{11}x_1^2 - 2P^b_{12}x_1x_2 - 2P^b_{22}x_2^2 - 2P^b_{23}x_2x_3 - 2P^b_{24}x_2x_4 \\
&\quad -P^d_2x_2 + P^d_3x_3\}/(\sum_k x_k)^2 \\
F_3(\boldsymbol{x}) &= \{2P^b_{12}x_1x_2 - 2P^b_{13}x_1x_3 - 2P^b_{23}x_2x_3 - 2P^b_{33}x_3^2 \\
&\quad -P^d_3x_3 + P^d_4x_4\}/(\sum_k x_k)^2 \\
F_4(\boldsymbol{x}) &= \{2P^b_{13}x_1x_3 + P^b_{22}x_2^2 - 2P^b_{14}x_1x_4 - 2P^b_{24}x_2x_4 \\
&\quad -P^d_4x_4 + P^d_5x_5\}/(\sum_k x_k)^2 \\
F_5(\boldsymbol{x}) &= \{2P^b_{14}x_1x_4 + 2P^b_{23}x_2x_3 - 2P^b_{15}x_1x_5 \\
&\quad -P^d_5x_5\}/(\sum_k x_k)^2 \\
F_6(\boldsymbol{x}) &= \{2P^b_{15}x_1x_5 + 2P^b_{24}x_2x_4 + P^b_{33}x_3^2\}/(\sum_k x_k)^2. \qquad (3.18)
\end{aligned}
$$

3.3.1 Time evolution

Figure 3.8 shows the change over time of the yield of clusters, obtained by solving the system of difference equations described above with the initial condition $\boldsymbol{x}(0) = (100, 0, ..., 0)$. It shows the time evolution of the yield for the cases of sequential aggregation (a) and one-shot aggregation (b). In Figure 3.8 (a), only 38.9 % of modules aggregate into full 6-clusters, which exemplifies the yield problem. Also, since there is no means for the system to disaggregate, it becomes almost stagnant after a certain number of interactions, that is, only a few modules continue the assembly process. However, in Figure 3.8 (b), 99.0 % of modules aggregate to form 6-clusters. Note that the one shot self-assembly shown in (b) takes much longer to reach a stable state than the sequential aggregation in (a). In our calculations, increase of yields are observable when the probability of disaggregation P^d is in the range from 1.0×10^{-8} to 5.0×10^{-2}. In Figure 3.8 (c) and (d), we plot the trajectories of the time evolution of each cluster, where both the x and y axes represent yields (sequential aggregation model in (c) and one-shot aggregation model in (d)). In Figure 3.8 (c), we see that clusters consisting of 3, 4, and 5 modules are temporarily formed and subsequently decrease in number by converting to larger-sized clusters. The convergence in the values represented in (c) denotes yield problem (indicated with *). In Figure 3.8 (d), we see the convergence of all the intermediate states and the growth of the number of 6-clusters[3]. In Figure 3.8 (e), we compare the transition of the yield for the two conditions, where the improvement in yield is clearly shown.

The mechanism of one-shot aggregation is illustrated in Figure 3.9 b, in contrast to sequential aggregation shown in Figure 3.9 a. The core of one-shot aggregation is that the system happens to have a chance to configure a targeted formation (product) with a small probability, while processing reactions combined with aggregations and disaggregations. Also the condition that a product is more structurally stable than the other configurations must be met. We call it "one-shot aggregation" for the sake of easy understanding of the phenomenon. Note that we are fully aware of the fact that reverse reactions assisting in the growth of yield of a product can be frequently observed in chemistry. Our contribution is that we demonstrated the concept using a macroscopic physical model.

The voltage (V) applied to the ceiling determines the level of perturbation introduced into the system. Thus it can be regarded as a kind of temperature (T) which is often employed as a control parameter in molecular self-assembly. The experimental results obtained show different voltages lead to different aggregation patterns. Moreover, by applying a large perturbation (e.g. $9\,V$), the system returns to its initial state, guaranteeing the reversibility of the reaction, which is a desirable property of our system. It allows the system to disaggregate undesired intermediate sub-assemblies.

3.3.2 Effect of morphology

In order to understand how the morphological properties of the modules influence the final state, we studied the stability of different configurations from

[3]In the mathematical model, we did not consider the "bank-effect", in which many modules become stuck together on a wall and stop their dynamical motion.

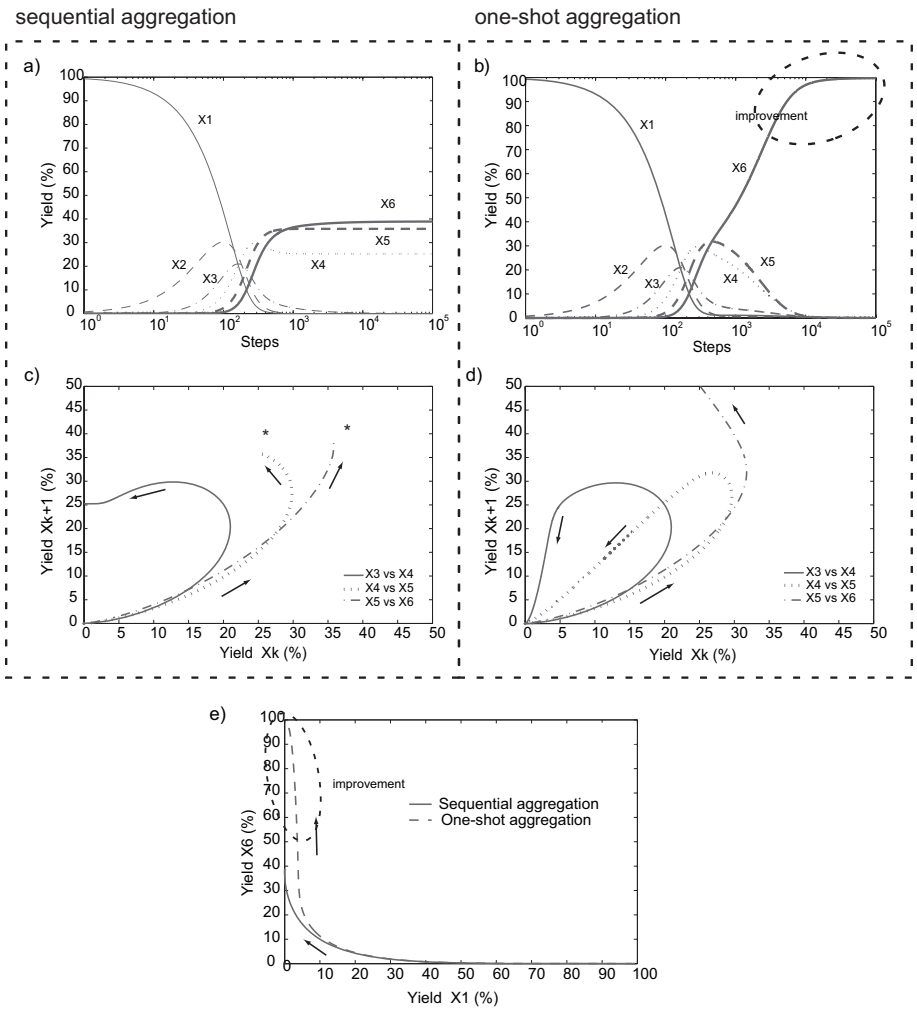

Figure 3.8: Change over time of the yield rate of clusters obtained by solving the model with the initial condition $\boldsymbol{x}(0) = (100, 0, ..., 0)$. (a, b): time evolution of the yield rate for sequential aggregation (a) and one-shot aggregation (b). (c, d): trajectories of time evolution of each cluster for sequential aggregation (c) and one-shot aggregation (d). (e): comparison of the transition of yield rate under the two conditions. The convergence in the values represented in (c) denote yield problem (indicated with *).

the perspective of the magnetic potential energy. In Figure 3.10, we plot the normalized potential energy (U'_{total}) as a function of the position of the magnet in the module. In this case, we moved the magnet along the symmetry axis of the module and measured its distance to the vertex (a). The figure suggests that shifting the position of the magnet closer to the rounded edge causes the system to produce dimers (2-clusters) with the rounded edges touching (from Figure 3.10, the limit is $a \approx 34 \times 10^{-3}\ m$). In our experiments, $a = 25 \times 10^{-3}\ m$, which implies that the full circle cluster has minimal energy[4]. For reference, we

[4]This example seems to indicate that it is also possible to perceive this change not as a shift in the position of the magnet, but rather as a change in the entire mass distribution

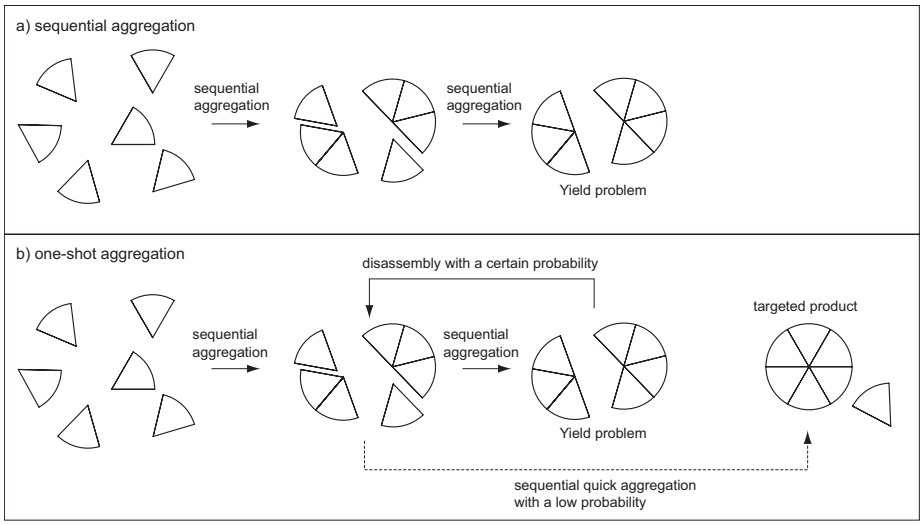

Figure 3.9: Mechanisms of aggregation. (a) Sequential aggregation leading to the yield problem. (b) One-shot aggregation leading to the increase of the targeted product.

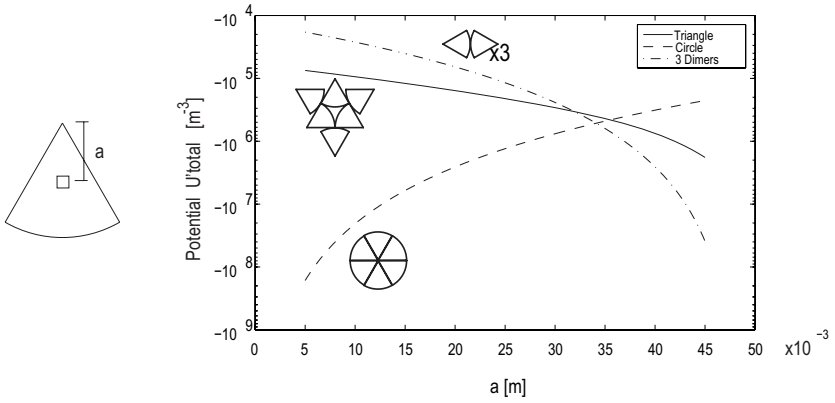

Figure 3.10: Potential energy of each configuration (full circle, 3 dimers, and triangular configuration) with respect to the distance of the magnet from the corner.

also considered the case of a triangle configuration which was observed occasionally. The calculations confirmed that this is a rarely produced configuration.

Figure 3.11 shows how the change of the spanning angle of the corner affects the yield of the self-assembly process in sequential aggregation. The yields are normalized by multiplying them by the number of modules required to construct a full circle (i.e., in the case of $\alpha = 60°$ the factor is 6; in the case of $\alpha = 180°$ the factor is 2), and plotted as a function of the angle α on a logarithmic scale. As can be seen in the figure, the narrower the angle becomes, the worse is the performance of the system. This result can be explained by considering that the number of clusters required to form the desired structure is inversely

(morphology) from the "force source" (here: magnets).

proportional to the angle. Interestingly, the relationship between yield and angle follows a power-law with a scaling exponent of 0.82. That is, the improvement of the yield saturates as the angle becomes wider. This result indicates that

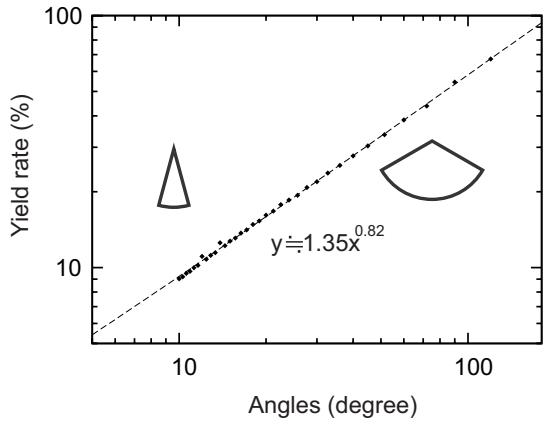

Figure 3.11: Yields as a function of the angle spanned by the circular-sector module in sequential aggregation. The relationship between yield and angle follows a power-law with a scaling exponent of 0.82.

there exists an optimal spanning angle for which both the aggregation rate and the number of identical modules can be maximized[5].

Finite Element Methods Magnetic Analysis

We employ the Finite Elements Method Magnetic (FEMM)[6], an open-source magnetic field solver to visualize the magnetic flux density and the magnetic field lines. For the analysis of the other clusters the appropriate numbers of magnets were added to the calculations. The body of the module itself only consists of plastic and its edges are only displayed for visualization purposes (they have no effect on the result). To keep the model simple we omit the vibration motor, electrode, pantograph and any other metallic objects from our analysis. Since we are interested in the magnetic properties surrounding the magnets we set the mesh grid size to only 0.1 for the complete model. For the magnet and air we use the preset material properties for NbFeB 40MGOe and air respectively. We want to model the magnetic field in an unbounded space while only modeling a finite region of that space. We create an asymptotic boundary condition that approximates the impedance of an unbounded, open space with

$$\frac{1}{\mu_r \mu_0} \frac{\partial A}{\partial n} + c_0 A + c_1 = 0 \tag{3.19}$$

where A is magnetic vector potential and μ_r is the relative magnetic permeability of the region adjacent to the boundary, in our case air with $\mu_r = 1$. μ_0

[5] In our circular-sector model, we considered the angle α to be an adequate parameter to measure the heterogeneity of the system. Although the 60° and 120° modules should be treated as different (heterogeneous) modules, once two 60° modules connect, a 120° module forms, which is obviously equivalent to a 120° module. This example tells us that the concepts "homogeneous" and "heterogeneous" cannot be separated from the context in which they are used.

[6] Available at: `http://www.femm.info/wiki/HomePage`.

is the permeability of free space, and n represents the direction normal to the boundary. For our asymptotic boundary condition, we need to specify:

$$c_0 = \frac{1}{\mu_r \mu_0 R} \tag{3.20}$$

$$c_1 = 0 \tag{3.21}$$

where R, here $10\,cm$, is the outer radius of a spherical problem domain.

Figure 3.12 shows the density plot of the magnetic flux field $|B|$ and the flux lines for the clusters $X1$-$X6$. It can be seen that the larger a cluster gets the more flux is contained within the cluster. Notice how the full circle cluster in Figure 3.12 f, the magnetic flux lines and most of the magnetic B-field is enclosed within the area covered by the clusters' body. This suggests that the morphological properties of the full circle cluster shields the magnets toward the outside effectively removing it from further magnetically interacting with other clusters in the system.

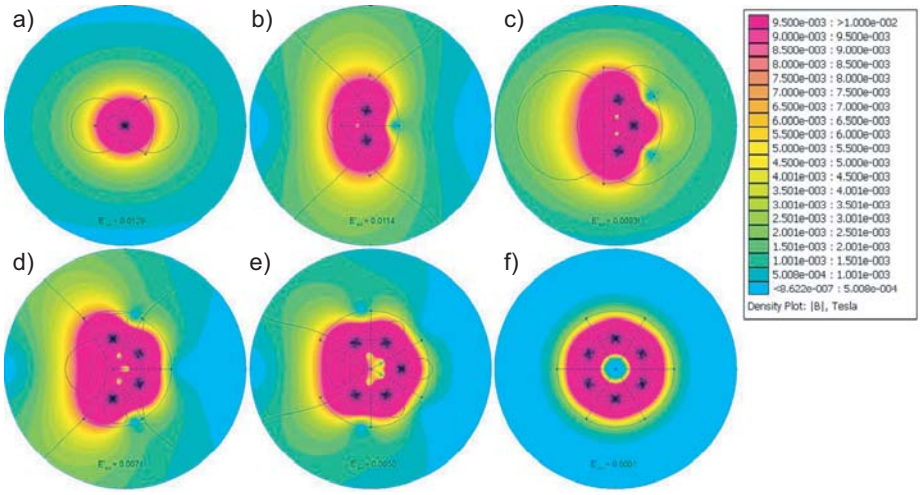

Figure 3.12: (a) - (f) Density plot of the magnetic flux field $|B|$ and the flux lines for clusters $X1$ - $X6$. It can be seen that the larger a cluster gets the more flux is contained within the cluster.

3.4 Degree of parallelism

In this section, we investigate the pattern of assembly focusing in particular on combinatorial matching patterns. The idea is to focus only on connections between components (neglecting the identity of each component), and to acquire information about the compounds. We now define the following variables:

To measure the geometrical connections of the modules, we define the local and global clustering degrees as:
Note that $C \neq c_i$ in general (see Figure 3.13). This measure allows us to characterize geometric topologies independent of the energy.

x_i	number of connections within the i-th cluster
x_{comp}	number of connections in a complete cluster
X	number of all connections ($\equiv \sum_i x_i$)
X_{comp}	number of connections within the complete configuration of clusters ($\equiv \sum x_{comp}$)

Local clustering degree of i-th cluster	c_i	$\equiv \frac{x_i}{x_{comp}}$
Global clustering degree	C	$\equiv \frac{X}{X_{comp}}$.

The *degree of parallelism* (DOP) H, as a function of the local clustering degrees (c_i), is used to quantify the aggregation paths [70], namely:

$$H = -\sum_{i=1}^{N} c_i \ln c_i. \tag{3.22}$$

Suppose that there exists a number N of clusters. From Shannon's lemma, it follows that the value H becomes maximum when the N clusters are all of the same size, namely:

$$\begin{aligned} H(X) &= -\sum_{i=1}^{N} c_i \ln c_i \\ &\leq -\sum_{i=1}^{N} \{\frac{1}{x_{comp}} \cdot \frac{X}{N}\} \ln\{\frac{1}{x_{comp}} \cdot \frac{X}{N}\} \\ &= -\frac{X}{x_{comp}} \ln\{\frac{1}{x_{comp}} \cdot \frac{X}{N}\}. \end{aligned} \tag{3.23}$$

The upper limit in Eq. (3.23), i.e. the maximal value for H, is obtained when $c_i = \{\frac{X}{x_{comp}} \cdot \frac{1}{N}\}$ for $\forall\, i$, that is, when there are equal numbers of clusters of the same size. This characteristic can be extended to general assembly processes, irrespective of the number of tiles or clusters.

The whole aggregation sequence can be quantified by the area covered by the DOP transition, namely:

$$H_{path} = \int_C H \, dC. \tag{3.24}$$

Figure 3.13 shows examples of clustering degrees with 6 modules in (a), and 12 modules in (b). The DOP of their intermediate states (left sides) are $H = 0.6452$ in (a), and $H = 1.2904$ in (b). Note that the DOP increases proportionately with the number of identical clusters. The concept can be extended and applied to assembly processes in general.

3.4.1 The case of 6 modules

In Figure 3.14, the DOP as a function of the global clustering degree C is shown for the case of 6 modules. Considering the combination patterns, the

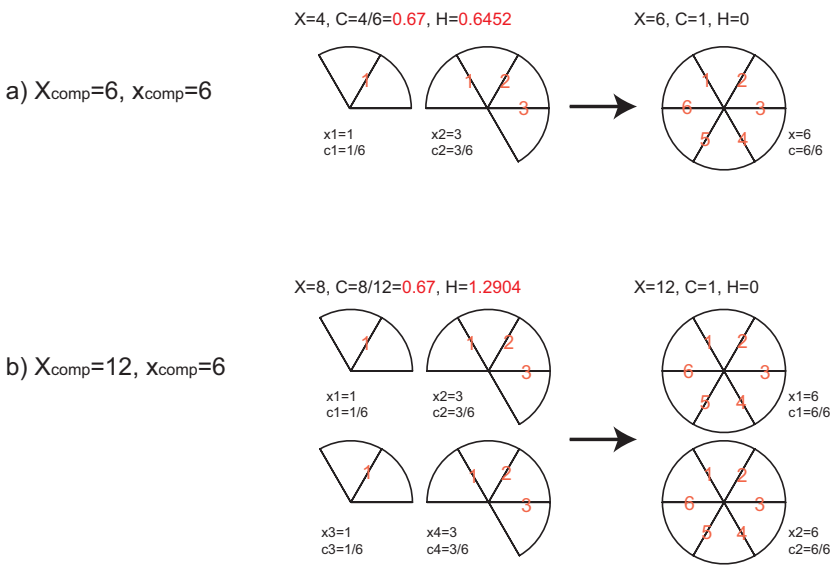

Figure 3.13: Examples of clustering degrees with 6 modules (a), and 12 modules (b). The DOP of their intermediate states (left sides) are $H = 0.6452$ in (a), and $H = 1.2904$ in (b). Note that DOP increases proportionately with the number of identical clusters.

probabilities of each transition are calculated and listed inside each path. The value P represents the probability of a state within the same C. For reference, the magnetic potential energies U are listed above each state.

The figure shows that as C increases, the DOP H increases, attaining a maximum for $C = 0.5$, and then decreasing to 0 for $C = 1$. Also, in each column (that is, within a group having the same number of connections), the more similar the clusters, the higher the DOP. In other words, high values are derived from states in which the connections are equally distributed. The highest DOP path (H_{path}), which goes through a state with $H = 0.8959$, has a value of 0.461, while the lowest DOP path has a value of 0.236 (which goes through a state with the lowest H). Note that the possible number of paths is 17 (neglecting disassembly), and the reactions always produce a full circle (the final state is marked with a yellow square).

3.4.2 The case of 7 modules

Conversely, the change in DOP for the case of 7 modules is shown in Figure 3.15. Surprisingly, the probability of configuring a full circle drops to 1/3 (the three possible final states are marked with yellow squares). Other configurations with $4 + 3$ clusters and $5 + 2$ clusters are calculated to both occur with a probability of 1/3. This is a typical illustration of the yield problem associated with self-assembly processes. Here the total number of paths is 25, if we neglect disassembly.

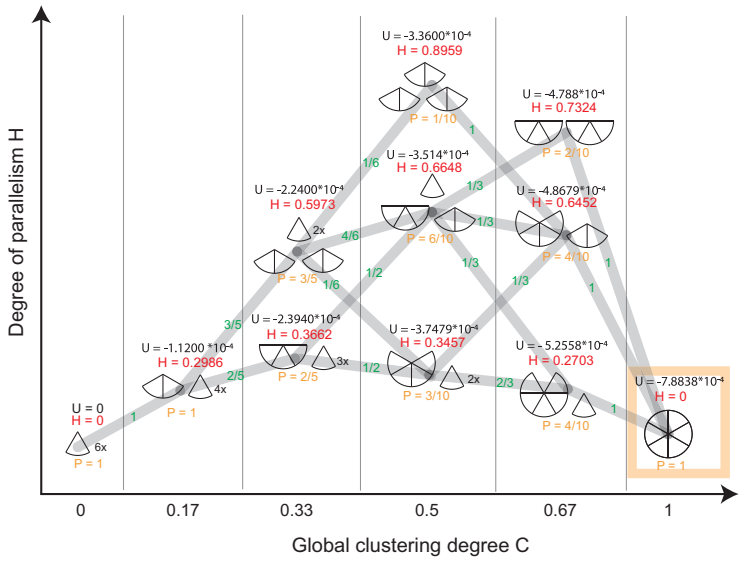

Figure 3.14: Change in DOP as a function of global clustering degree (6 modules). The more that assembly proceeds in parallel, the larger the value becomes. The highest DOP path (H_{path}), which goes through a state with $H = 0.8959$, has a value of 0.461, while the lowest has a value of 0.236 (which goes through a state with the lowest value of H). Note that the possible number of paths is 17 (without considering disassembly), and the reactions always produce a full circle (the final state is marked with a yellow square).

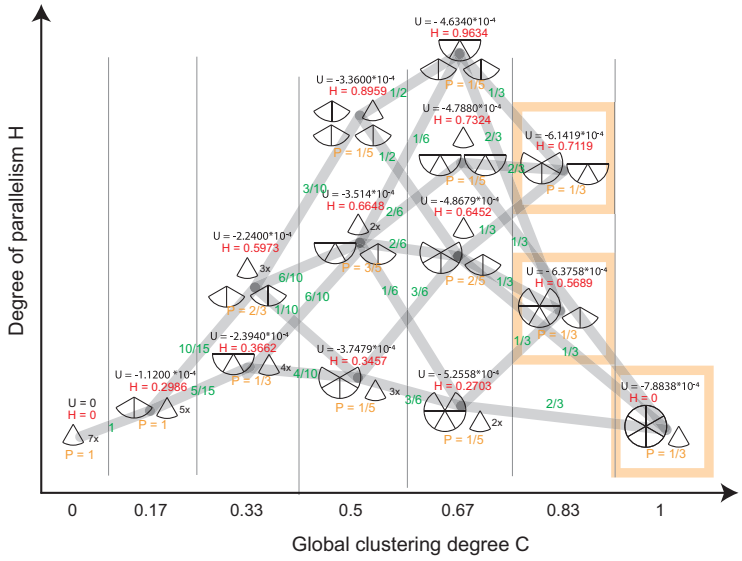

Figure 3.15: Change in DOP as a function of global clustering degree (7 modules). The probability of configuring a full circle drops to 1/3 (the three possible final states are marked with yellow squares).

3.5 Conclusion

This work showed an influence of reverse reactions on the improvement of yields of targeted products of stochastic self-assembly. By using a platform designed for the analysis of self-assembly systems, we observed a unique aggregation pattern at a specific stochasticity level - a number of modules instantly composed a product while avoiding converging to undesired geometric configurations. We hypothesized that this is mainly due to the disaggregation (reverse reaction) of undesired configurations that block the system, re-enabling modules to compose a product at a certain probability. We investigated the model using kinetic rate calculations and validated the hypothesis. In this regard, the discussion of the yield problem from a combinatorial perspective in Section 3.4 clearly depicts the causal reason. We believe this paper projects an insight on the macroscopic frame on chemical systems, and deepens the theoretical understanding to realize scalable self-assembly systems.

Appendix 3A - Diffusion by Random Walk

In our system, we suppose that a vibrating module randomly moves in a field, inducing Brownian-like motion. As a measure of a traveling diffusion, we consider a situation where a particle randomly moves in one dimension [44]. Given that the distance of each step is one, and the probability that the particle moves either left or right are both $\frac{1}{2}$. In order for the particle to be at position m after n steps, it should move + direction $\frac{n+m}{2}$ times, and - direction $\frac{n-m}{2}$ times. After n steps, the particle moves to + direction for $(n+m)/2$ times and to - direction for $(n-m)/2$ times in order to be at the position m after n steps. Considering that $(n+m)/2$ and $(n-m)/2$ are both integer number, the number of moving patterns of the particle can be given by

$$ {}_nP_{\frac{n+m}{2}} = \frac{n!}{\left(\frac{n+m}{2}\right)!\left(\frac{n-m}{2}\right)!}. \tag{3.25} $$

The number of possible movement after n steps is 2^n. Therefore the probability that the particle positions at position m after n steps $P(m,n)$ is

$$ P(m,n) = \frac{n!}{2^n\left(\frac{n+m}{2}\right)!\left(\frac{n-m}{2}\right)!}. \tag{3.26} $$

Suppose n and m are big enough, we assume $m/n \ll 1$. By utilizing Stirling's formula:

$$ \ln(x!) \simeq \left(x+\frac{1}{2}\right)\ln x - x + \frac{1}{2}\ln(2\pi) \tag{3.27} $$

we obtain

$$ \begin{aligned} \ln P(m,n) \quad \simeq \quad & \frac{1}{2}\ln\frac{2}{\pi n} - \frac{n}{2}\Big[\Big(1+\frac{m+1}{n}\Big)\ln\Big(1+\frac{m}{n}\Big) \\ & +\Big(1+\frac{1-m}{n}\Big)\ln\Big(1-\frac{m}{n}\Big)\Big]. \end{aligned} \tag{3.28} $$

Considering that $m/n \ll 1$, Eq. (3.28) can be transformed as

$$ \ln P(m,n) \simeq \frac{1}{2}\ln\frac{2}{\pi n} - \frac{n}{2}\Big(\frac{m}{n}\Big)^2 + \cdots. \tag{3.29} $$

Therefore the proportion of the probability is asymptotic to the following distribution:

$$P(m,n) \simeq \sqrt{\frac{2}{\pi n}} \exp\Big[-\frac{n}{2}\Big(\frac{m}{n}\Big)^2\Big]. \tag{3.30}$$

Supposing l_f as the step width, and τ_f as the time taken to move to the next site, we obtain $x = ml_f$ and $t = n\tau_f$. The probability that the particle can be observed in the region $[x, x + dx]$ is therefore given by

$$P(x,t)dx = P\Big(\frac{x}{l_f}, \frac{t}{\tau_f}\Big)\frac{dx}{2l_f}. \tag{3.31}$$

Considering that the diffusion coefficient D is described as

$$D = \frac{l_f^2}{2\tau_f} \tag{3.32}$$

we obtain

$$P(x,t)dx = \frac{1}{\sqrt{4\pi Dt}} \exp\Big(-\frac{x^2}{4Dt}\Big)dx. \tag{3.33}$$

The derived distribution shows that the positioning probability of x follows diffusion equation (cf. Eq. (1.4)). In our 2D system, however, due to the asymmetric motion induced by a vibration motor, the system often showed unique behaviors (see also Appendix 3B).

Appendix 3B - The Ability to Express Various Behaviors

Here we present examples of the diverse behaviors exhibited by the proposed models. Experiments carried out with various types of modules are shown in Figure 3.16 [7]. We used different types of primitive shapes, such as circles or triangles, and demonstrated their ability to express a range of behavior in different combinations. The modules containing vibration motors are indicated by "V". Some were powered via the ceiling plate (a, e, g, h), while the others were powered through a wire controlled by hand (c), or sustained by hand (b, d, f).

- **Figure 3.16 a: A set of homogeneous modules automatically aligns into a straight configuration.** Each rectangular module contains a vibration motor and a horizontally attached magnet directing to the long edges. The fluctuation breaks apart unstable formations (directing short edges together, which is a local minimum state) and causes the long edges to attach.
- **Figure 3.16 b: The large module at the center rotates the small modules around it. At the same time the small modules rotate individually.** One vibrating module is manually placed in the center. The magnets are vertically attached to all the modules attracting / repelling each other. Mutual attraction occurs between the large module

[7] Some of the movies can be seen at: http://tribolon.com/

at the center and the small modules around it, while the small modules repel and stay apart from one another. The movement of the large module forces the small modules to rotate around itself and at the same time they rotate in the opposite direction to the movement.

- **Figure 3.16 c: A vibrating module can produce a string of modules.** Modules with a magnetic north pointing upwards and those with a magnetic south pointing upwards can become wound around the manually fixed and controlled module rotating in the opposite direction.

- **Figure 3.16 d: A simple gear system is created by the combination of attractive magnetic forces and repulsive friction.** This example shows how far the rotational movement generated by the vibrating modules can be transferred. In general, a triangular module is able to trap a module at one side of the edges, due to the relatively short distances from the edges to the magnet.

- **Figure 3.16 e: Modules attract each other and create coupled modules (dimer).** One horizontal magnet attached to each 6 modules between the center and the end causes the formation of the couple, impeding the attachment of a third module.

- **Figure 3.16 f: A global rotational movement occurs through local interactions.** A triangular module rotates three circular modules along its edges. The friction from the triangular module causes the circular modules to move from the center of the edge, where the magnet is closest, and to push the edge of the triangle module. This imposes a rotational movement on the group.

- **Figure 3.16 g: A bike-like configuration follows the wall.** A triangular module with a vibration motor inertially follows the wall by striking it. Subsequently, when two circular modules are manually placed next to it, they turn into "wheels" and the whole cluster starts following the wall. This happens because the circular modules are attracted to the wall by capillary forces while the vibration motor pushes the wheels into one direction.

- **Figure 3.16 h: Bending motion can be achieved by exploiting shape.** Four modules contain vibration motors, and the magnets are attached horizontally (similar to case (a) above). By applying a voltage, the vibration motors rotate into the same directions and generate a bending force via friction. Also, an inverted voltage enables the cluster to bend in the opposite direction.

These examples are typical outcomes that we obtained with the described settings, though this does not mean that these are the only outcomes with the given configurations. Table 3.1 lists their properties (isometric configuration, stability of the product, motion, controllable parameter, function) attributed to the particular configurations shown in Figure 3.16 a to h, respectively. It should be mentioned that the reactions responsible for the structuring of the system act at a strictly local level, that is, all behaviors described above emerge spontaneously and autonomously through a decentralized process. Nevertheless,

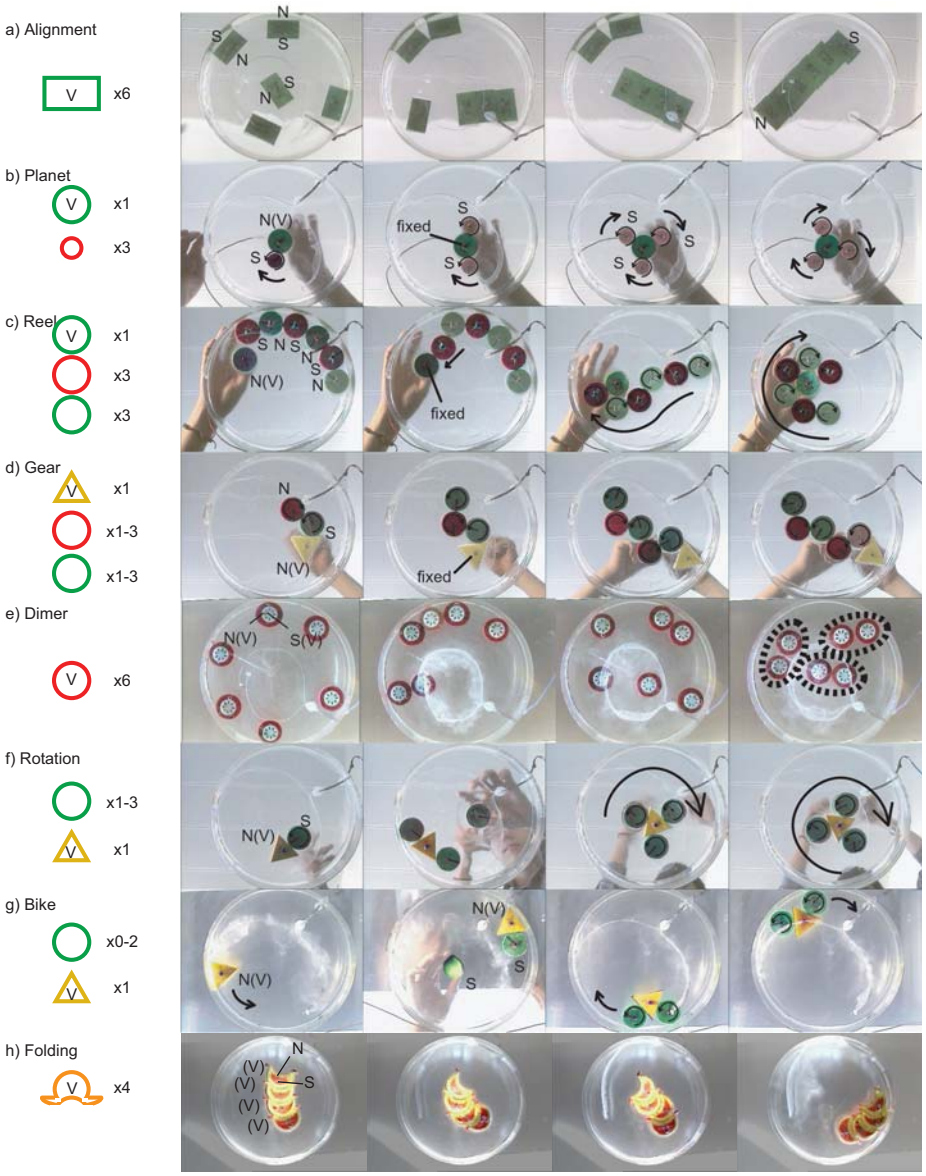

Figure 3.16: The ability to express various behaviors. The modules containing vibration motors are indicated with letters "V". Some modules were powered via the ceiling plate (a, e, g, h), while others were powered through a wire controlled by hand (c), or sustained by hand (b, d, f). The findings could shed light on how interaction between primitive organisms evolved. Some of the videos can be found at http://tribolon.com/

by contrast to traditional manufacturing processes, less control is required for the assembly. The process and the configurations are typically robust against unforeseen damage (a, b, e, g, h), implying that the system could recover from failures and external disturbances to some degree. A special attention is dragged by g, in which the compound acquires mobility function. The findings could shed

Table 3.1: Attributes of the systems shown in Figure 3.16 a to h.

	isometric	stability	motion	controllable parameter	functionality
a) Alignment	N	stable	static	-	-
b) Planet	N	stable	dynamic	rotational speed, number of passive modules	torque transformation
c) Reel	Y	-	dynamic	-	number and size of outer layer modules
d) Gear	Y	-	dynamic	size and number of modules	torque transformation
e) Dimer	N	stable	static	-	-
f) Rotation	N	-	dynamic	size of circular modules rotational speed	torque transformation
g) Bike	N	stable	dynamic	driving speed	**mobility**
h) Folding	N	stable	-	folding angle	distortion

light on how interaction between primitive organisms evolved.

We further investigated the assembly process presented in Figure 3.16 f, g. Figure 3.17 shows an example of the representative behavior observed in an experiment. We initially positioned three passive modules (colored green) along the wall such that they were equally distributed, and manually placed a module with a vibration motor (active module, colored white) at the center of the tank (Figure 3.17 **a**). Once a voltage was applied the following actions took place: an assembly motion (the 1st assembly, Figure 3.17 **b**), wall following behavior driven by the active triangle module (Figure 3.17 **c-d**), the 2nd and the 3rd assembly (3rd: Figure 3.17 **e**), rotational movement (Figure 3.17 **f**, **g**), and wall following (Figure 3.17 **h-j**). The rotational movements were observed when at least one passive module was attached to an active module, and the whole body has no contact to the wall. The assembly motion, the rotational movement, and

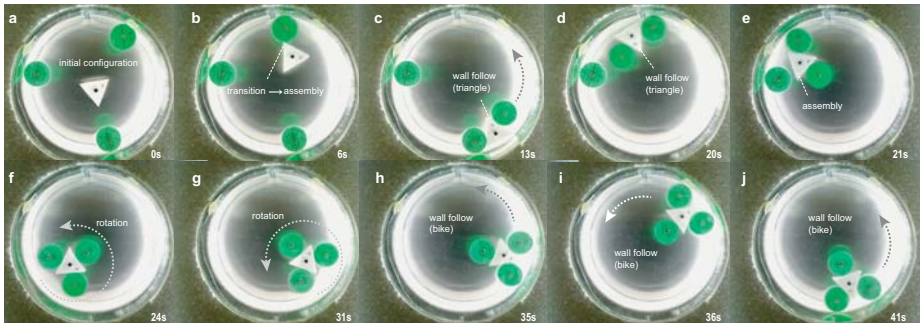

Figure 3.17: Typical observed behavior, consisting of assembly motion (1st assembly, Figure 3.17 **b**), wall following behavior driven by active triangle module (Figure 3.17 **c-d**), 3rd assembly (Figure 3.17 **e**), rotational movement (Figure 3.17 **f**, **g**), and wall following indirectly managed by passive modules (Figure 3.17 **h-j**).

the wall following behaviors can be recognized in Figure 3.18, where the time evolution of x-positions of all the modules are displayed. The rotation of the whole body can be recognized in 120°-phase delay (highlighted in dotted boxes),

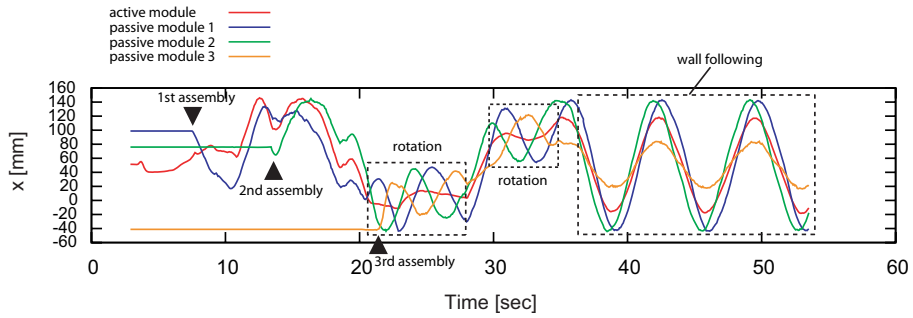

Figure 3.18: Time evolution of the x-positions of all the modules. The timing of assembly (indicated with triangular arrows), rotational movements, and wall following behaviors can be seen (highlighted in dotted boxes).

and the wall following behavior can be seen as coherent phases (highlighted in dotted boxes). These dynamical motions are thought to be attractors in the dynamical system.

In general, magnetic attraction, which plays the main role for the assembly process, merely works when modules are apart. An active module has to rove around the field to attain physical contacts to the passive modules. Figure 3.19 **a** shows the assembly time of 15 trials (n=15) that took for the 1st and the 2nd assembly. We treated some trials which doesn't show any assembly process for 30s as "trapped" trials and removed them from the statistics. Such "trapped" trials were observed 6 times out of 21 trials (therefore the success rate with two passive modules in this condition is 71.4 %). The measured average time for the 1st assembly was 2.92s, and for the 2nd assembly was 11.88s, which represents the ease of the 1st assembly compared to the 2nd. The observed trapped states

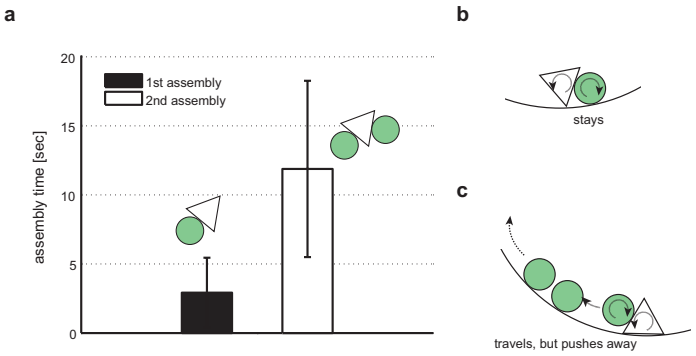

Figure 3.19: Assembly time (a, 7V), and "trapped" patterns (b, c).

are illustrated in Fig. 3.19 **b c**. Figure 3.19 **b** represents the state in which an active triangular module and a passive circular module pull each other in opposite directions. Consequently, the whole body stays. This convergence is avoided if there exists another active module, which is capable of promoting the couple of active and passive modules to escape from this state. Another observed converged state is illustrated in Figure 3.19 **c**, where the active module carrying an

passive module pushed other passive modules, and eventually hinders further assembly.

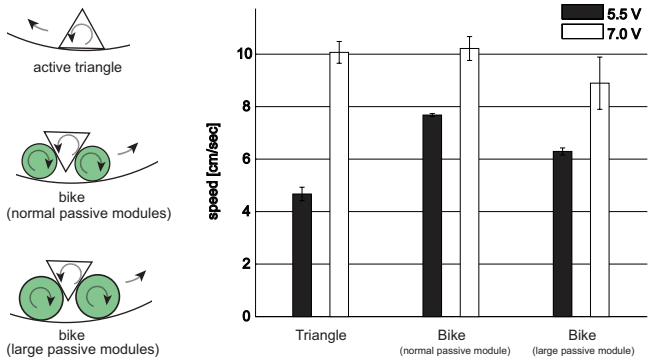

Figure 3.20: Velocity for the wall following behavior with different configurations (5.5V, 7V).

As we described above, the wall following behavior was observed (1) when an active triangle module kicks the wall by itself, and (2) when an active module kicks two attached passive modules (Figure 3.20, termed bike configuration). Adhesion force between the modules and the wall was provided by capillary force. We examined the velocity in the wall following behavior with respect to the applied voltage (Figure 3.20, the number of each trials is 5). In general, the higher the applied voltage was, the higher the velocity ($4.67\,cm$ to $10.07\,cm/s$ with triangle, and $7.68\,cm/s$ to $10.22\,cm/s$ with bike configuration). The speeds of triangle and bike configurations under $7\,V$ showed similar velocities[8]. In order to evaluate the influence of the size of the passive modules, we conducted similar experiments with large passive modules and measured the velocity (10 % increase in size, Fig. 3.20 **d**). Interestingly, the velocity decayed in both conditions (i.e. $5.5\,V$ and $7.0\,V$) with large passive modules (18.1 % decrease in the speed at $5.5\,V$, and 12.9 % decrease in the speed at $7.0\,V$ from normal bike configuration, respectively).

[8]Note that the velocities can be changed to negative by applying negative voltage to the system.

Chapter 4

Detection Mechanisms of Global Configurations

Sensor mounted model for logical self-assembly

Self-assembly is a process in which individual components form an organized structure as a consequence of local interactions. When using magnets to create interaction forces, the magnetic flux distribution of a self-assembling system changes as its assembly state varies. Since Hall-effect sensors are a convenient and effective means to detect changes in the magnetic field, we explore their applicability to monitoring the morphology of such magnetically self-assembling systems. We find that optimal positions for the sensor can be found where the flux changes maximally. Our analysis is applied to two different systems by deriving the flux changes for all possible states, and theoretical flux changes are verified with experiments. In addition, we show that a small number of sensors is sufficient for robust state determination. In addition to state detection, experiments show the potential for angle measurement for compliant cylindrical magnet joints using a single Hall-effect sensor.

keywords
magnetic flux distribution, Hall-effect sensor, global configuration, opto-coupler

[1]Parts of the material in this chapter previously appeared in; Z. Nagy, S. Miyashita, S. Muntwyler, Ashish K. Cherukuri, J. J. Abbott, R. Pfeifer and B. J. Nelson (2009) "Morphology Detection for Magnetically Self-Assembled Modular Robots", *IEEE/RSJ International Conference on Intelligent Robots and Systems (IROS)*, pp. 5281-5286.

4.1 Magnetic Detection

To study self-assembling systems at the cm scale, it is convenient to use magnets to provide sufficient interaction forces and torques, and thus motion, without the need for additional power. Magnetic interaction has been shown to scale favorably to the micro and nanodomain, implying that knowledge gained at the cm-scale will translate well to the sub-mm domain [22].

The morphology, i.e. the shape, of a magnetically self-assembled system is not only characterized by its geometrical boundary, but also by the distribution of the magnetic field—as the shape of the system changes, so does the magnetic field distribution. If this change is unique, then knowledge of the field variation leads to knowledge of the morphology variation. In this paper, we numerically and experimentally investigate the existence of such unique mappings for two different situations: detection of individual self-assembly states, i.e. online monitoring of the stochastic self-assembly process, and determination of the relative position of the modules separated by compliant joints.

In [66,69] the stochastically self-assembling Tribolon system was introduced. It consists of triangular modules floating on water and eventually assembling into a final, hexagonal configuration. The modules feature one magnet providing the intermodular attraction force, and a vibration motor generating a random motion component. The assembly of the final hexagonal configuration is known to be affected by the so-called yield problem, where clusters of either 4 or 5 modules cannot attach together and remain as "garbage" [46].

Another solution is based on low-level control in which case the formation of the clusters is restricted to a maximum of three modules and only such clusters can attach to one another. Our goal here is to achieve this end without the need for intermodular communication. This requires that the global information of the cluster size is available to each module locally. In Section 4.2 we propose a solution that allows a given module to detect its state transitions, and thus the size of the cluster it is in, and demonstrate simple behavior with three modules.

A Hall-effect sensor is a device for measuring magnetic fields. The main advantage of using Hall-effect sensors is that they can be sealed and used in harsh environments. Moreover they are able to sense magnetic fields beyond obstacles, also through the direct neighbor. The modules we used for the experiments are equilateral triangles (Figure 2). The magnet providing the attraction and bonding force between them is placed 15mm from the tip of the module facing left with its south pole. Two hall-effect sensors with a size of approximately $3 \times 4mm$ are placed on the edge of each module where the distance to the own magnet and the magnet of the neighbor is the shortest. Hall-effect sensors are widely used in position and orientation sensing applications, and, in this work, we are interested in their applicability to the detection of self-assembly states.

4.1.1 Detecting Changes in Magnetic Fields

The output voltage of the Hall-effect effect sensor we use in our experiments (A1302 from Allegro Microsystems Inc.) is proportional to the magnetic flux density across it. In particular, the change in voltage ΔV is related to the flux change $|\Delta \mathbf{B}|$ through the sensitivity $S = 13\text{mV/mT}$ of the sensor as $\Delta V = S|\Delta \mathbf{B}|$. The Hall-effect sensors are interfaced to a PC using a National Instruments USB-6008 data acquisition card and LabView.

We are interested in using as few sensors as possible to determine the required information. Therefore, we numerically determine the optimal position of the Hall-effect sensor for a given problem. This optimal position is characterized by the largest change in the magnetic flux as the system changes from one configuration to another and, thus, allows for the least ambiguous sensing of the state transition.

For the numerical optimization, the magnetic field of the magnets is computed using the surface charge models provided in [31] and partially reproduced in the Appendix. These equations can be used to determine the field of nearby multipole structures, and are computationally effective as no discretization of the space is necessary (as opposed to finite-element-based methods). When the inter-magnet distance is much larger than the magnet size, a simple point-dipole model is sufficient.

We begin by a qualitative analysis of the flux change. Let $\mathbf{B}_{\mathcal{S}_1}$ and $\mathbf{B}_{\mathcal{S}_2}$ be the flux distributions of a first shape $\mathcal{S}_1$ and a second shape $\mathcal{S}_2$, respectively. Then, for an arbitrary reference frame j

$$\begin{aligned} \mathbf{B}^{\mathbf{j}}_{\mathcal{S}_1}(\mathbf{x}^{\mathbf{j}}) &= \sum_{i=1}^{n} g_{ji}\mathbf{B}^{\mathbf{i}}(\mathbf{x}^{\mathbf{i}}) = \sum_{i=1}^{n} g_{ji}\mathbf{B}^{\mathbf{i}}(g_{ij}\mathbf{x}^{\mathbf{j}}), \text{ and} \\ \mathbf{B}^{\mathbf{j}}_{\mathcal{S}_2}(\mathbf{x}^{\mathbf{j}}) &= \sum_{i=1}^{n+m} g_{ji}\mathbf{B}^{\mathbf{i}}(\mathbf{x}^{\mathbf{i}}) = \sum_{i=1}^{n+m} g_{ji}\mathbf{B}^{\mathbf{i}}(g_{ij}\mathbf{x}^{\mathbf{j}}) \end{aligned}$$

where $\mathbf{x}^{\mathbf{j}} \in \mathbb{R}^3$ is the point where we are computing the field, expressed in the frame j, $\mathbf{B}^{\mathbf{i}}$ is the field of magnet i in its own frame i, g_{ji} is the homogeneous transformation from frame i to frame j, with $g_{ij} = g_{ji}^{-1}$, n is the number of magnets in the first shape, and m is the number of additional magnets in the second shape. The flux change at $\mathbf{x}^{\mathbf{j}}$ follows as

$$\Delta\mathbf{B}^{\mathbf{j}}(\mathbf{x}^{\mathbf{j}}) = \mathbf{B}^{\mathbf{j}}_{\mathcal{S}_2}(\mathbf{x}^{\mathbf{j}}) - \mathbf{B}^{\mathbf{j}}_{\mathcal{S}_1}(\mathbf{x}^{\mathbf{j}}) = \sum_{i=n+1}^{n+m} g_{ji}\mathbf{B}^{\mathbf{i}}(g_{ij}\mathbf{x}^{\mathbf{j}}) \tag{4.1}$$

That is, the flux change is simply equal to the flux of the additionally introduced magnets. In the simplest case ($n = m = 1$), $\mathbf{B_1}$ is provided by a single magnet on a given module, and $\Delta\mathbf{B}$ by a second magnet on another module. Thus, to optimally detect the presence of the second module with sensors inside the first module, the position of the maximal flux due to the second module's magnet occurring inside the first module is required. This position is close to the second magnet as the magnetic flux generally decreases with distance from a magnet. We conclude that the optimal position is near the boundary of the first module.

For the numerical analysis, the field equations are implemented in MATLAB and used in the numerical maximization of the flux change between two morphologies as follows. We choose $j = 1$, i.e. we express the fields in the frame of magnet 1 and omit the superscript from now on. We identify the different occurring shapes $\mathcal{S}$ and derive the transformations g_{1i}. Then, we use MATLAB's `fmincon` to solve the optimization problem in each component B_i of $\mathbf{B}$

$$\begin{aligned} &\text{minimize} && -\Delta B_i \\ &\text{subject to} && \mathbf{x} \in \mathcal{C}, \end{aligned} \tag{4.2}$$

and designate the optimal position as $\mathbf{x}^\star$, $\mathcal{C}$ designates the feasible region for $\mathbf{x}^\star$—that is, the region where we could realistically place a Hall-effect sensor. Considering the individual components in the optimization process, rather than the norm $|\Delta\mathbf{B}|$, also considers situations where $\mathbf{B}$ rotates while its magnitude remains constant. Additionally, if the optimal position for two components i and j is the same, an optimal orientation of the Hall-effect sensor can be derived as $\theta = \arctan(\Delta B_i/\Delta B_j)$.

4.2 The Model and Experiments

Self-assembling systems at the cm scale are typically considered as distributed systems, implying that there are uncertainties in the knowledge of the components' global information. Due to the lack of a central controlling system to coordinate and control the modules, each module is required to possess any necessary information of the global configuration. Fig. 4.1a) shows the Tribolon modules employed in this work. The modules are equilateral triangles (see Fig. 4.1b)), and the magnet ($B_r = 1.4$T) providing the attraction force between them is a cube of 5mm sidelength magnetized along the x-axis (perpendicular to the symmetry axis) and placed at $L = 15$mm from the tip of the module.

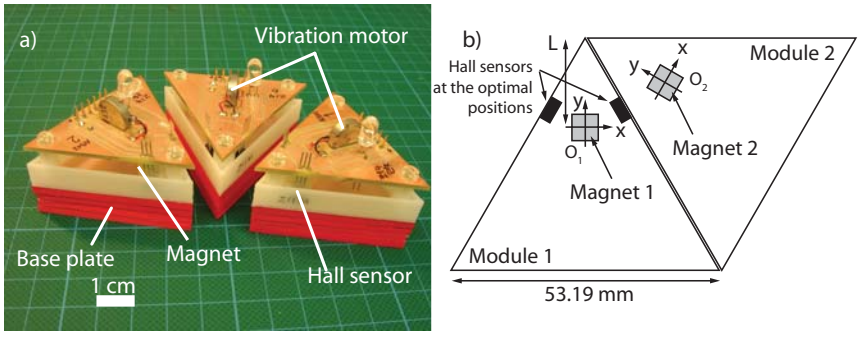

Figure 4.1: Tribolon modules. a) Photo, b) Employed coordinate frames.

The morphologies that may occur during the self-assembly process are depicted in Fig. 4.2. We wish to determine the number and position of the Hall-effect sensors to enable a given module to sense the size of the cluster it is in, i.e. know how many left and right neighbors it has. We begin by determining the optimal position to detect one neighbor—the situation depicted in Fig. 4.1b)—and define $\mathcal{S}_1$ as the state without any neighbor, and $\mathcal{S}_2$ as the state with one right neighbor (R). Then,

$$g_{12} = \begin{bmatrix} 1/2 & -\sqrt{3}/2 & 0 & \sqrt{3}L/2 \\ \sqrt{3}/2 & 1/2 & 0 & L/2 \\ 0 & 0 & 1 & 0 \\ 0 & 0 & 0 & 1 \end{bmatrix}. \tag{4.3}$$

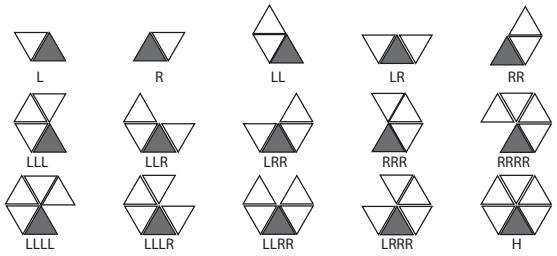

Figure 4.2: Possible morphologies that may occur during the Tribolon self-assembly process. The nomenclature reflects the number of (L)eft and (R)ight neighbors of the gray module, and H designates the self-assembled hexagon.

With the feasible region $\mathcal{C}$ being the whole module 1 except the position of the magnet, and $x_0 = [4, 4, 0]$mm, we find the optimal position to be at $\mathbf{x}^\star = [2.6, 9.8, 0]$mm, which is at the boundary of the module. Also, we find that the change of both flux components ΔB_x and ΔB_y is maximal at this position, therefore, the Hall-effect sensor should be oriented to capture the flux at the angle $\arctan(\Delta B_y/\Delta B_x) = \pi/6$ (perpendicular to the wall of the module).

We also find that the flux change at the symmetric position $\mathbf{x_2}^\star = [2.6, -9.8, 0]$ is negligible, therefore, it can be used to optimally detect a (L)eft neighbour. Thus, we equip the modules with two Hall-effect sensors at $\mathbf{x}^\star$ and $\mathbf{x_2}^\star$ and investigate this configuration for its utility in detecting state transitions. Fig. 4.3 shows the percentage change in the flux for both sensors for all possible state transitions (except for symmetry). We observe that every transition causes a flux change of at least 1% which can be detected with appropriate hardware. For robustness of detection, one could implement the possible transitions onto the module given a certain cluster size. Then, the number of possible transitions is greatly reduced. Either way, we conclude that the information on the global shape and size of the cluster, as well as the position of a given module inside this cluster, can be made available locally on the module.

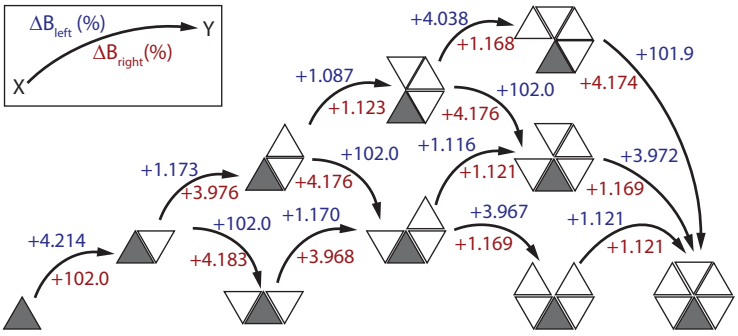

Figure 4.3: Flux change (in %) for two optimally positioned Hall-effect sensors on the gray module (see Fig. 4.1b)). Each state transition is unique and allows the gray module to monitor the size of the cluster.

Experimentally, we investigate the yield problem introduced earlier. To constraint the size of the cluster to three modules, it is necessary that a given module detects the states L, R, LL, LR, and RR. To show this, we implemented

the following simple rule on one module: run the vibration motor as long as the cluster size is 1 or 2, else stop it. Before running the experiment we determined the voltage limits of the Hall-effect sensors for the different states as shown in Table 4.1. The sensor readout and the motor power supply were passed from and to the module by means of a cable, and the control was done in LabView. The other two modules were passive, i.e. their sensors and motor information was not processed. Snapshots of typical assembly states are shown in Fig. 4.4 together with the state of the module (a movie is provided as supporting material).

Table 4.1: Voltage limits for the different Tribolon states

	Left Sensor		Right Sensor	
State	$V_{\max}$	$V_{\min}$	$V_{\max}$	$V_{\min}$
N	0.8	0.7	1.3	1.2
R	0.8	0.728	1.2	0.88
L	0.7	0.45	1.3	1.208
RR	0.8	0.7	0.873	0.85
LL	0.727	0.45	1.208	1.2
RL	0.8	0.43	0.879	0.8

We show the experimental result of the effect of a Hall-effect sensor in Figure 4.4. The insets in each window indicate the state of module a1 of the motor (green indicates that the motor is running) and the state of the hall-effect sensors (one green dot at one side indicates that there is one neighbor on that side; two dots indicate two neighbors at that side.) of the controlled module.

In a), the motor is running, all the neighbors keep enough distance and hence are not detected. In b), the motor is running and one neighbor is connected and detected on the left side of the module. In c) and d) the motor is turned off because two modules are detected. The process of neighbor detection is efficient because it exploits the characteristics of the decay of magnetic strength with respect to the distance (inversely proportional to the 4th power of distance).

4.3 Conclusions & Future Work

Based on the premise that the flux distribution of a magnetically self-assembling system changes as its geometric shape changes, we have shown that linear Hall-effect sensors can be used to uniquely identify the current state of the system. In addition, we have numerically derived optimal locations and orientations for the sensors for maximal flux change. We have also demonstrated the efficiency of Hall-effect sensors because the number of the necessary sensors for unique state detection can be very low.

Only two sensors per module allow the distinction between sixteen shapes. This enables a given module to have local information on the global morphology of the cluster it is in.

In addition to the examples presented in this work, our methodology can readily be extended to virtually any system undergoing a flux distribution change upon shape change.

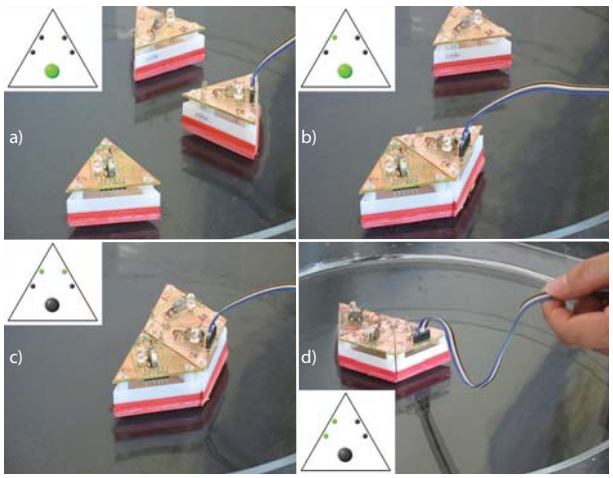

Figure 4.4: Example for Tribolon state transition. In a), the motor is running, all the neighbors keep enough distance and hence are not detected. In b), the motor is running and one neighbor is connected and detected on the left side of the module. In c) and d) the motor is turned off because two modules are detected. The process of neighbor detection is efficient because it exploits the characteristics of the decay of magnetic strength with respect to the distance (inversely proportional to the 4th power of distance). (see Fig. 4.2)

Appendix 4A - Surface Charge Models

For a rectangular bar magnet with edge coordinates (x_1, x_2), (y_1, y_2), and (z_1, z_2), and magnetization $\mathbf{M} = [0, 0, M_s]^T$ the $\mathbf{B}$-field outside the magnet is given by

$$
\begin{aligned}
B_x(x,y,z) &= \frac{\mu_0 M_s}{4\pi} \sum_{k=1}^{2} \sum_{m=1}^{2} (-1)^{k+m} \\
&\quad \times \ln\left[F(x,y,z,x_m,y_1,y_2,z_k)\right] \\
B_y(x,y,z) &= \frac{\mu_0 M_s}{4\pi} \sum_{k=1}^{2} \sum_{m=1}^{2} (-1)^{k+m} \\
&\quad \times \ln\left[H(x,y,z,x_1,x_2,y_m,z_k)\right] \\
B_z(x,y,z) &= \frac{\mu_0 M_s}{4\pi} \sum_{k=1}^{2} \sum_{n=1}^{2} \sum_{m=1}^{2} (-1)^{k+n+m} \\
&\quad \times \arctan\left[\frac{(x-x_n)(y-y_m)}{(z-z_k)}\right. \\
&\quad \left. \times\, g(x,y,z,x_n,y_m,z_k)\right]
\end{aligned}
$$

with the remanence being $B_r = \mu_0 M_s$, and

$$
\begin{aligned}
F &= \frac{(y-y_1)+[(x-x_m)^2+(y-y_1)^2+(z-z_k)^2]^{1/2}}{(y-y_2)+[(x-x_m)^2+(y-y_2)^2+(z-z_k)^2]^{1/2}} \\
H &= \frac{(x-x_1)+[(x-x_1)^2+(y-y_m)^2+(z-z_k)^2]^{1/2}}{(x-x_2)+[(x-x_2)^2+(y-y_m)^2+(z-z_k)^2]^{1/2}} \\
g &= \frac{1}{[(x-x_n)^2+(y-y_m)^2+(z-z_k)^2]^{1/2}}
\end{aligned}
$$

More details on surface charge models can be found in [31].

Appendix 4B - Consequential Attraction

In self-assembly systems at the macroscopic scale (including our platform), generally exploit magnetic attraction as a long-range interactive force. However, the magnetic force decays in proportional to the distance of the order of 4 (r^{-4}), which acts as relatively short-range force. As Boncheva *et al.* mentioned once in his optimistic eye on the possibility in employing magnetism for self-assembly; *"The solutions developed for self-assembly in nature may not be optimal for self-assembly using non-biological components. As one example, magnetic interactions are essentially never used in self-assembly in biology"* [14], molecular systems utilize environmental diffusion as traveling aid and achieve high efficient assembly matching per unit time. This provides us with a good reasoning especially in a circumstance of utilizing small size magnets are preferable. In our case, where diffusions could aid magnetic systems, the same effect of attraction can be realized by stopping repulsion (here vibrational motion) at an appropriate position.

For the investigation of this scenario – consequential attraction, we focus on opto-couplers as sensors. An opto-coupler is an electrical device which optically detects the presence of an object in front. It consists of a pair of infrared light emitter and detector and the maximum detectable distance that we used varies from 3mm to 15mm according to the adjustment setting. This infrared emitter/detector is a compact-package of phototransistor output and reflective photo interrupter, with emitter and detector facing the same direction.

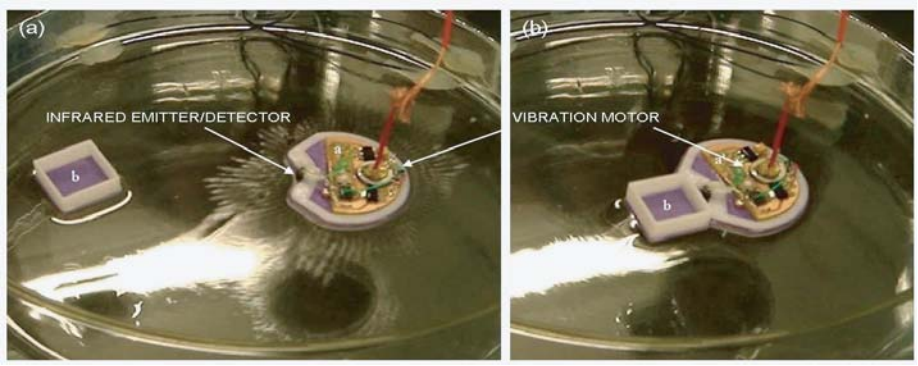

Figure 4.5: Demonstration of halting vibration with an opto-coupler model.

The effect is demonstrated in Figure 4.5, in which a module with an embedded opto-coupler detected a square-shaped objects and stopped its vibrational motion. Note that if the module does not stop the motion, the square object would leave from the place.

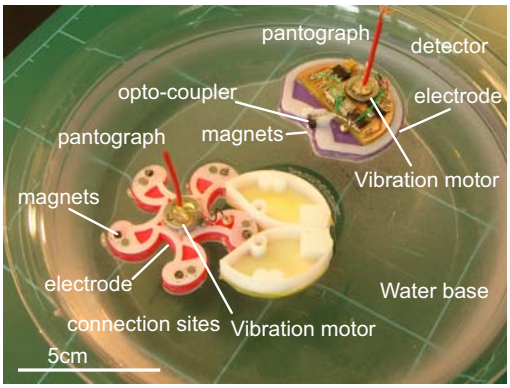

Figure 4.6: The developed system. The purple module (detector) features opto-coupler, and the red module (connection sites) possesses 10 magnets in which 2 of them are placed in pairs orienting opposite direction.

For the experiments, a module (termed *detector*) featuring an opto-coupler (purple color module in Figure 4.6), and a module with 5 magnetized bonding sites (red color module in Figure 4.6) were installed. Both modules are equipped with vibration motors, a pantograph systems, and (a) pairs of magnets, such that they attract each other (the red module (termed *connection sites*) is equipped with 10 magnets in which 2 of them are placed in pairs orienting opposite direction).

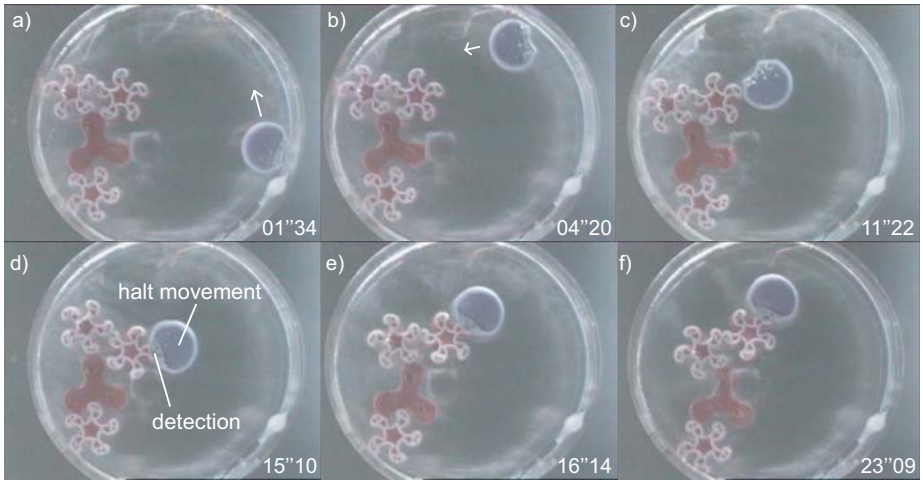

Figure 4.7: Snapshots of the experiment. It is shown that the detector collides into bonding sites (c), and eventually attracted by magnets of bonding sites when it got close to the bonding sites (d). After all, halting motion of the detector can be recognized in (e, f).

We show an exemplary experimental result in Figure 4.7 with the snapshots. It is shown that the detector collides into bonding sites (Figure 4.7 c) following the wall of arena (Figure 4.7 a b), and eventually attracted by magnets of bonding sites when it got close to the bonding sites (Figure 4.7 d). After all, halting motion of the detector can be recognized in (Figure 4.7 e f).

Chapter 5

Peltier-Based Freeze-Thaw Connector for Logical Self-Assembly

Connector mounted model for logical self-assembly

Manufacturing technologies and industries heavily rely on robots. For macroscopic objects industrial robots are not only economical but are also reliable, fast, and accurate. Such robots, however, hit a barrier – entailing lower yields and higher fabrication costs – as the assembled objects become too complex. One potential solution to this problem is to exploit processes of self-assembly, that is, processes in which the interaction of pre-existing components leads to organized structures without human intervention. Such components could be, for instance, identical mechanical units (modules). Self-assembly is of crucial importance in the biological realm at all scales, e.g. for the formation of the protein shells of viruses and for cell organization. In this chapter, we present a novel type of inter-module connection mechanism for waterborne modular robotic systems. The proposed mechanism exploits the thermoelectric effect to cool down and freeze the water between two modules thus causes them to attach to each other. We validate the feasibility of this mechanism by embedding a Peltier heat pump ($m = 0.8\,g$) in two types of *cm* scale self-assembly systems, one in which the modules are free to move and one in which the modules are linked together by hinges. Our experimental results demonstrate that the proposed Peltier-based connector has (a) a high bond strength/weight ratio for a rather large range of temperatures and (b) is rather robust against misalignments between docking modules, making it a useful alternative to current connection mechanisms for small scale high autonomy self-assembly systems.

keywords
Peltier Freeze-Thaw Connector, self-reconfigurable robot, self-assembly, hinge, chain, degree of freedom

[1]Parts of the material in this chapter previously appeared in; S. Miyashita, F. Casanova, M. Lungarella and R. Pfeifer (2008) "Peltier-Based Freeze-Thaw Connector for Waterborne Self-Assembly Systems", *IEEE/RSJ International Conference on Intelligent Robots and Systems (IROS)*, pp. 1325-1330.

5.1 Related Work

By taking inspiration from nature, many inroads have already been made to realize self-assembly systems. For instance, the possibility of using self-assembly for the fabrication of structures from a given set components (potentially of nano- or micrometer scale) has been suggested by Winfree [123], Rothemund [92] or Whitesides *et. al* [12, 16, 62, 122]. In the related field of self-reconfigurable systems, research effort has been devoted to realizing robots that can rearrange the connectivity of their structural units and create new topologies to accomplish a task [72]. Special attention has been paid to the design and construction of basic building blocks of a typically small repertoire, binding or docking interfaces allowing transfer of mechanical forces and moments, electrical power, and the sharing of information between the modules [18, 19, 24, 30, 53, 57, 76–78, 93, 126, 131].

Most modular systems are "deterministically self-reconfigurable" implying that the exact location of the unit is known all the time. That is, the units are moved or directly manipulated into their target locations through deliberate active motion. In contrast to such systems, self-assembly systems are "stochastically self-reconfigurable" implying that (1) there are uncertainties in the knowledge of the modules' location (the location is known exactly only when the unit docks to the main structure); and (2) the modules have only limited (or no) computational (deliberative) abilities. To date, a few self-reconfigurable modular robots relying on stochastic self-assembly have been built [8, 38, 69, 82, 102, 119, 120]. Although in all these systems the units interact asynchronously and concurrently, a certain amount of state-based control is still required for the modules to move, communicate, and dock. Such docking/undocking is one of the main challenges towards the realization of self-assembly system (other two challenges are how to actuate the modules, so that they can move, and how to supply power to them).

In this paper, we address the docking/undocking challenge by presenting the design and construction of a novel kind of connection mechanism. The connector works by freezing water close to it so that when another module is in its neighborhood, the two modules stick to each other. We also show how this connector can be embedded in a stochastic modular robot. In the following section 5.2, we provide a brief review of available connection mechanisms with a special emphasis on the ones used in the field of modular robotics. Then, in section 5.3, we describe our Peltier-based freezing-thawing connection mechanism and validate its functioning as a connector. In section 5.4, we describe the experiments of proposed connector by embedding it into a group of modular robots. This is followed by a discussion (section 5.5), some pointers to future work and a brief conclusion (section 5.6).

5.2 Connection mechanism

Table 5.1: Classes of connectors (μm - cm scale)

type	sub-type	main problem	reference
surface tension	-	weak bond / controllability	Boncheva 2003 [12], Rothemund 2000 [92], Hosokawa *et al.* 2005 [47], Bowden *et al.* 1997 [16], Chengde Mao *et al.* 2002 [62]
permanent magnets	-	detachment	Hosokawa *et al.* 1994 [46]
	+ electrical actuator	heavy weight	Bishop *et al.* 2005 [8]
	+ SMA spring	duration to detach	Murata *et al.* 1999 [78]
electrical magnets	-	strength-to-weight ratio	Murata 1994 [76]
	+ electrical actuator	heavy weight	Kotay *et al.* 1998 [57], Zykov *et al.* 2005 [131], Bhat *et al.* 2006 [7]
mechanical (hook, latch, lock)	-	actuation / alignment	Penrose 1959 [87] [a]
	+ electrical actuator	heavy weight	Yim 1994 [126], Rus *et al.* 2001 [93], Jørgensen *et al.* 2004 [53], Murata *et al.* 1998 [77], Terada *et al.* 2004 [109]
	+ electrical magnets		Griffith 2005 [38]
	+ SMA		Fukuda *et al.* 1988 [30], Castano et al. 2002 [18]
Velcro	-	detachment	
	+ pneumatic actuator	energy consumption	Shimizu *et al.* 2005 [102]
	+ electrical actuator	heavy weight	Moeckel *et al.* 2005 [71]
Peltier	-	heat dissipation	López *et al.* 2007 [117] [b]

[a] turbulence was controlled
[b] as a microgripper

For a modular robot, the ability to attach to and detach from another module or to parts of the environment is of fundamental importance. With the connection mechanism introduced in this paper we tackle the following problems that arise especially at smaller scales (<1 *cm*): (1) The actuation that is necessary for mechanical connectors is not easy to scale down. (2) The connection strength has to be sufficiently strong to fulfill the robot's purpose. (3) The precise alignment of the connector is crucial for a successful binding for some connection types. (4) The electromechanical complexity of the connector has to be small enough to allow for mass fabrication.

Table 5.1 lists various popular connection types for modular robots. In what follows, we will review some of them.

The exploitation of surface tension through the use of hydrophilic and hydrophobic materials provides a binding mechanism for modular robots in a fluidic environment that is often used for research on *cm*-scale stochastic self-assembly systems [12, 16, 47, 62]. The connection strength is weak compared to other mechanisms but is sufficient because the modules are lightweight. Additional properties make this mechanism useful: (1) no power has to be provided for attachment and detachment; (2) the alignment is done by the connecting force itself; and (3) the connection mechanism is easy to produce.

Permanent magnets are a second type of popular connection mechanism for modular robots. They have many useful properties: (1) they do not require any power for binding; (2) the relatively strong attractive force eases the alignment problem; and (3) they are rather straightforward to manufacture. However, because their attractive force is constantly active, a repelling force is necessary to revoke the connection. Some robots use a mechanism to push modules away from each other until the attraction force has no more effect, for example with a Shape Memory Alloy (SMA) [78]. Others rotate the permanent magnets so that they repel each other [8]. Permanent magnets are useful at the *cm* scale though their attractive force decreases with third power with respect to the size.

A third type of popular connection mechanism are electro-magnets. They allow for selective connections and are simple to fabricate and implement. However, they need to be constantly powered to ensure the connection, and their strength-to-weight ratio decreases with size. It follows that for the use on a scale smaller than the *cm* scale they are not applicable.

Mechanical connectors such as latches, lock and key, as well as hooking mechanisms provide a high connection strength. The docking and undocking is usually driven by electrical motors. However, they are not a viable solution at small scales because of the high demands on the precision of the required alignment. Furthermore, it is a difficult engineering task to build and actuate small and robust mechanical systems.

Velcro has the advantage that the connection mechanism itself does not have to be actuated [71, 102]. A repelling force has to be provided only for the detachment (through an actuator). A further advantage of Velcro is that it does not have to be aligned precisely to connect and also works at small scales.

5.3 Peltier-based freeze-thaw connector for lightweight self-assembly robots

The size of 1 *cm* is a critical size for self-assembly systems. For objects in water around that size, viscosity is as important as inertia; for such objects, the Reynolds number (the ratio of inertial forces and viscous forces) is ≈ 1. It follows that objects smaller than that size are affected more by viscous forces whereas larger objects are affected more by inertial forces. In order to make a step towards smaller and more lightweight systems, we propose a novel connection mechanism: the water close to the docking interface of one module is frozen to ice building a local bridge to another module.

5.3.1 The Peltier connector

The core of our connector is the Peltier heat pump – a double-faced cooling-heating device that can transfer thermal energy from one side of the device to the other, with consumption of electrical energy. We used the Peltier device to freeze (and thaw) the water between two modules and thus realize binding (and unbinding) between modules. The polarity of the current applied to the device defines which side is cooled down or heated up. The device consists of different types of semiconducting materials that are connected in series to take advantage of the so-called thermoelectric or Peltier effect. This effect is the direct conversion of an electric voltage into a temperature difference and *vice versa*, and allows the element to work as a heat pump. Peltier devices are available in various sizes. For our purpose we used an 8×8 *mm* element that weighs 0.8 *g* (Fig. 5.1). Theoretically, the Peltier heat pump can induce a temperature difference of up to 72 $^\circ C$ while consuming approximatively 2.60 W. The connection mechanism is as listed in Figure 5.1 c). The faces of Peltier elements are initially organized such that the water within the gap can be cooled down by running current. The energy pured in is enough to alter the hydrogen bond of water, and to structure a piece of ice between the Peltier elements. We expect the ice formed is strong enough to sustain the physical connection of the Peltier elements.

One particular advantage of this type of inter-module connection mechanism is due to the absence of mechanical parts which makes it scalable. The fact that the connector is devoid of moving parts makes it also intrinsically less prone to failures. One disadvantage is that in order to sustain the connections, energy has to be supplied permanently to the heat pump. For the detachment process, however, there is no need to supply energy because the ice melts when it is not cooled down; moreover, the flow of heat from the hot surface supports the thawing process speeding it up.

Figure 5.2 demonstrates the strong force that can be achieved with two Peltiers. The precisely measured data will be listed in Chapter 5.3.2.

5.3.2 Feasibility study

To confirm the use of Peltier devices to build a connector, we conducted two experiments. First, we tested the connector's functionality for different water temperatures. Second, we measured how much force was required to separate

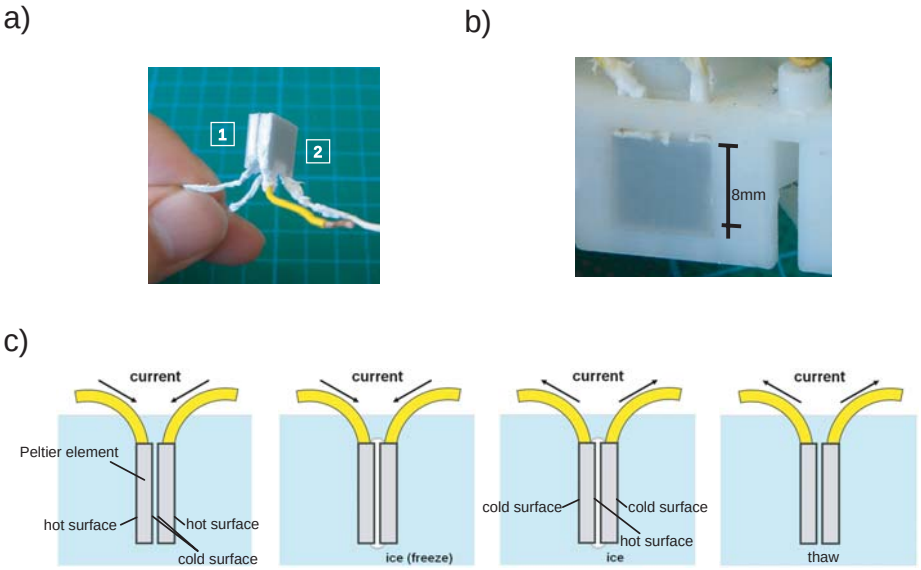

Figure 5.1: Illustration of Peltier elements. a) Frozen Peltier elements ($8 \times 8\ mm$) sticking together. b) A Peltier element embedded into a module. c) The proposed connection mechanism.

Figure 5.2: Strong sticking force by Peltier elements.

two modules (once they had connected to each other) also for different water temperatures.

Table 5.2 shows the conditions for which a connection was realized as a function of the voltage V applied to the Peltier elements and the time T necessary to achieve a connection. On average it took about one minute to establish a connection. For low temperatures and high voltages the two Peltier devices bound quickly to each other, for higher temperatures, however, the required time increased (e.g. at room temperature for $V = 2\ V$, it took $T = 3\ min$).

Although the time for the connection takes more time than for most other types of interconnection, the duration and the energy required for freezing decreases with the square of the size of the element's active area (the smallest commercially available Peltier elements have an area of approximately 1 mm^2, and we assume that a reduction in size can solve the heat dissipation problem which comes with this device).

We measured the bond strength for several water temperatures by applying a force perpendicular to the binding side until the connection broke (Fig. 5.3). A voltage of $V = 2\ V$ was applied to two Peltier elements for 60 seconds to bond, and the two elements were separated by hand from each other. On average,

Table 5.2: Experimental results of establishing a connection under different conditions ($Voltage$ [V], $Time$ [$seconds$]).

water temperature 0 °C

$V \setminus T$	30 s	60 s	120 s
0.5 V	×	√	√
1 V	√	√	√
2 V	√	√	√

water temperature 5 ° C

$V \setminus T$	30 s	60 s	120 s
0.5 V	×	×	×
1 V	×	×	√
2 V	√	√	√

water temperature 10 °C

$V \setminus T$	30 s	60 s	120 s
0.5 V	×	×	×
1 V	×	×	√
2 V	√	√	√

water temperature 15 °C

$V \setminus$ T	30 s	60 s	120 s
0.5 V	×	×	×
1 V	×	×	×
2 V	√	√	√

the connector withstood a pulling force of 17.56 N (the standard deviation was $\sigma = 2.03$). Considering the weight cumulated of the two Peltier elements (1.6 g), it becomes clear that the bond strength/weight ratio is higher than for other known connection mechanisms (Table 5.1). Moreover, we observe that the bonding force remaines roughly constant for different water temperatures. This is because the volume of ice that the two Peltier elements built up stayed relatively constant irrespective of the water temperature. A further advantage is that in order to connect, the two Peltier elements do not have to be aligned precisely. This property allows the system to be not only strong and scalable, but also robust to misalignments.

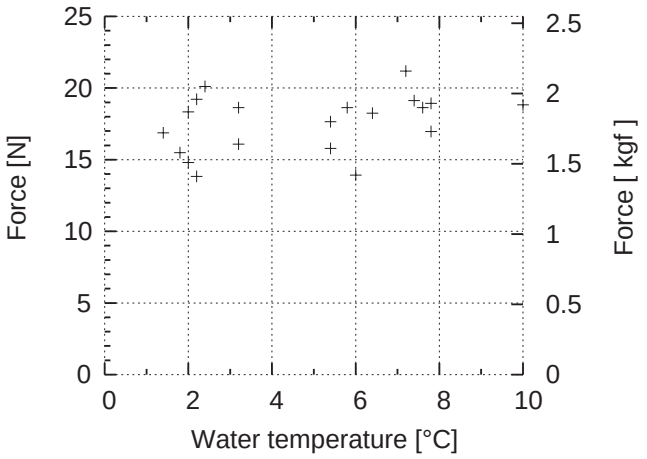

Figure 5.3: Temperature - bonding strength comparison. X-axis: water temperature [°C], Y-axis: force to detach [N, kgf]

5.3.3 Scalability

Figure 5.4 lists required energy to cool down a surface of Peltier element for 1 °C depending on the size (samples are taken from the products listed in the

website of Quick-Ohm Kupper & Co. Gmbh). The shown plots obey power-law,

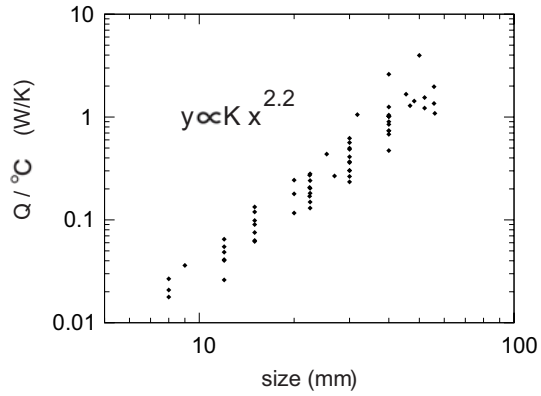

Figure 5.4: Required energy to cool down a surface of Peltier element for 1 °C depending on the size (samples are taken from the products listed in the website of Quick-Ohm Kupper & Co. Gmbh).

showing the competency of smaller device use.

5.4 Implementation of the Peltier connectors to Self-assembly robots

Followed by the feasibility of the connector idea (described in Section 5.3), we embedded the Peltier-based connector into two types of stochastic modular robots.

5.4.1 Kite-shaped model

The experimental setup was composed of a power supply, a metallic ceiling, a water tank, and six modules immersed halfway in water (Fig. 5.5). Each module consisted of a kite-shaped wedge made of durable plastic (acrylnitrile butadene styrene; ABS) spanning angles of 60 degrees and 30 degrees. The modules (H: 13 mm, L: 30 mm) contained a permanent magnet oriented orthogonally to their main axis to attract or repel other modules (Fig. 5.6 a). A vibration motor was used to endow the modules with a minimal locomotive ability which allowed the modules to move randomly around – vaguely reminescent of Brownian motion. Rather than using batteries, electricity was supplied to the modules through a pantograph that drew current from a metal ceiling. This solution not only led to lightweight modules ($m = 6.0\ g$), but it ensured that all modules received approximately the same amount of energy in a particular experiment. When an electrical potential was applied to the metallic ceiling plate, current flowed through the pantograph to the vibration motor returning to ground via the electrodes (platinum) immersed in the water (8 % concentration of electrolyte (salt) was added to the water to make it conductive). To speed up the connection between two modules, the water in which the modules moved was cooled down to approximately -3 °C (due to the concentration of salt this was slightly higher than the freezing temperature). Two diodes were used to switch

the direction of the current. Current flowed either through the Peltier element or the vibration motor depending on the direction of the voltage applied to the system (Fig. 5.5c, switch).

We first carried out experiments to test the reliability of the connector and to investigate the reconfigurability of our self-assembly system. The result is shown in Fig. 5.6. In the beginning of the experiment the modules were placed in the arena (Fig. 5.6 a) and arranged by hand to form a hexagonal shape (Fig. 5.6 b). Voltage was applied via the metallic ceiling (Fig. 5.6 c). After one minute, all six modules were connected to each other forming one unit (Fig. 5.6 d). We then flipped the polarity of the current supplied through the pantograph. The Peltier connectors stopped cooling and the vibration motors started to vibrate causing a disassembly of the hexagonal shape into 6 separate modules (Fig. 5.6 e). As a result of the vibrations of the motor, the modules moved around in the arena where they eventually got magnetically attracted by another module and started to form triangles (Fig. 5.6 f,g). The experiment was considered completed when the six modules had formed two triangles (Fig. 5.6 h). We conducted the experiment several times. For sufficiently long waiting times T, we always observed two different ways of convergence to the final states: one is in Fig. 5.6h (two 3-clusters), the other is three 2-clusters (not on the picture, yield problem [46]).

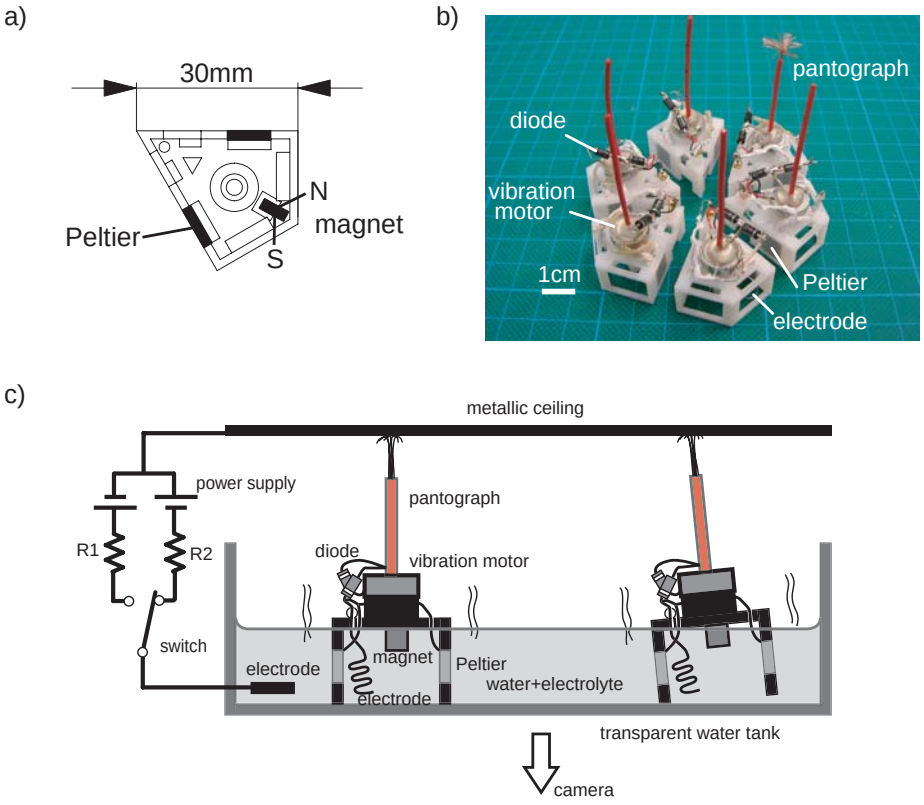

Figure 5.5: Experimental setup. a) Schematic illustration of a module (bottom view). b) Picture of 6 modules. c) Experimental setup with 2 modules.

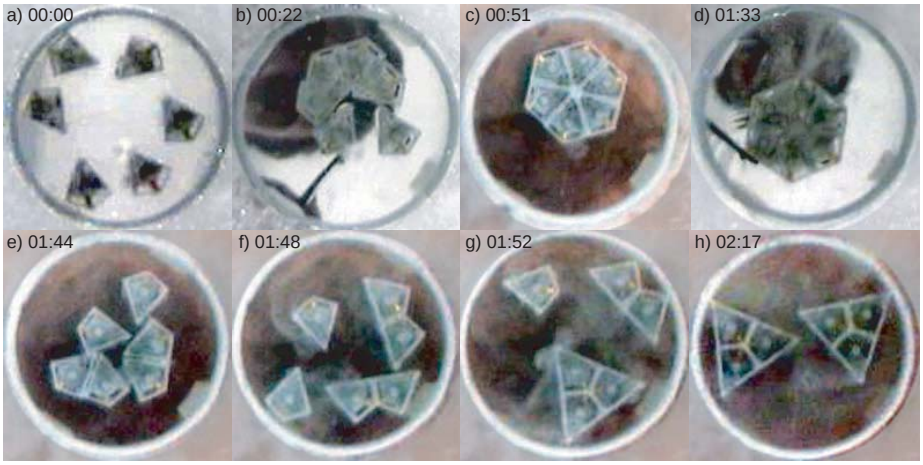

Figure 5.6: Snapshots of the experiment. Initially, the modules were arranged by hand to form a hexagonal shape (a-b). Voltage was then applied via the metallic ceiling (c). After a minute, all six modules were connected to each other forming one unit (d). We then flipped the polarity of the current supplied through the pantograph. The Peltier connectors stopped cooling and the vibration motors started to vibrate causing a disassembly of the hexagonal shape into 6 separate modules (e). As a result of the vibrations of the motor, the modules moved around in the arena where they eventually got magnetically attracted by another module and started to form triangles (f,g). The experiment was considered completed when the six modules had formed two triangles (h).

5.4.2 Hinge-connected chain model

The outcome of the experiments described in section 5.4.1 led to the question of how to take our modular system to another level of operation. To answer this question, we took inspiration from protein folding and linked modules through hinge joints and formed a chain model expecting a drastic reduction of dimensionality of the search space (Fig. 5.8, $m = 12.8\ g$). As a case study to see the effect of designed chain model, we set the task such that a configuration of a system scales up the size through self-assembly, sustaining the same geometry after all.

The main advantage of this implementation is that it avoids a crucial problem: the increased number of magnets generates also undesired configurations. Note that the positions of all the other magnets were replaced and rearranged. Only the center module (red colored, Fig. 5.8b) had a large magnet oriented orthogonally to the symmetry axis. The other small cylindrical magnets were oriented vertically – "S"outh poles attracting "N"orth poles and *vice versa*. As in the modules described in the previous section, diodes were used to direct the current flow. Depending on the polarity of the applied voltage, current only flowed either through the Peltier elements ($12\ V$) or through the vibration motors ($10\ V$).

The aimed reconfiguration process is shown in Fig. 5.8. Initially, two modules are connected by Peltier connector and form a hexagonal shape. By applying inverted current, it can unfreeze the connection and eventually configure an triangle guided by magnets inserted to the module. Once the triangular shape

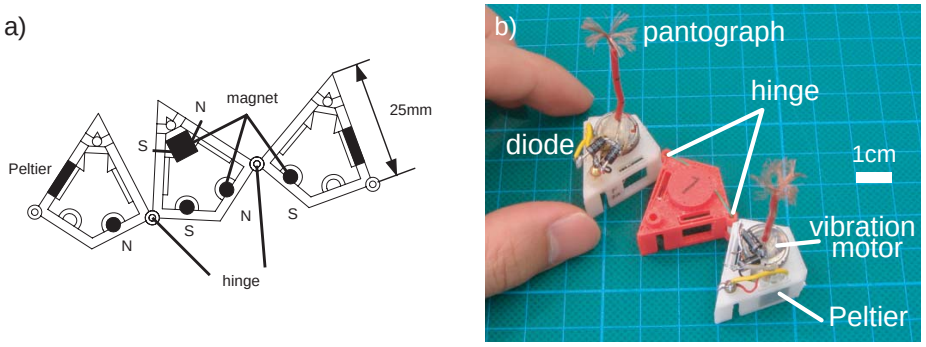

Figure 5.7: Chain model. a) Schematic illustration of a chain. b) Picture of a chain. Three modules are connected by hinges.

is formed, using the large magnets at the top, it is expected to configure a large hexagonal shape.

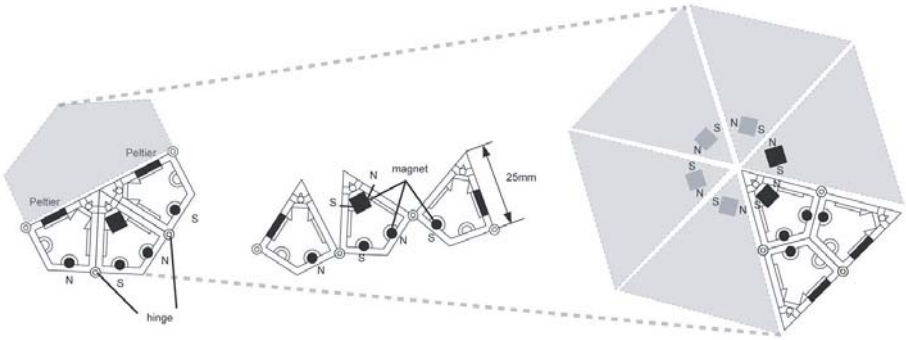

Figure 5.8: The aimed reconfiguration process. Initially, two modules are connected by Peltier connector and form a hexagonal shape. By applying inverted current, it can unfreeze the connection and eventually configure an triangle guided by magnets inserted to the module. Once the triangular shape is formed, using the large magnets at the top, it is expected to configure a large hexagonal shape.

Snapshots from a representative experiment are shown in Fig. 5.9. At the beginning of the experiment, we arranged by hand two chains of 3 modules each to form a hexagonal shape (Fig. 5.9b). Voltage was applied to the system so that the Peltier elements were powered (Fig. 5.9c). After one minute, an ice layer built up between the modules causing them to attach to each other yielding one single piece (Fig. 5.9d). We then inverted the polarity of the applied voltage and let the current flow to the vibration motors (Fig. 5.9e). The ice melted and the modules altered their configuration guided by the magnetic forces (Fig. 5.9f,g). The transformation was completed in a minute, and two magnetically connected triangle chains were obtained (Fig. 5.9h). The success rate of the reconfiguration just described was not as high as expected. We suspect that this low yield rate was mainly due to a design problem: the position of the large magnet was too close to the edge of the module. Therefore a rather strong movement of the modules was required to induce a disassembly of the initial hexagonal

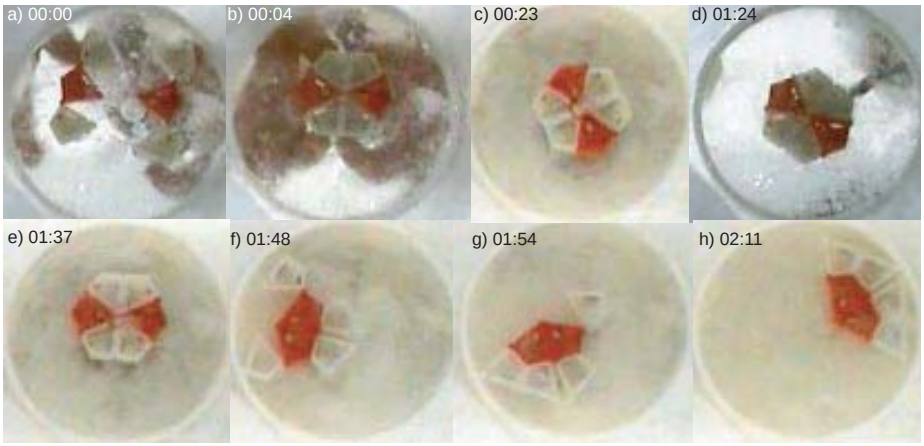

Figure 5.9: Snapshots of the experiment with chain modules. At the beginning of the experiment, we arranged by hand two chains of 3 modules each to form a hexagonal shape (b). Voltage was applied to the system so that the Peltier elements were powered (c). After a minute, an ice layer built up between the modules causing them to attach to each other yielding one single piece (d). We then inverted the polarity of the applied voltage and let the current flow to the vibration motors (e). The ice melted and the modules altered their configuration guided by the magnetic forces (f,g). The transformation was completed in a minute, and two magnetically connected triangle chains were obtained (h).

configuration.

The main implication of the two experiments described in this section 5.4 is that the restriction of the geometric constraint of modules, in other words, the "dimensionality reduction" of the reconfiguration problems enables the system to transit to a different level of functionality, bringing the modules to magnetically connected triangular clusters while avoiding undesirable formations (yield problem).

5.5 Discussion

In order to achieve highly autonomous self-assembly modules, the realization of a sufficient number of degrees of freedom that are controllable is necessary for such small scale autonomous-distributed systems. In particular, because of the difficulty in including different types of attractive forces within the same system, realizing a new kind of connection mechanism endows the module with a better means of reacting in the environment. In this sense, the idea of a connector exploiting the thermoelectric effect may open yet another possibility for the state of the art of self-assembly systems. The summarized characteristics are following:

- Pros:
  - Strong bonding force per weight ($1.79kgf$ / $1.6g$)
  - Robust alignment
  - Scalability

  - Polarity less connection
  - Continuous use (Repeatability)
  - No interference by magnetism
  - Ideal niche use: exploitation of under water environment for heat dissipation
  - Graceful degradation (fail safe)
  - Consumer level availability and easy maintenance
  - Silent

- Cons:
  - Energy required to sustain the connection
  - No energy/information transfer between neighboring modules

An important goal of the growing field of self-assembly is the development of a better formal understanding of the specific mechanisms and general principles underlying it. It is clear that the discovery of principles which hold at all scales will require substantial input from various fields. At the molecular scale, biological systems are one of the examples that achieve robust self-assembly system through an intricate web of well ordered reactions. Attention must be paid to the fact that all components are passively interacting even if it looks as if they are actively reacting [59].

5.6 Conclusion

We presented a novel type of connection mechanism for small-scale modular robotic systems. The mechanism exploits the thermoelectric effect to cool down the temperature and freeze water close to the modules and induce a strong bonding between modules. To test the connector, we embedded it into water-based modular robots. The results obtained in this research demonstrate the utility of the proposed connection mechanism for lightweight self-assembling systems, and open a door towards more resilient self-assembly system at smaller scales.

Chapter 6

Magnetic Enzyme Catalysis

Logical model

The decay in structure size of manufacturing products has yielded new demands on spontaneous composition methods. The key for the realization of micro self-assembling robots lies in how to order the assembly sequence in a bottom-up manner, where the parts have only limited (or no) computational (i.e. deliberative) abilities. In this paper, we focus on the role played by enzymes that regulate biochemical transaction paths in living systems, and propose a cm-sized enzyme model based on water floating components that are capable of inducing cascade conformation changes and thus regulating the reaction speeds. The model consists of two major parts - enzymes (activators or inhibitors) and a substrate set - which are all equipped only with permanent magnets, and can trigger conformation changes (with activator enzyme) or inhibit (with inhibitor). Experiments performed with 5 sets of components showed new possibilities of magnetically realized enzymes, which is a purely distributed system capable of performing catalysis by passively following the local rules of magnetic interactions.

keywords
magnetic enzyme; cascade conformation change; morphological computation; distributed system; activator; inhibitor.

6.1 Introduction

Micro/Nano-fabrication based on photolithography technology provided remarkable progress to engineers in the last few decades. Researchers from various domains, such as robotics, micro-device physics, synthetic chemistry, microbiology have been exploiting this technology aiming at their valuable potential. As for roboticists, the progress has opened up a new frontier, namely, the creation of autonomous micro-robots in small scales.

Together with the advancement of robotic technology, medical treatments employing autonomous robots have gained much attention. Recent applications illustrate the potential of edible robotic tablets that assemble in a stomach [43,80], and drug blending in vivo by autonomous micro sized capsules [60]. Recent development in tele operating micro objects has shown the capability to control micro-sized components (robots) in untethered manner, prospecting a challenge for spontaneous assembly mechanism [25, 27, 84, 104]. Their main focus was spotted on the actuation under externally added magnetic field environment, some with corkscrew configuration [45, 49], or the other exploiting resonated frequency [97,116]. Another attempt was carried out using chemistry as actuation means [118]. A state-of-the-art of the microrobotics is introduced in [103]. Along with the progress on fabricating micro-devices, some work from micro electro mechanical systems (MEMS) have shown noticeable outcomes, e.g. rod-like building blocks that form a series of single-layer superstructures consisting of bundles, tubes, and sheets [51, 83]. Leong et al. entered this new domain from chemistry [60]. They demonstrated spatially controlled chemical reactions, by which two containers are spatially controlled and diffuse chemicals.

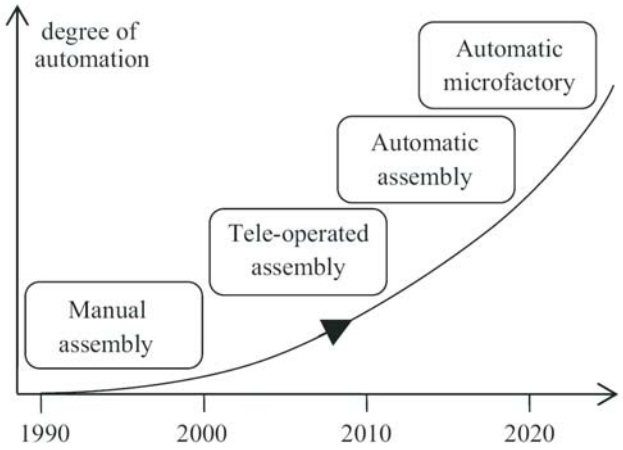

Figure 6.1: Different levels of assembly processes (cited from Gendreau et al., 2010 [32]). The figure, which exactly fits to our perception of the field, denotes the present transition period from tele-operated assembly to automatic assembly.

In Figure 6.1, Gendreau et al. classify the progress of the field on different levels of assembly processes [32]. The X-axis represents years, and the Y-axis represents the degree of autonomy of a component on assembly. The figure, which exactly fits to our perception of the field, denotes the present transition

period from tele-operated assembly to automatic assembly. However, as the demand of fabricating small sized complex robots has increased tremendously, the lack of construction techniques has become an outstanding constraining factor.

In contrast, biological systems have solved this problem in a bottom-up fashion, where a vast number of molecules autonomously construct a structure in a decentralized manner, so called self-assembly. Self-assembly is a key phenomenon to understand nature, which was recently redefined by Whitesides et al. as *the autonomous organization of components into patterns or structures without human intervention* [122], and there have been numerous attempts undertaken in various fields to tackle the self-assembly challenge. Pioneering experiments toward this aim were tackled by Penrose half a century ago [87], where a provoking mechanical model of natural self-replication in a stochastic environment was presented. It was followed by speculations about the clustering patterns of passive elements, focusing on the role of shape on template and components matching [21], and on their time evolution [46]. A series of studies were conducted by the group of Whitesides with achievements in the realization of positional coordinate of molecule-mimetic chemistry [15,124], circuit functionality [12,36], reversible aggregation [62], folding structure [10], rotation of magnets [41], rotation of rotors [40]. Similarly, numerous research efforts have been devoted to the investigation of morphology [106]. Artificial chemicals that can form in several ways, such as polymers and dimers, depending on the temperature of the system were demonstrated in [17]. Different aggregation patterns with various sizes of components were shown in [125]. An intelligent self-assembling block, which can represent multiple states by the units' rotational angle, was designed by [113]. The system can physically conduct XOR calculation on a 2D plane. To date, a few robots that can self-assemble relying on stochastic environment have been built. The modules are usually settled on a ground with low friction, being agitated for the achievement of locomotive transitions. The way of agitating varies, from adding mechanical turbulence to the ground [119] to air-jet turbulence [8, 37, 54]. Other type of environment includes oil to which fluidic turbulence is added [120]. Yokoi et al. took robotic and chemical approaches, in which they developed a physically connected multi-robots system and a system that can control a drop of mercury [128].

6.2 Enzyme

Enzymes play one of the major roles in regulating biochemical transaction paths in living systems. They are large protein molecules of which activated parts specifically combine with substrates such that they accelerate chemical reactions at least a million times [108]. They act on a protein whose configuration will be changed such that it exposes new bonding sites for a further reaction. First, an enzyme ($\mathcal{E}$) combines with a substrate ($\mathcal{S}$) and configure enzyme-substrate complex ($\mathcal{ES}$). Then it induces a conformation change of the substrate ($\mathcal{EP}$) and eventually produces a product ($\mathcal{P}$) (Figure 6.2).

$$\mathcal{E} + \mathcal{S} \underset{k_{-1}}{\overset{k_{+1}}{\rightleftharpoons}} \mathcal{ES} \overset{k_{+2}}{\longrightarrow} \mathcal{E} + \mathcal{P}. \tag{6.1}$$

Such a chemical reaction is caused by the enzyme acting on a free enthalpy

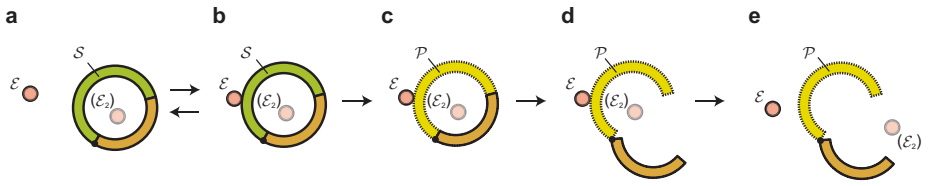

Figure 6.2: Illustration of a catalysis. enzyme($\mathcal{E}$) + substrate($\mathcal{S}$) $\rightleftharpoons$ enzyme-substrate complex($\mathcal{ES}$) $\rightarrow$ enzyme-product complex($\mathcal{EP}$) $\rightarrow$ enzyme($\mathcal{E}$) + product($\mathcal{P}$).

(Δ G, internal energy) of each reaction, such that the whole system can reach to a further stable state (Figure 6.3). In this process, which is so called catalysis,

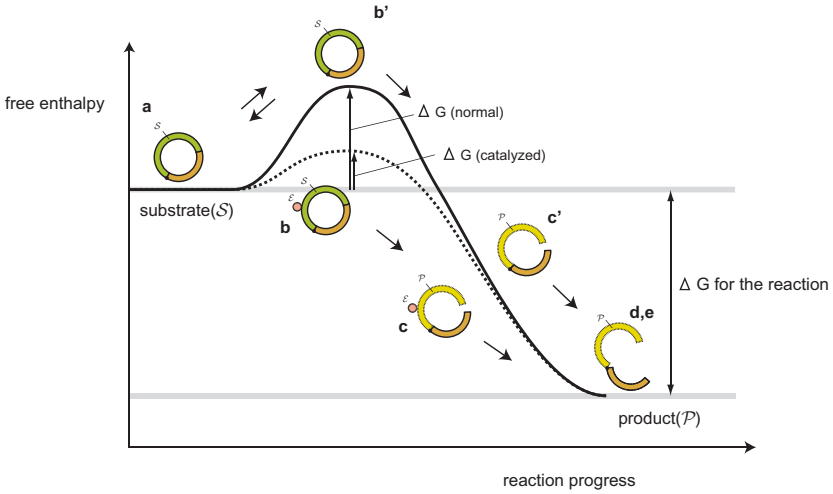

Figure 6.3: Enzymes speed up reactions by decreasing the free enthalpy. Two distinct reaction paths can be recognized: one driven by thermal agitation ($\mathbf{a} \rightarrow \mathbf{b} \rightarrow \mathbf{d}$), and the other assisted by enzymes ($\mathbf{a} \rightarrow \mathbf{b}' \rightarrow \mathbf{d}$).

the energy triggering the reaction of a substrate is regulated by the enzyme. The enzyme regains its initial state and becomes able to react upon another target to proceed further reactions [52]. As the targeted structure becomes complex, ordering the assembly process arises as a fundamental issue.

In general, it is known that the rate of product formation (v) can be described by Michaelis-Menten kinetics as:

$$v = \frac{d[\mathcal{P}]}{dt} = \frac{V_{max}[\mathcal{S}]}{K_{\mathcal{S}} + [\mathcal{S}]}, \tag{6.2}$$

where $V_{max} = k_{+2}[\mathcal{E}]_0$ ($\mathcal{E}_0$ is the total concentration of enzyme), $K_{\mathcal{S}}$ is the dissociation constant that is defined as $K_{\mathcal{S}} = \frac{[\mathcal{E}][\mathcal{S}]}{[\mathcal{ES}]}$.

6.3 Proposed Magnetic Enzyme

The decay in structure size of manufacturing products has yielded demands the spontaneous composition method. However, the available existing devices, such as microchips, sensors, actuators, and batteries, are mostly limited to the cm-order scale, and thus restrict the possibility to realize small scale robots [67]. Thus, the key for the realization of small scale self-assembling robots lies in how to order the assembly sequence in a bottom up manner, where the parts have only limited (or no) computational (i.e. deliberative) abilities. The aim of this study is to realize an innovative self-assembly method that can lead to a logical construction of small scale robots. More specifically, we attempt to design and fabricate components that can self-assemble by mechanically switching to different properties. This entails advancing the current tele operated self-assembly systems to automatic self-assembly systems (Figure 6.1). Referring to the knowledge that has been acquired through our past studies, we structured the prerequisites for enzyme reactions as follows:

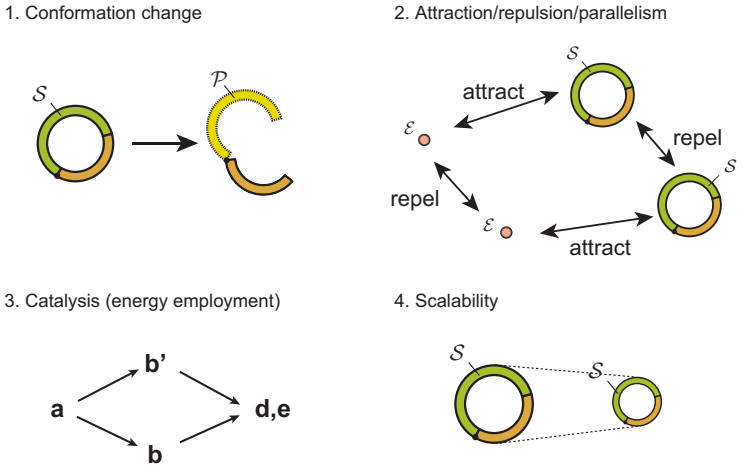

Figure 6.4: Four prerequisites for enzyme reactions. 1: Conformation change. 2: Attraction/repulsion/parallelism. 3: Catalysis (energy employment, **a-e** corresponds to the same letters of Figure 6.3). 4: Scalability.

1. **Conformation change.** The component should be able to exhibit new properties by changing the physical conformation (Figure 6.4 **a**, we often call conformation change "reaction" hereafter).

2. **Attraction/repulsion/parallelism.** For aimed reactions, it is desired that enzymes attract substrates, and *vice-versa*, while enzymes themselves or substrates repel each other (Figure 6.4 **b**), such that it can be able to cope with parallel assembly.

3. **Catalysis (energy employment).** The stored energy of a system should be systematically consumed inducing conformation changes. Particularly for an enzyme reaction, two different energy convergence paths should exist, such that one can be triggered kinetically, the other can be achieved by enzyme assist (Figure 6.4 **c**, see also Figure 6.3).

4. **Scalability.** The component architecture should be scalable down (ideally) to the order of sub-*mm* scale, where inertial effect can be minimized (Figure 6.4 **d**)

As concluded in the previous chapter, the methodology for the realization of such self-assembling robots lies in the order of the assembly sequence, in a bottom up manner, where the parts have only limited (or no) computational (i.e. deliberative) capabilities. Once a set of experimental conditions is invoked, components are expected to act in parallel, following local causal rules of the given environment.

Having considered the prerequisites above, we particularly focused on magnets as driving force and energy. Figure 6.5 illustrates the design principle of employing magnets. We firstly started focusing on that two magnets have

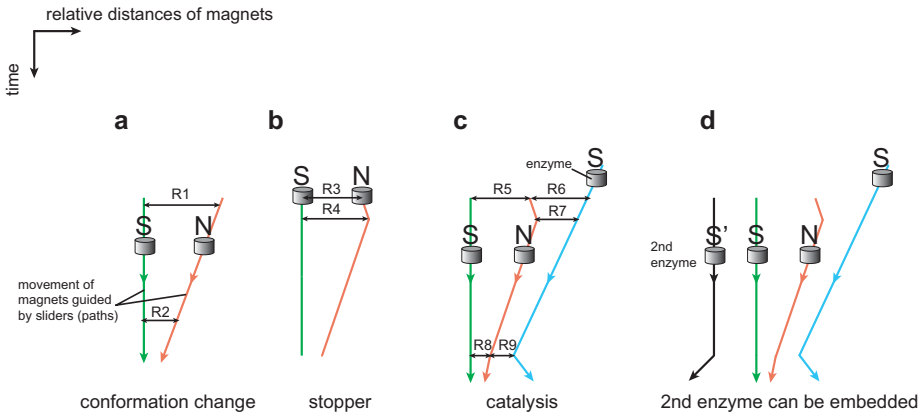

Figure 6.5: The design of a magnetic catalysis. **a:** Two magnets have substantial potential to induce conformation change by reducing the distance (consuming the magnetic potential energy, R1>R2). **b:** A stopper can be introduced by the path that can suppress the conformation change (R3<R4). Note that perturbation may still be able to invoke the conformation change. **c:** The third magnet (enzyme) can assist the trapped magnet (N) to step into the original path and trigger the conformation change (R5>R6>R7>R9), and moreover, bear off the enzyme (R8<R9). **d:** Depending on the displacement, an additional magnet(s) can reside in the system (S').

substantial potential to induce conformation change by reducing the distance (consuming the magnetic potential energy, R1>R2, Figure 6.5 **a**). Then introduced a stopper by the path such that it can suppress the conformation change (R3<R4, note that perturbation may still be able to invoke the conformation change, Figure 6.5 **b**). We employed the third magnet (enzyme) so that it can assist the trapped magnet (N) to step into the original path and trigger the conformation change (R5>R6>R7>R9), and moreover, bear off the enzyme (R8<R9, Figure 6.5 **c**). Finally, we added an additional enzyme to the system (Figure 6.5 **d**).

The proposed model only employs magnetic forces for the attractive/repulsive interactions, yet it can exhibit complex dynamical behaviors. It consists of three units - a substrate set (combined with left substrate and right substrate) and two enzymes (either two activators or two inhibitors) (Figure 6.6). The directions of magnets on each unit are arranged such that the left substrate attracts

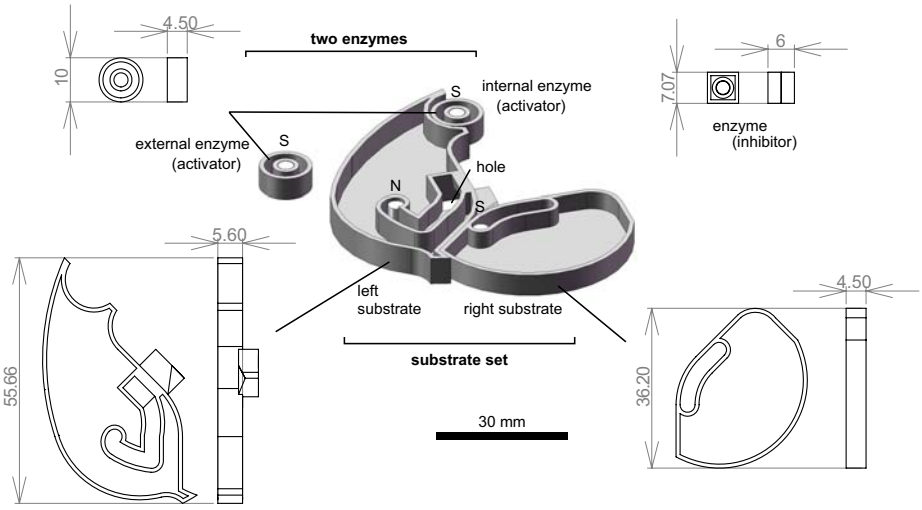

Figure 6.6: The proposed enzyme model.

the other three units (two enzymes and the right substrate) - only the magnet in the left substrate faces upward (North is up), whereas the other three magnets (two in enzymes and one in the right substrate) face downward (South are up).

The conformation changes induced by an activator and by an inhibitor are respectively illustrated in Figure 6.7 **a** and **b**. In Figure 6.7 **a**, an external ac-

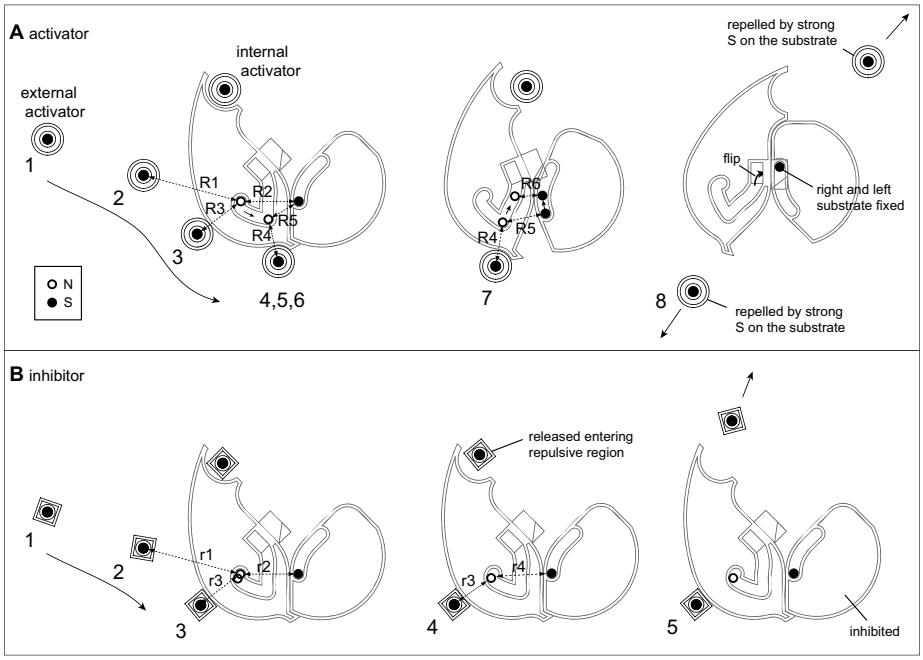

Figure 6.7: The conformation changes with an activator (**a**) and an inhibitor (**b**).

tivator approaching from the left side triggers a conformation change of the

substrate set, releasing the internal activator while it itself eventually moves away from the substrate set after the contact. More concretely, the external activator having reached to the left substrate drags a magnet of the left substrate and delivers it to a certain position by rolling over the edge of the left substrate (positions 3-5 in Figure 6.7 **a**). Then the magnet of the left substrate gets attracted by another one on the right substrate, causing a conformation change (5 in Figure 6.7 **a**). Eventually the sliding magnet enters a hole and connects to the other magnet of the right substrate (6 in Figure 6.7 **a**). Hence, the number of activators is doubled, capable of leading to cascade reactions with multiple substrate sets. Cascades are used in many cellular functions especially to amplify intensities of chemical signals.

An inhibitor has the same magnetic arrangement as an activator but with square shaped body. Due to its shape which restricts the rotational movement, it inhibits the conformation change by fixing a magnet of the left substrate (position 4 in Figure 6.7 **b**). Nevertheless, the second inhibitor is released due to the magnetic distribution and the number of free inhibitors is preserved. Note that after the reaction by an inhibitor, the substrate set cannot neither change its conformation nor attract another enzyme anymore.

The behaviors of both activators and inhibitors are summarized in Table 6.1, in which the numbers on the most left column correspond to the number in the Figure 6.7.

Table 6.1: Summarized description of the conformation changes by activators and inhibitors shown in Figure 6.7 **a** and **b**, respectively. The numbers on the most left column correspond to the number in the Figure 6.7.

	Activators	
1 2	R2<R1	The substrate set keeps an initial configuration. An external activator is gravitated by a magnet on the left substrate.
3	R3<R2	The external activator having reached to the left substrate drags a magnet of the left substrate.
4	R4<R3	The external activator rolls over the edge of the left substrate, delivering the magnet on the left substrate to a certain position.
5	R5<R4	The magnet of the left substrate gets attracted by another one on the right substrate.
6	R6<R5	The magnets on the left and right substrates attract each other, causing a conformation change.
7 8	R7<R6	The magnet on the left substrate enters a hole and connects to the other magnet on the right substrate by turning the orientation 180°.
	Inhibitors	
1 2	r2<r1	The substrate set keeps an initial configuration. An external inhibitor is gravitated by a magnet on the left substrate.
3	r3<r2	The external inhibitor having reached to the left substrate drags a magnet of the left substrate, however, due to its shape which restricts the rotational movement, it inhibits the conformation change by fixing a magnet of the left substrate.
4	r3<r4	The second inhibitor is released due to the magnetic distribution and the number of free inhibitors is preserved.

The degradation of distances of targeted magnets were designed such that it occurs on circumference of circles (Figure 6.8). As it can be seen in the figure, the path of a magnet on the left substrate consists of 4 traces that can compose circles and a straight line. Setting the aimed trajectory of an enzyme by shifting the center and altering the radius of such circles that compose paths, the distances of guided two magnets can be gradually reduced, as discussed in

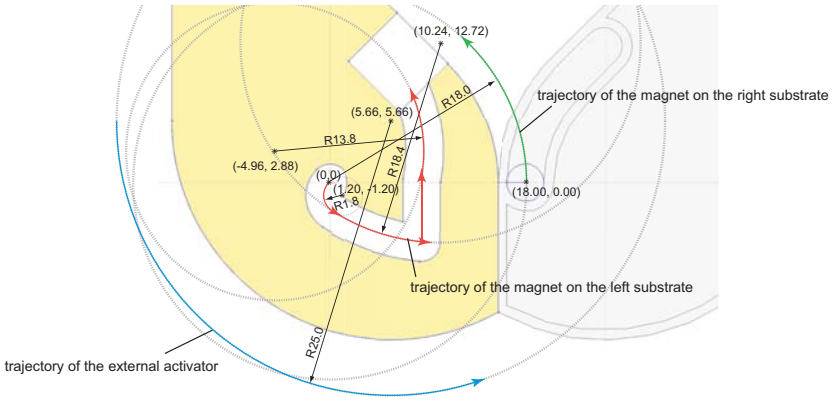

Figure 6.8: The degradation of distances of targeted magnets were designed such that it occurs on circumference of circles. The path of a magnet on the left substrate consists of 4 traces that can compose circles and a straight line (unit: mm, the corresponding paths are identically colored in Figure 6.5)

Figure 6.5.

The attractive region ($F_x > 0 \wedge F_y > 0$) of a substrate set for an external enzyme is illustrated as a red colored region in Figure 6.9, in which **a** represents the attractive region before the reaction, and **(b)** after the reaction. An enzyme

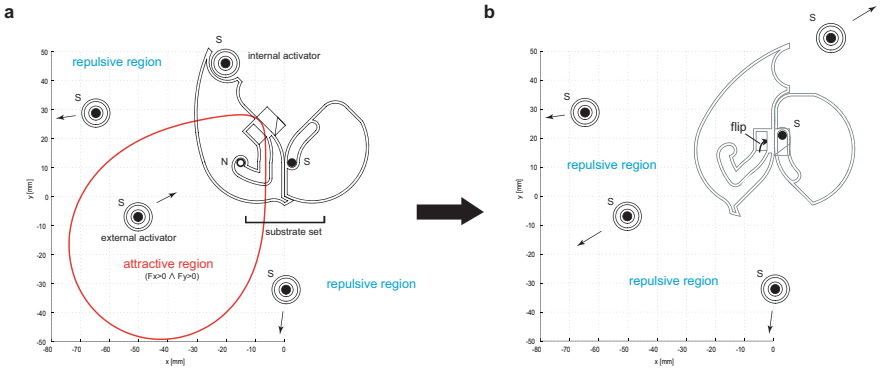

Figure 6.9: The attractive region ($F_x > 0 \wedge F_y > 0$) for an external enzyme. **(a)** before the reaction, and **(b)** after the reaction. Note that attractive region in practice is larger than it is shown in the figure, for a substrate can rotate and often captures an enzyme near the region.

in this region can be attracted by the substrate set and causes a conformation change of the substrate set. In principle, enzymes out of this region are repelled by the substrate set. However, in practice, the repulsive torque induces a rotational movement of the substrate set and often captures an enzyme near the region. The shape of the attractive region is determined by the placement of three magnets (two on a substrate set and one on an internal enzyme unit). The shape of the attractive region for the inhibitors is the same as the activators, for the same magnetic arrangements.

To investigate the reliability of designed reaction, we conducted 20 trials for both activators and inhibitors each, and obtained the success rate of 100.0 % for both cases. We show snapshots of reactions with an activator and an inhibitor in Figure 6.10 and Figure 6.11, respectively. In both cases, initially the external enzyme was placed manually at 8 cm left from the center of the substrate set. Drifting motions were frequently observed (Figure 6.10 **g-i**) in trials with

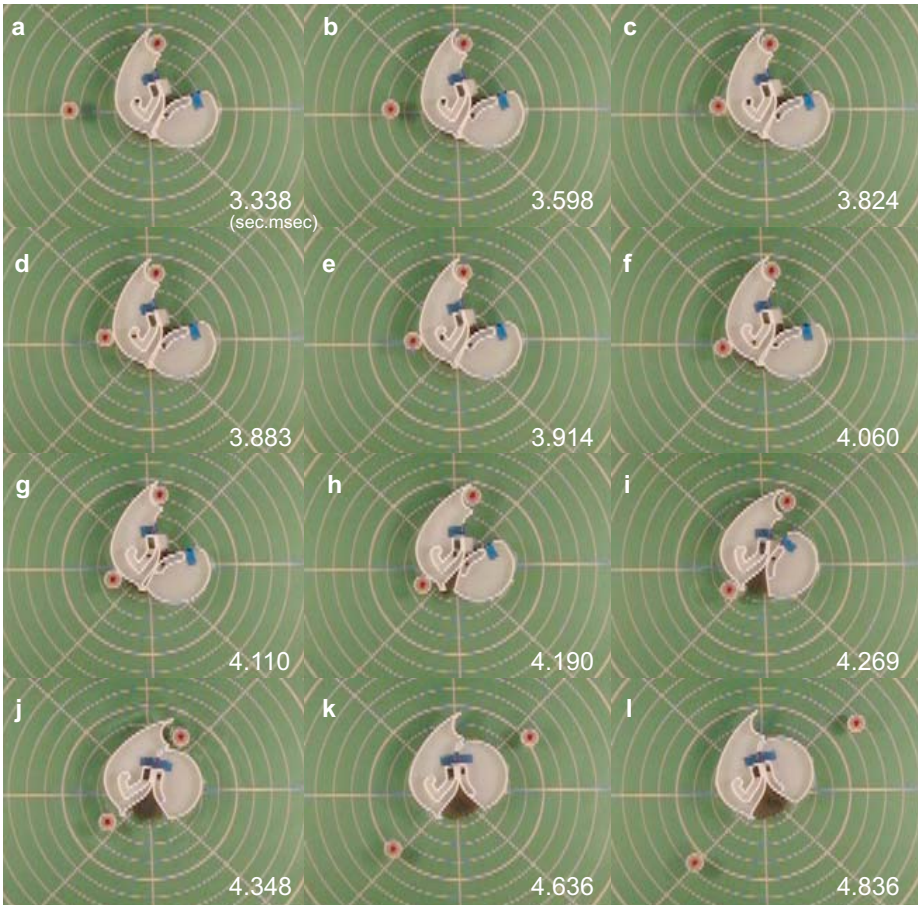

Figure 6.10: Reaction with activators. The time taken for the conformation change (the time after the first contact of an activator till the completion of the conformation change) was 1.012 s, and the success rates of conformation change was 100.0 % in 20 trials.

activators. This is because the time needed for the conformation change is relatively longer than the magnets' transitional movement. This phenomenon is supposed to disappear with scaling down the system, due to the decay of inertial influence. This reminds that the size is an important issue for self-assembly systems. For objects of mm scale or less in water (the world of low Reynolds number), viscosity is dominant compared to inertia, thus inducing static motion. The results show an advantageous circumstance for sub-mm scale self-assembly systems, which may eliminate undesired magnet fluctuations encountered in cm-scale self-assembly. The reaction time of the activator, which is the time after

the first contact of an activator till the completion of the conformation change, was 1.012 s.

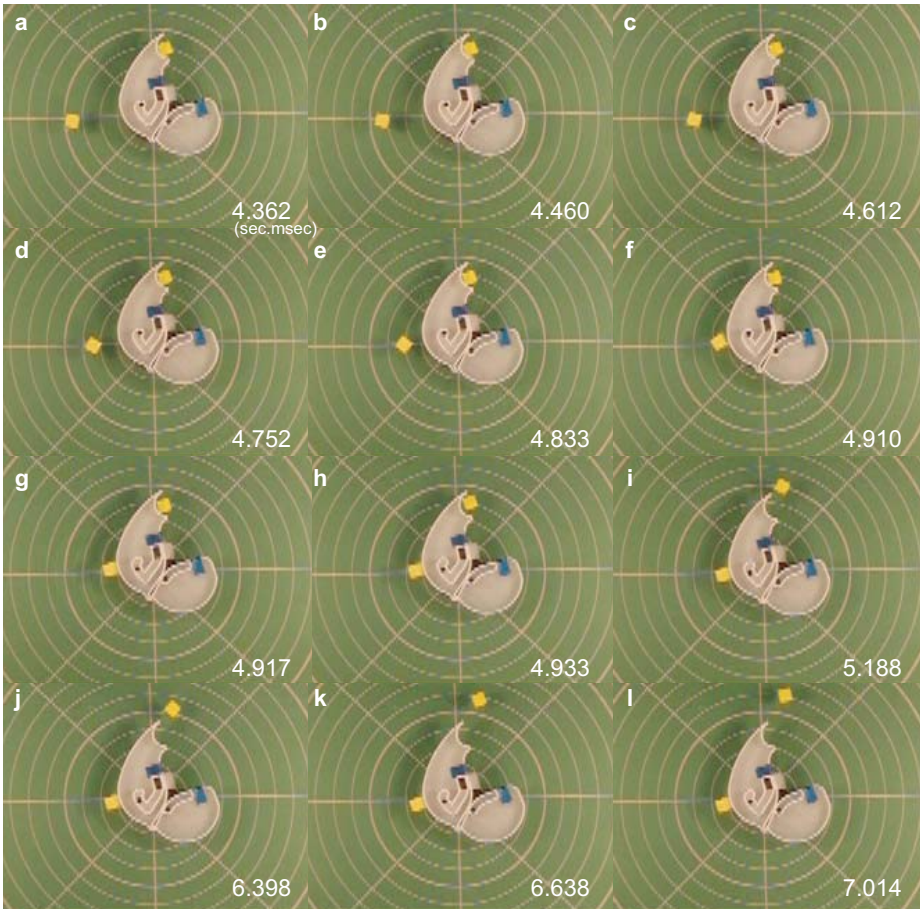

Figure 6.11: Conformation change by an inhibitor. An inhibitor inhibits the conformation change of the substrate set, due to its angular shape, which is unsuitable to rolling over (**g-l**). The success rates of conformation change was 100.0 % in 20 trials.

Figure 6.12 shows the relative distances of the magnets on the right substrate (green color) and external activator (blue color), measured from the magnet on the left substrate (red color). Note that an inversion of the distances, one between the activator and the magnet on the left substrate, and the other between the magnet on the left substrate and the magnet on the right magnet, is clearly shown (ref. Figure 6.5).

The magnetic potential $\phi_j(\boldsymbol{r})$ at a position $\boldsymbol{r}$ from the magnetic moment $\boldsymbol{m}_j$ is given by

$$\phi_j(\boldsymbol{r}) = \frac{\mu_0}{4\pi} \frac{\boldsymbol{m}_j \cdot \hat{\boldsymbol{r}}}{r^2} \tag{6.3}$$

where $\mu_0 = 4\pi \times 10^{-7} Tm/A$ is the permeability of free space, and $\hat{\boldsymbol{r}} \equiv \boldsymbol{r}/|\boldsymbol{r}|$ assuming that $|\boldsymbol{r}| = r$ is much larger than the size of the magnet. The magnetic

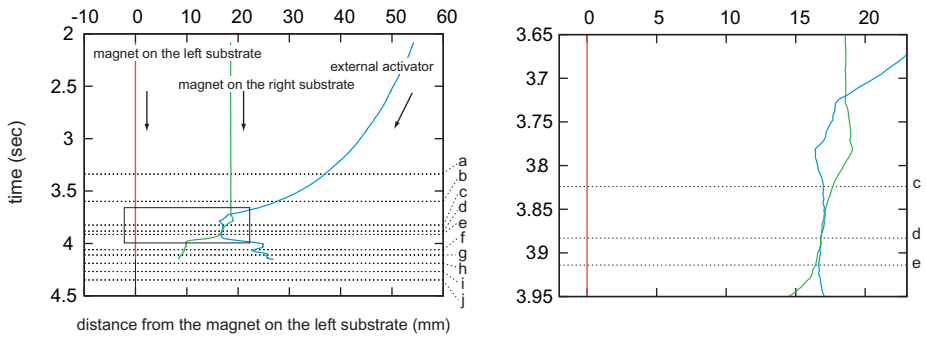

Figure 6.12: The relative distances of the magnets on the right substrate (green color) and external activator (blue color), measured from the magnet on the left substrate (red color). The magnification of the square region is shown on the right side. Labels **a-j** correspond to the same labels in Figure 6.10. The green, blue, and red color correspond to the same color in Figure 6.5 and Figure 6.8, representing the corresponding trajectories.

flux of the dipole is then found as

$$\boldsymbol{B}_j = -\nabla\,\phi_j \tag{6.4}$$

and the magnetic potential energy U_{ij} acquired by a second dipole $\boldsymbol{m}_i$ placed in the field of $\boldsymbol{m}_j$ is given by

$$U_{ij} = -\boldsymbol{m}_i \cdot \boldsymbol{B}_j. \tag{6.5}$$

Then, the force between the two dipoles is found by differentiating (6.5) with respect to $\boldsymbol{r}$.

Since in our case the magnets are identical, we have $|m_i| = |m_j| = m$, and because they are parallel, the energy and the force expressions simplify to:

$$U_{ij} = -\frac{\mu_0}{4\pi}\frac{m^2}{r_{ij}^3} \tag{6.6}$$

$$F_{ij} = -\frac{dU_{ij}}{dr} = \frac{3\mu_0}{4\pi}\frac{m^2}{r_{ij}^4}, \tag{6.7}$$

and we can determine the total potential energy of the system as

$$U_{total} = \frac{1}{2}\sum_{i,j\ i\neq j}\{-\sigma_{ij}\ \frac{\mu_0}{4\pi}\frac{m^2}{r_{ij}^3}\}, \qquad \sigma_{ij} = \frac{\boldsymbol{m_i}\cdot\boldsymbol{m_j}}{|\boldsymbol{m}_i||\boldsymbol{m}_j|}. \tag{6.8}$$

Finally, we normalize the energy as $U'_{total} \equiv U_{total}/(\frac{\mu_0}{4\pi}m^2)$. Note that normalizing by this positive number, will make the self-assembly system tend towards a maximum of U'_{total} instead of a minimum.

Figure 6.13 **a** and **b** display the transitions of magnetic potential energy shown in Figure 6.10 and Figure 6.11, respectively. The corresponding frames (**a** - **l**) are indicated in each figure with dotted lines. The difference between the two transitions is remarkable. In the case with activators, the energy decreases to less than $-0.0015\,m^{-3}$, while with inhibitors, it stops above $-0.0005\,m^{-3}$,

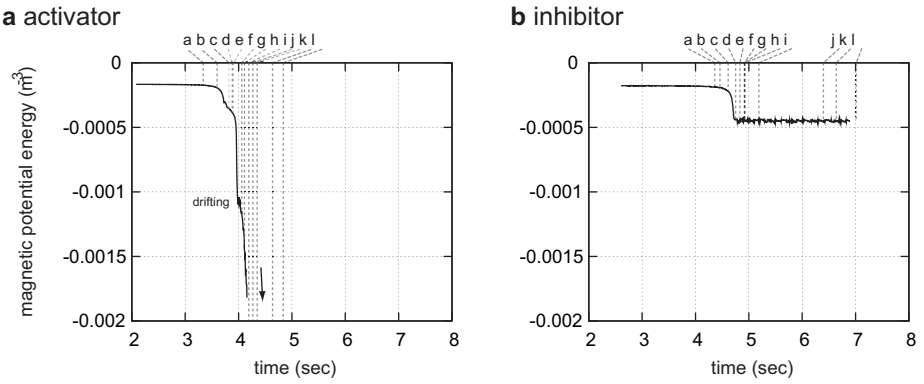

Figure 6.13: Transition of magnetic potential energy of (**a**) activator, and (**g**) inhibitor (cf. Figure 6.3 (**a** → **b** → **d**)).

representing the incompletion level. The monotonically decreasing energy curve of the activator tells it does not require inertial velocity to proceed the reaction, but geometrically able to achieve. This is a good indicator that the system shall work at smaller scales. Note that we are aware that if we invoke a conformation change not with an activator but by agitating the water tank, the curve should rise provisionally to overcome the magnetic potential barrier, and eventually drops. In this case, the rise of both the magnetic potential energy and the turbulence level (which correspond to a temperature at the microscopic level) corresponds to the rise of enthalpy in Figure 6.3 (**a** → **b**′ → **d**).

6.4 Cascade Conformation Changes

In order to investigate the validity of the designed system, we performed experiments with multiple number of components. Experiments were carried out in a water tank of 40 cm diameter with 5 substrate sets as an initial condition. Snapshots of one of the trials are shown in Figure 6.14 with activators and in Figure 6.15 with inhibitors, respectively. In order to avoid situations in which the substrate sets repel each other and gather around the boarder of the tank, we circularly submerged 5 metallic plates ($\phi\, 3cm$), such that they weakly attract the substrate sets. We initially placed 5 enzyme units at the middle of two substrate sets by hand (Figure 6.14 **a**, and Figure 6.15 **a**), and triggered conformation change reactions. Trials which didn't show any reactions for more than one minute are removed from the results.

In Figure 6.14, the first conformation change was triggered at time 57.420 s after a while of quasi-steady state (Figure 6.14 **d**) (we set time 0 as when the last enzyme unit was released). Release of an internal activator can be recognized in Figure 6.14 **e**. Followed by another conformation change that can be seen in Figure 6.14 **g**, it can be recognized that one of the released internal activators also triggered conformation changes (Figure 6.14 **k**, **n**, and **p**).

In Figure 6.15, the first conformation change was triggered at time 5.214 s, which occurred relatively quicker than the case of activators, shown in Fig-

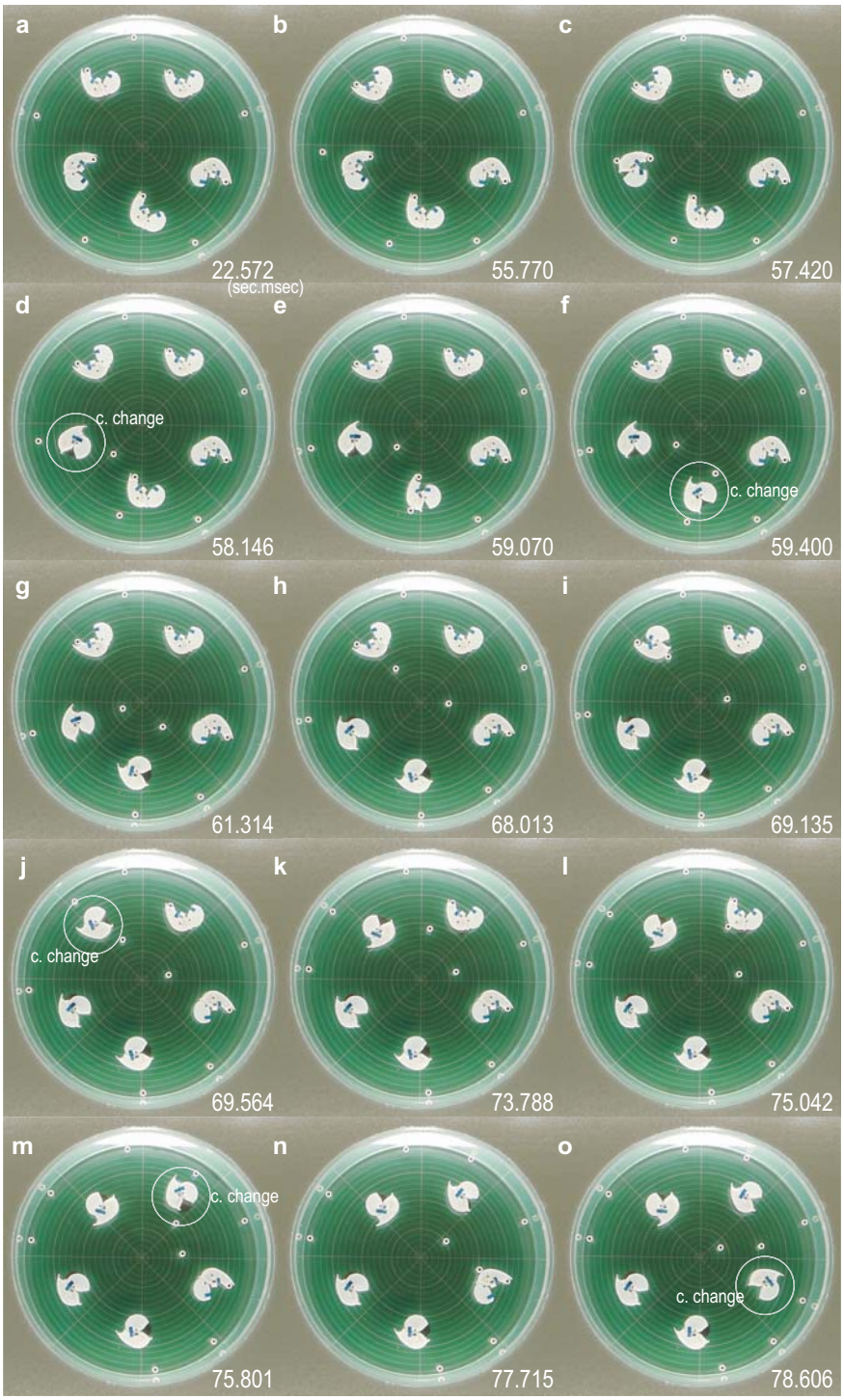

Figure 6.14: Snapshots of a trial with activators.

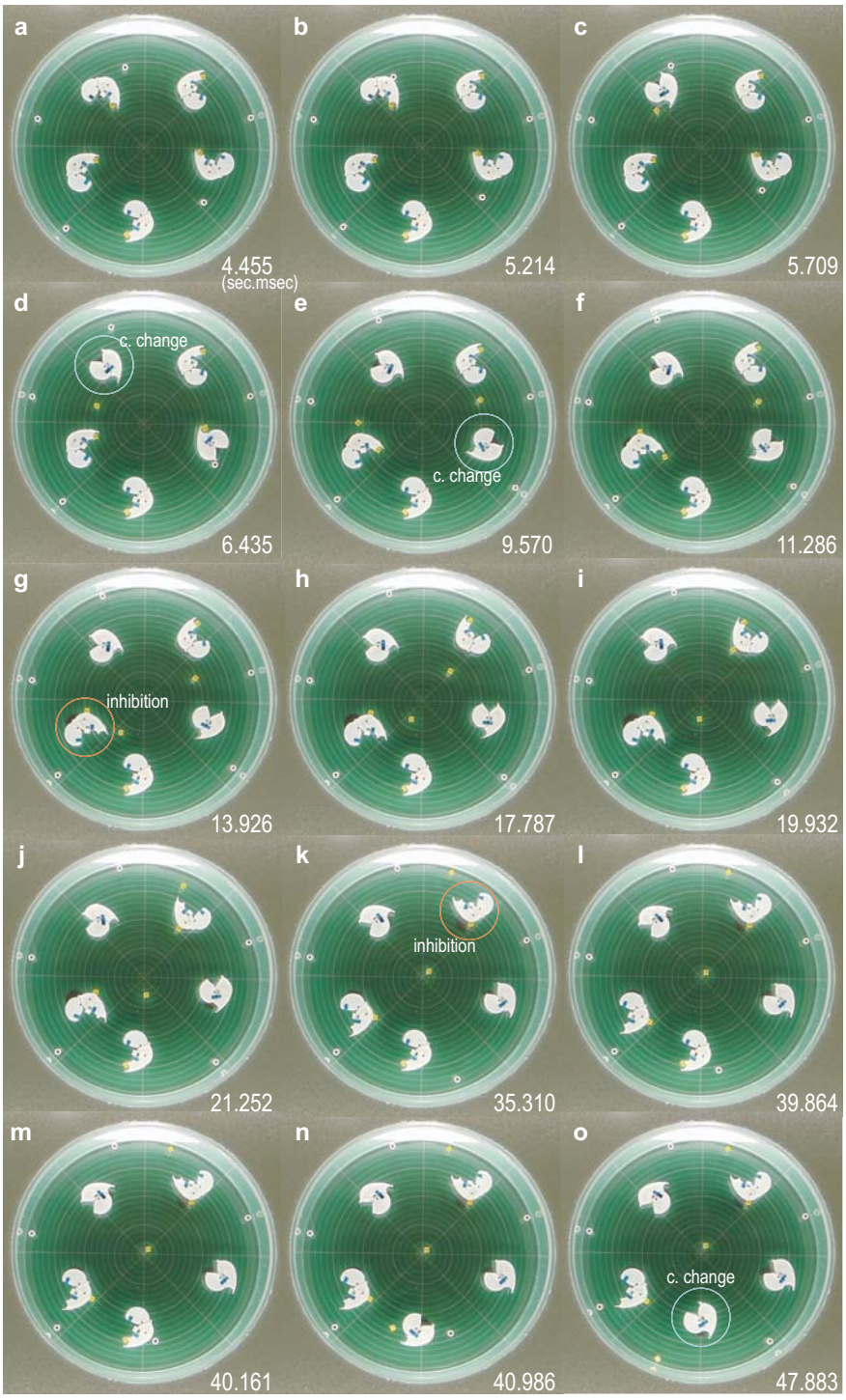

Figure 6.15: Snapshots of a trial with inhibitors.

ure 6.14. In general, the time of a first reaction is strongly dependent on the (randomly) orienting angles of each substrate sets, and this has little influence on the time taken in the later conformation changes. After two conformation changes had been triggered, pre-released internal inhibitors inhibited substrate sets (Figure 6.15 **h** and **l**).

Summary of the whole experimental results are shown in Table 6.2 and in Figure 6.16. In total, successful trials with activators and inhibitors were carried out 38 times and 47 times, respectively.

Table 6.2: Results of trials

	activator	**Inhibitor**
number of success trials	38 trials	47 trials
total number of reactions	228 times	282 times
observed conformation changes	228 times (100 %)	238 times (84.4 %)
observed inhibitions	(-)	46 times (15.6 %)
running time per trial (average)	78.29 s	51.932 s
running time per conformation change (average)	15.66 s	10.739 s

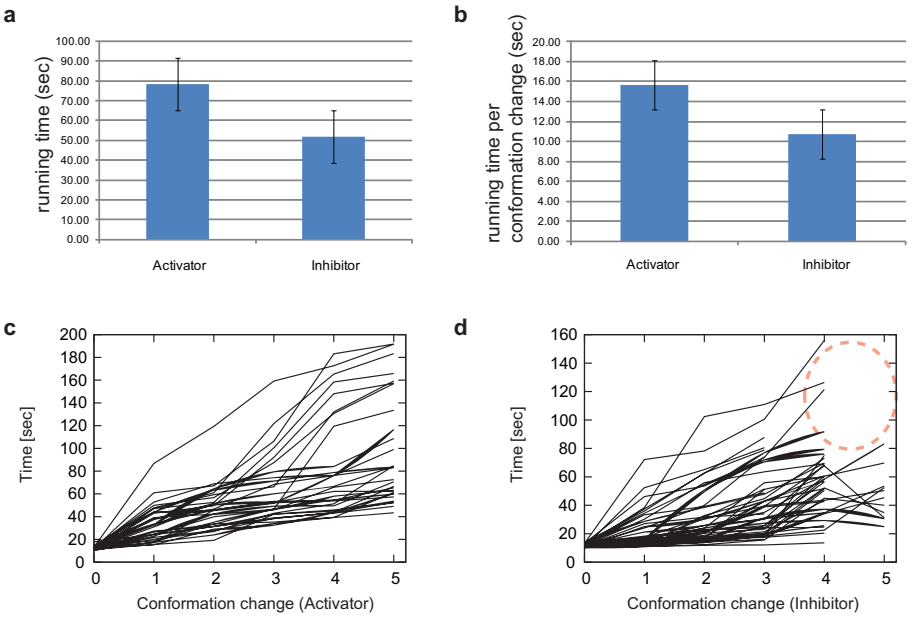

Figure 6.16: Result of trials. **a:** running time per trial, **b:** running time per conformation change (average), **c:** progress of conformation change with activators, **d:** progress of conformation change with inhibitors.

The total running times of each reaction with activators and inhibitors are respectively listed in Figure 6.16 a. It is shown that in general, the case with activators took longer time than that with inhibitors to complete a trial. This tendency can also be seen in the Figure 6.16 b, where running time per conformation change with activators and inhibitors are compared. We suspect that this is because substrate sets that finished changing their conformations acted as strong repulsive components for activators, hindering their path by creat-

ing potential "walls". Differently from the case with inhibitors, probably the magnetic potential energy with activators acts as if it increases when a magnet on the left substrate flips. That is, this is a specific phenomenon due to the fact that the components are constraint in a 2D plane. Among all the 38 trials with activators, 228 times of conformation changes were observed. Where as in the case with inhibitors, 238 conformation changes and 46 inhibitions (which is 15.6 %) occurred out of total 282 reactions. This effect of inhibitions can be seen in Figure 6.16 c and Figure 6.16 d, where the number of reactions are plotted against the time taken. Quite a few trials with inhibitors didn't finish conformation changes 5 times (namely, 15.6 % of all the trials; marked with dotted circle).

6.5 Discussion

The term *morphological computation* was originally coined by C. Paul, when she was questioning whether it may be possible for the morphology, or the physical body of the robot, to perform computation [73]. In the same way as she discovered the link between the two, morphology and computation, performance of our developed system can be regarded as a logical operation conducted through morphology. In this context, the "input" for a substrate is either an activator or an inhibitor, and the outputs are the state of the substrate and the released enzymes. A substrate acts as a gate, distinguishes the input through the morphology, and determines the action - an output. In spite of the analogue design of the system, the reaction is achieved in a digital manner, and this mechanism enables the system to temporally and spatially order the reaction sequence.

As introduced in Chapter 1.3.4, the incipient studies of realizing computation by physical entities were originally initiated by the group of DNA computation / self-assembly in the 90s. By utilizing a set of available/constructive "tools" (i.e., molecules, DNAs, controllable thermal agitation, etc.) in chemistry, the researchers in the field showed the possibility of realizing computation with physically grounded substances.

One of the main contributions of this study is the achievement of basic computation by combination of morphology and magnetism, that are realized in the same physics layers, likewise nature carries out, but based on a different technique. In the processes, all the resources for computation (e.g., memory, sensor, actuator, etc.,) are realized on a physics basis, in other words, these supplies are effectively outsourced to the components' morphology. We believe that the presented study provides a good platform, where one can find the tight interdependencies between mechanics (component design), physics (magnetism), chemistry (enzyme reaction), and logic (computation), that all jointly reside.

6.6 Conclusion

In this paper, aiming for alternative innovative techniques to realize logical self-assembling systems at small scales, we designed and developed a cm-sized enzyme model based on water floating components. The designed components showed the capability to invoke conformation changes in a bottom-up manner, which is a basic, but has sufficient functionality in regulating assembly order.

The system, by which we mimic the mechanism of enzymes, orchestrates magnets' transitions through the morphology - which are ideally scalable - by following local causal rules, and induces conformation changes of the components in parallel. The model was investigated in experiments with five enzyme-substrate sets and checked for reliability.

Chapter 7

Discussion

In this chapter, we discuss the obtained results in relation to the initial aims of this thesis (in Section 7.1), and in relation to the ultimate goal of realizing living systems (in Section 7.2). We conclude the thesis in Section 7.3.

7.1 Summary of Results

As described in Chapter 1, the aim of the present thesis was to design an innovative self-assembly system that complies with the following prerequisites.

1. **The system should be distributed in a stochastic environment.**
2. **The components should be sufficient to attain logical assembly.**
3. **The component architecture should be scalable.**

The models shown in Chapter 2 to Chapter 6 all subscribe to a distributed approach, and thus lack central control. The interactions were mainly managed by the embedded magnets on each module, though some global parameters did exist (the level of agitation of the tank in Chapter 2, or the applied voltage in Chapter 3). All these variables led models to assemble in parallel and stochastic manner, giving rise to different aggregation patterns. The study in Chapter 2 was designed to examine how shape influences the assembly dynamics, specifically from a mechanical point of view. The results in our experiments clearly showed that each shape induces distinctive assembly dynamics, leading to shape-dependent variations in the aggregation patterns. Consequently, they revealed a clear correspondence between shape, behavior, and function. In the experiments, the assembly patterns of differently shaped tiles (circular, square with rounded corners, and square) were investigated. For instance, rounded tiles (e.g., circular tiles or rounded square tiles) were capable of rolling over other components due to the system's energetic stabilities, whereas angulated tiles (square tiles) showed difficulty in movement, requiring larger environmental agitation to overcome the magnetic potential barrier. These differences in local interactions resulted in differences in aggregation patterns (e.g., the quick assembly with square tiles showed a multiplicative aggregation pattern). We further discuss this issue in Section 7.2.2.

In order to explore the possibility of self-propulsive self-assembly systems at the macro-scale, and the effect of stochasticity, we developed a second model that can self-propel (Chapter 3). The novel aspect of this model was the employment of vibration motors for induction of random motion, combined with an electricity supply mechanism that mimics a pantograph system. The advantage of such a mechanism is that modules no longer have to carry their own power supply, and therefore become more lightweight without compromising their power. Apart from wheeled robots, the model showed the first possibility of robots at this scale assembling stochastically even without environmental agitation. The self-propulsive mechanism also enabled the system to provide different stochasticity levels dependent on the voltage applied to the system. The analyzed results revealed qualitatively different aggregation patterns, and moreover, some of them showed a positive effect in improving *the parallel yield problem*.

As described in Chapter 1, the need for realizing logical assembly is noteworthy, specifically for removing *the topological dead end problem*. By developing the modules described in Chapter 4, we pursued the sensing capability of modules. Consequently, we utilized two types of sensors, an opto-coupler and a hall sensor, the former of which can optically detect the presence of other modules within a given range of distance, and the latter of which can measure a magnetic field beyond obstacles, and thus can detect the environment. We further attempted to realize a controllable attachment/detachment mechanism in Chapter 5. The proposed mechanism exploits the thermoelectric effect to cool down and freeze the water between two modules, thereby causing them to attach to each other. We validated the feasibility of this mechanism with Peltier elements, and demonstrated that it has several advantages over the other existing mechanisms, such as a higher bond strength/weight ratio, and robust alignment capability between modules. In particular, the difficulty in including different types of attractive forces within the same system is an intricate problem in self-assembly. Hence, realizing a new kind of connection mechanism which endows the module with better and various means of interaction is critical. The development of these models led us to the following question: *how do molecular systems achieve their sensing capabilities and manage such complex assembly without having distinctive sensor-motor mechanisms?* This riddle led us to the next model, which, after all, although equipped only with permanent magnets, was capable of performing logical assembly behavior in a passive way.

In Chapter 6, we designed a model that can logically invoke conformation changes of components. More specifically, the system orchestrated magnets' transitions through the morphology by consuming the potential energy, and was capable of regulating the reaction speeds by performing catalytic reactions in a bottom-up fashion. The developed system showed a possibility of realizing "passive but reactive"self-assembly components that are scalable, but can act logically and in parallel, following local causal rules imposed by the environment.

Considering the fact that the adequate physical laws vary depending on the structure targeted through self-assembly, it is also worth mentioning that the models described in Chapter 2 and Chapter 6 feature only magnets, apart from the constituent body parts. Consequently, this type of structure promises certain scalability of the system. Moreover, the advocated connection mechanism utilizing Peltier effect owes its scalability to the semiconductor design, which also holds promise for downscaling.

7.2 Design Principles

After the tidal challenge of investigating "life as it could be" in 90s, the trend which tries to answer to the question "what is life?" seems to have saturated in its progress. In this section, on the basis of our current experience in designing, constructing and controlling self-assembly systems, we discuss the current state of our system with respect to Figure 1.3, as well as the particular design principles that are bridging the gap to living systems.

To begin with, knowing that exceptions can always be found to each definition of life, let us define it as a generic term for **dynamical, self-assembling, and self-regulative physical causality**. We project our view in Figure 7.1, which is a modified version of Figure 1.3. As such, we take stochasticity as the X-axis, and the degree of autonomy of components as the Y-axis. Each barometer was considered as an indicator to assess the level of autonomy of the system in comparison with living systems, and discuss in detail below.

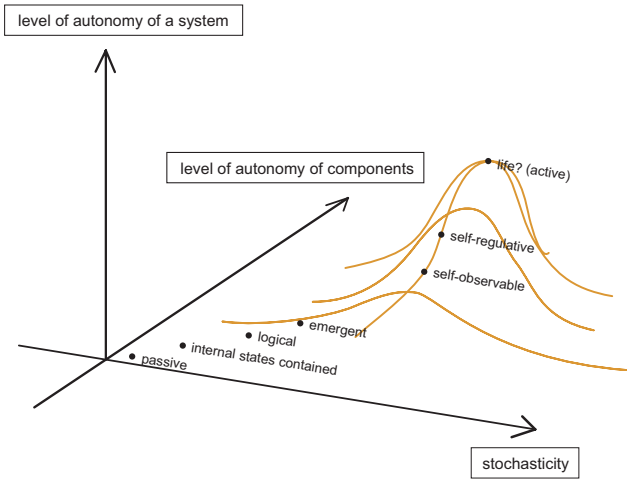

Figure 7.1: The level of autonomy realized as a system as a function of stochasticity and the level of autonomy of components (cf. Figure 1.3).

7.2.1 Level of Autonomy of Components

In this section, we discuss the level of autonomy of components from two perspectives: functionality and allostericity.

Functionality

Figure 7.2 demonstrates that the same functionality can be realized in two ways: by changing the shape of tiles, or by changing the position of magnets that are embedded on the tiles. In each trial (**a** to **d**), a set of magnets are complementarily mounted on the tiles, such that the tiles attract each other on a water surface. In a demonstration in Figure 7.2 **a**, a rotational motion of tiles

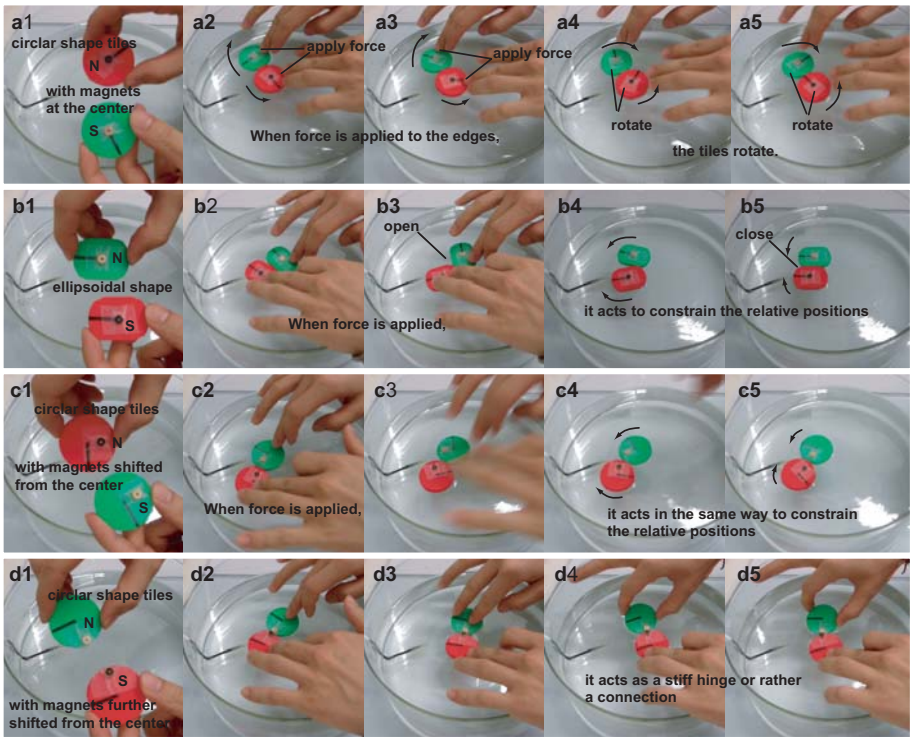

Figure 7.2: Changes in functionality induced by varying the shapes of tiles (**b**) and the positions of magnets (**c**). Both changes result in a restricted rotation.

is induced when a force is applied to the edges of the tiles. The demonstration in Figure 7.2 **b** shows that the whole demonstration shows that a constraint in the rotational motions can be introduced by using ellipsoidal tiles. A didactic demonstration can be found in Figure 7.2 **c**, in which the same constraint is realized by using circular tiles with magnets shifted from the center. If we attach the magnets further away from the center, the attraction is nearly as strong as a bond (Figure 7.2 **d**). Together, these demonstrations imply that an essential role is often played by the distribution of the body parts from the "origin of the force" (i.e. the magnets), rather than the overall geometry.

Recall the experimental results by the use of circular sector modules in Chapter 3. We often observed that the modules tended to form dimers (2-clusters) orienting the rounded edges toward each other instead of forming a circle, when we shifted the position of the magnets closer to the rounded edge or after we perturbed the water (Fig. 7.3 **a**). This is attributable to the same cause, since the convergence of assembly dynamics was chiefly driven by the stability of the potential energy. As we illustrate in Figure 7.3, these examples indicate that the positional change of a magnet has the same effect as the change of the entire morphology, and this implies the difficulty of realizing a lightweight actuator.

A practical approach is to evaluate shape from an energetic perspective, and develop a scheme to ground the phenomenon in the context of physics. Figure 7.4 describes a geometry in which two components change the absolute angles (θ_1, θ_2) keeping the contact. The case shown is a generic instance of eval-

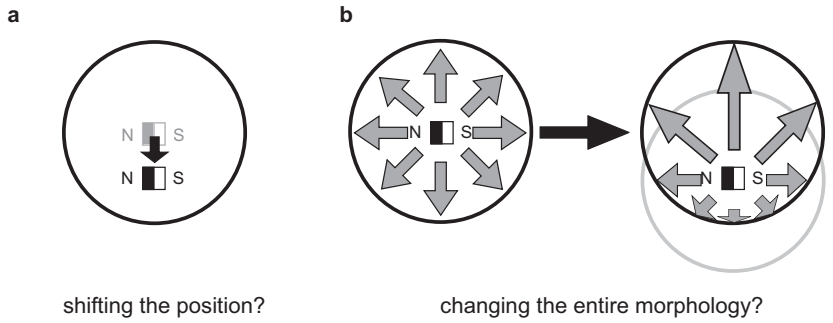

Figure 7.3: Two interpretations of the change. a) Shifting the position of a magnet. b) Changing the entire morphology.

uating shape as a measure of the potential energy of the system (e.g. magnetic potential energy) by independently varying the variables (here, θ_1, θ_2), and deriving the system's energy as a function. The "shape" of the derived function reflects the stability as well as the expectation of the system's convergence. As

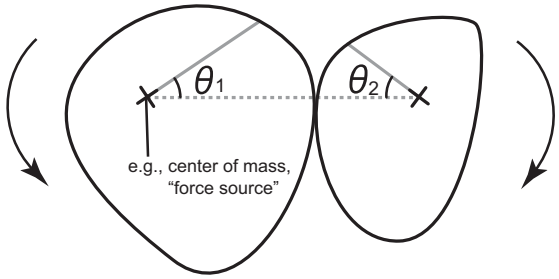

Figure 7.4: Evaluation of shape by assessing the potential energy. By varying the angles (θ_1 and θ_2), a function $f(\theta_1, \theta_2)$ can be derived.

we previously showed in Figure 2.15 in Chapter 2, the shape of components constrains the interaction, mainly due to the energetic stability of components. Connection mechanisms, such as Peltier elements, act to prevent the modules from converging to an energetically global configuration. The effect of such connection mechanisms is essentially to regulate the transitions of the system that minimize the energy. In that sense, a connection mechanism behaves as an increment of the system's degree of freedom.

As we noted, it can be said that one of the roles of a component is to alter the interaction with other components and with the environment through morphology. Besides, as it can be seen in the "bike" configuration in Appendix 3B, where a combination of two circular modules and a triangular module yielded functional mobility, combinations of basic components often exhibited a meaningful behavior, or in other words, functionality[1]. Another example that we consider from the perspective of functionality can be found in the formed lattice structures in Chapter 2 (i.e., Figure 2.9). In this case, the stability of

[1] not to mention, the system's observer ultimately defines what is functionality

the formed structures were intrinsically determined by the shape of constitutive tiles. Besides, rounded tiles, induced folding motion, which was hardly observed in sharp-cornered tiles, enabling the clusters to smoothly converge to further stable states. It is also worthy to mention that addressing capability of bonding was commonly reinforced by component's morphology. Desired connections demonstrated in this thesis made use of shape matching in addition to magnetic pole matching to restrict the bonding condition. One final point of functionality found at the component level is boundary formation (e.g., Figure 3.12). Depending on the shape of components, the geometry of formed structure prohibits/enables further reactions. These examples advocate that the components intrinsically comprise "functionality" especially when they make up a compound with other components.

Allostericity (internal states)

In biology, molecular compounds often exhibit different behaviors acting as logical machines [5,26]. By carefully observing the molecular interactive networks, one notices that the aggregation processes take place in a well organized pathway. For instance, a protein A can only dock on a protein B by first coupling with a protein C: A+B+C $\rightarrow$ AC+B $\rightarrow$ ABC. It follows that, through coupling with protein C, protein A can acquire a different level of functionality, which then enables the interaction with protein B. In this example, only C requires internal state (i.e. C'), one which enables bonding with B. As the scale grows smaller, the control of the order of reactions becomes a crucial matter. These deliberations on the molecular level of life remind us of the need to examine an appropriate level of autonomy implemented in a component.

Suppose there are two different components/clusters A and B. In general, interactions of two components/clusters are considered to be able to describe with combinations of the following three reaction steps, namely:

(I)	Forward reaction	$A + B \rightarrow AB$
(II)	State change	$A \rightarrow A'$
(III)	Backward reaction	$AB \rightarrow A + B.$

A state change can be any conformational/internal change inducing the acquisition of another functionality of the component, e.g., conformation change of a protein, protruding a sticking site (charged site) out of the body such that it can react with another protein. In distributed systems, this sort of acquisition of functionality is normally accompanied with combining to another component, and can be described as

(I)+(II)	*Allosteric plus*	$A + B \rightarrow A'B$
(II)+(III)	*Allosteric minus*	$AB \rightarrow A' + B,$

which we termed Allosteric plus and Allosteric minus, respectively. In *Allosteric plus* reaction, a component connects to another component and eventually obtains a different characteristic. Such an acquisition of functionality spontaneously leads to the next reaction. Note that the reaction order can be sorted through this process, and this shall be the only way to sort the aggregation sequence in assembly processes. In *Allosteric minus* reaction, which is the opposite

case, a cluster disassembles a part of itself, and obtains a different characteristic. In this way, all the reaction processes in a system can be described algebraically employing causal analysis.

In addition to the logical model presented in Chapter 6, the identical functionality as an allosteric effect can also be achieved as a combination of a simple set of components, such as the self-assembly process in Figure 2.13. As the attractive region for the external tiles depends on the configuration of the constitutive tiles, the system differentiates its characteristics through the structure's morphology. The difference between functionality and allostericity is that while the former mainly exerts influence to the system in an analogue manner, the latter one operates in a digital way, and its features are mostly distinctive. In addition, an allosteric component is not only capable of playing roles of two different types of components, but also generates various temporal causalities. Heterogeneous systems which consist of many different types of components, on the other hand, often encounters divergence of components' combinatorial problems, in which enrolled components regularly yield undesired compounds, due to the lack of reaction's temporal constraint.

Homogeneous systems, such as biological organisms, that commonly consist of homogeneous cells and thus feature redundant properties are thought to be robust, e.g., self-repairable. In self-assembly systems, however, as we saw in Chapter 6, having elaborated internal states that enable the component to physically express a/various state(s) is a trade-off in two ways: it leads to vulnerability against the environmental turbulence, and it induces overweight of components and hinders rapid motions and structural stability. The benefit of having different types of components compensates for such problems, and eventually guarantees the diversity of reactions, while maintaining the complexity of the causal rule. In other words, fertility in heterogeneity lightens the mechanical load of components. Finding a suitable level of heterogeneity must become one of the capital issues in artificial self-assembly systems.

7.2.2 Stochasticity

Dynamics

In molecular assembly, three conditions are known to be necessary: weak interaction, thermal agitation, and nucleation. The mechanism behind molecular assembly is numerous trial and error iterations of the connections till the connection strength reaches a sustainable level, which is beyond the pressure of proofreading through the environmental turbulence. This is one of the fundamental differences from pick-and-place style (deterministic) assembly. Through such a process, the system gradually shifts to a more energetically stable state. In artificial self-assembly systems at macro-scale, due especially to the inertial effect, the frequency of collisions has a practical limit. This low capacity of collision-matching of macroscopic self-assembly invokes a demand of accurate bondings, and the need for long-range instructions that guide to accurate alignments in the bonding processes.

Parallelism is another keyword which describes the characteristics of stochastic self-assembly. Unlike the conventional multi-tasking assembly systems, self-assembly systems deal with multi-degree parallelism in their assembly processes. The parallelism occurs not only in the spatial dynamics, but also along a tempo-

ral dimension, where the progress of different stages of reactions can be observed simultaneously. Such as we set in one of the prerequisites in the logical model developed in Chapter 6.5 – *enzymes attract substrates, and vice-versa, while enzymes themselves or substrates repel each other*, most of our systems suppose magnetic attractions between desired attachments, and either repulsions or no relation between undesired attachments. This postulate prevents the system from further extension in the diversity in the type of components, and hence, in the complexity of reaction paths. The solution may be, as we discussed before, (i)

A dynamical equilibrium state represents one of the unique characteristics of dynamical systems, which show certain (in)stabilities in their intrinsic dynamics. This aspect can be seen in the results of mathematical analyses carried out in Chapter 3, where we observed some counterintuitive behaviors in the assembly dynamics of modules (Section 3.3). There, the number of targeted clusters consisting of 6 modules increased by premising the disassembly of the intermediate-state clusters[2]. This happened because disassembly of the intermediate-state clusters provoked multiple single modules, which were subsequently supplied to the same group of intermediate-state clusters such that they formed targeted (6-) clusters with better efficiency. The dynamically stable states show different characteristics from statically stable states. The formed "structure" can exist only by consuming energy and often shows robustness against external turbulence.

Passive and self-propulsive

In our model, modules with vibration motors are often regarded as an "active" system (e.g. Section 3). However, it is most likely that a similar assembly process can be derived by externally applying turbulence (e.g. an external rotational magnetic field), which is, as a result, expected to induce torque on the modules' magnets. As it is often discussed from *the frame of reference problem* [88], the difference between "passive" and "active" is simply a matter of the point of view of the observer. Therefore, the concept "self-propelled", which more appropriately describes the difference, is preferably used. In this regard, the distinction resides not in the way the modules are powered, but in the difference in a module's behavior toward its neighbors, that is, in the functional asymmetry among modules. As we discussed above, molecules exploit thermal agitation as their means of mobility. In contrast, self-assembly at more than μm scale needs to compromise the lack of stochasticity. The demand of self-propulsion may rise for this reason. From the perspective of mechanisms in biological systems with respect to autonomous and distributed systems, it can be noticed that the components which form the morphology are not always highly autonomous [5]. When we discuss autonomy of components in the context of autonomous and distributed systems, the crucial point might not be whether the units are passive or active, but whether the units are passive or "reactive".

Entropy

In chemistry, systems whose molecules' molar mass is less than approximately $100\,g/mol$ tend to be governed by internal energy. This is our assumption

[2]some unique results can also be found in [68].

when we design self-assembly systems. It is also known that molecules whose molar weight is over $10,000\,g/mol$ tend to be affected by entropy. In general, thermodynamic entropy S can be expressed as

$$S = k_B \ln D \tag{7.1}$$

where k_B is the Boltzmann constant, and D is a measure of the disorder in the system.

If the system has a constant temperature and a pressure, Gibbs free energy defines the change of free energy (ΔG). The ΔG is given by the combination of change of the Enthalpy (ΔH) and the Entropy (ΔS), namely

$$\Delta G = \Delta H - T\Delta S, \tag{7.2}$$

where T is the temperature of the system. The Enthalpy is the sum of the internal energy as well as the work produced by the system [110]. Entropic effects, often termed "entropic forces", play an increasingly important role as the length of the scale decreases (e.g. the self-assembly of lipid phases is almost exclusively driven by entropic effects). The fact that entropic effects can be neglected on macroscopic scales is connected to the fact that the bigger the scale the smaller the (relative) fluctuations. At first glance, the absence of fluctuations may appear to be beneficial; for self-assembly it certainly is not, because entropic forces are powerful driving mechanisms for self-assembly on the scale of up to several tens of nanometers. In our system, we consider the internal energy to consist mainly of kinetic and magnetic energy. As we expected, the influence of entropy was merely seen, for the small number of components and large scale of components.

7.2.3 Level of Autonomy of a System

The basic design principles derived from our case-studies have provided a pathway toward more complex/dynamical systems, yet they have merely accommodated a convincing feeling on what is life. Let us return to the question formulated in the Introduction: to what degree can we make our system approximate a living system? This section discusses the gap laying down between our current models and the living systems.

Emergence

One of the capabilities that we have not yet specified precisely is emergence, which is known as the effect of local interactions that end up with a global phenomenon. The difference between emergence and self-organization is that the former implies bidirectional influences between local interactions and (global) phenomena, whereas the latter implies that there might exist only local to global influences. In our work, the formation of a propeller-like rotating aggregate (Figure 3.5 **a** and **b**) is an instance of emergence, whereas the examples listed in Figure 3.16 **a** to **h** in Appendix 3B are instances of self-organization, where the local interactions caused global phenomena, but with only one-directional influence. In the process of propeller-like rotation, due to the stable configuration, each module constantly touched the ceiling, and thus steadily increased in power as well as physical contacts with the ceiling, which in turn caused a

resonance frequency of the body dynamics coupled with the vibration motors. The rotational behaviors were observed with two different directions, namely clock-wise and counter clock-wise, depending on the environmental conditions (the applied voltage and the length of the pantograph). At this point, the system was stable not only as a composed structure but also as an attractor within a dynamical system.

Meaning of being active (Programmed vs. Controllable)

Control is an important concept in robotics. It could also be said that roboticists only deal with entities that can be controlled. On the other hand, with regard to self-assembly, researchers in this field tend to take the opposite approach, namely, pre-programming the reaction paths by arranging appropriate components situated in their systems (embodiment). For them, "control" parts should be implemented to the systems so that the entities involved only need to follow the local physics rules and perform desired actions. This attitude can be confirmed in Heslop-Harrison's quotation on self-assembly of biological cells '*... control must be exerted only at certain strategic points, in determining what shall associate with what, and in what order, and in mapping out, in interaction with the cell environment, where the greatest probabilities will be for association to begin.*' (Heslop-Harrison (1972) [50]). In this respect, the unbridged valley lying between our self-assembly models and living systems is essentially equivalent to the gap between programmed components and active components, and this discriminates objects out of life. As our system showed, solely programmed behaviors are yet to be merely passive systems. Systems that can "consciously" determine their actions without any external control are still a dream of engineers.

It could be said that life is a blind engineer, because the components, e.g., molecules, self-construct into organisms in a completely bottom-up fashion.

7.3 Conclusion

Self-assembly is of crucial importance in the biological realm at all scales. This thesis has explored the potential for developing artificial self-assembly systems that are applicable to different scales. The contribution of this work is twofold: (i) achievement of an artificial self-assembly system that fulfills the elemental prerequisites in the thesis (distributed system in a stochastic environment, logical assembly, and scalability) and (ii) elucidation of the effect of morphology in the context of self-assembly. The achieved self-assembly processes were all carried out and realized in a distributed and stochastic manner, that is, once a set of experimental conditions was invoked, components acted in parallel, following local causal rules imposed by the system. By utilizing basic materials and methods, such as a magnet or a thermal bond, the designed component architecture left open a possibility of scalability of the system, ideally, for the miniaturization. Apart from that, various technological advancements of the models provided a new possibility of artificial self-assembly systems to engineering. In addition, the designed components showed a capability to logically assemble, exploiting the morphology. During the process, the system orchestrated magnets' transitions through the morphology, and intrinsically ordered

the assembly sequence. The obtained results further give rise to unique insight into the interdependencies between the components' morphology, systems' stochasticity, and complexity of assembly paths. The revealed influence of shape and stochasticity cast light on the design principle of components, and enabled the optimization problem solving in designing assembly pathways. We believe that this research deepens the theoretical understanding of the formation of spontaneous structure and function, which firmly provides the key knowledge for the realization of scalable self-assembly systems, and will, ultimately, shed some light on the nature of "living" systems.

Figure 7.5: What is life? (Courtesy of Tjep. [111])

Bibliography

1. `http://www.pdimages.com/web9.htm`.

2. J. J. Abbott, Z. Nagy, F. Beyeler, and B. J. Nelson. Robotics in the small. *IEEE Robotics & Automation Magazine*, 14:92–103, 2007.

3. L. Adleman. Linear self-assemblies: Equilibria, entropy and convergence rates. In *Sixth International Conference on Difference Equations*, 2001.

4. L. M. Adleman. Toward a mathematical theory of self-assembly (extended abstract). Technical report, 1999.

5. B. Alberts, A. Hohnson, J. Lewis, M. Raff, K. Roberts, and P. Walter. *Molecular biology of the cell*. Garland Science, 2002.

6. M. A. Bedau, J. S. McCaskill, N. H. Packard, S. Rasmussen, C. Adami, D. G. Green, T. Ikegami, K. Kaneko, and T. S. Ray. Open problems in artificial life. *Artificial Life*, 6:363–376, 2000.

7. P. Bhat, J. Kuffner, S. Goldstein, and S. Srinivasa. Hierarchical motion planning for self-reconfigurable modular robots. In *IEEE/RSJ International Conference on Intelligent Robots and Systems (IROS)*, pages 4108–4115, 2006.

8. J. Bishop, S. Burden, E. Klavins, R. Kreisberg, W. Malone, N. Napp, and T. Nguyen. Programmable parts: A demonstration of the grammatical approach to self-organization. In *IEEE/RSJ International Conference on Intelligent Robots and Systems (IROS)*, pages 3684–3691, 2005.

9. H. Bojinov, A. Casal, and T. Hogg. Multiagent control of self-reconfigurable robots. In *International Conference on Multi-Agent Systems*, pages 143–150, 2000.

10. M. Boncheva, S. A. Andreev, L. Mahadevan, A. Winkleman, D. R. Reichman, M. G. Prentiss, S. Whitesides, and G. Whitesides. Magnetic self-assembly of three-dimensional surfaces from planar sheets. *PNAS*, 102:3924–3929, 2005.

11. M. Boncheva, D. A. Bruzewicz, and G. M. Whitesides. Millimeter-scale self-assembly and its applications. *Pure and Applied Chemistry*, 75:621–630, 2003.

12. M. Boncheva, R. Ferrigno, D. A. Bruzewicz, and G. M. Whitesides. Plasticity in self-assembly: Templating generates functionally different circuits from a single precursor. *Angewandte Chemie International Edition*, 42:3368–3371, 2003.

13. M. Boncheva, D. H. Gracias, H. O. Jacobs, and G. M. Whitesides. Biomimetic self-assembly of a functional asymmetrical electronic device. *PNAS*, 99:4937–4940, 2002.

14. M. Boncheva and G. M. Whitesides. Making things by self-assembly. *MRS BULLETIN*, 30:736–742, 2005.

15. N. Bowden, A. Terfort, J. Carbeck, and G. M. Whitesides. Self-assembly of mesoscale objects into ordered two-dimensional arrays. *Science*, 276:233–235, 1997.

16. N. Bowden, M. Weck, I. S. Choi, and G. M. Whitesides. Molecule-mimetic chemistry and mesoscale self-assembly. *Accounts of Chemical Research*, 34:231–238, 2001.

17. J. Breivik. Self-oranization of template-replicating plolymers and the spontaneous rise of genetic information. *Entropy*, 3:273–279, 2001.

18. A. Castano, A. Behar, and P. M. Will. The conro modules for reconfigurable robots. *IEEE/ASME Transactions on Mechatronics*, 7(4):403–409, 2002.

19. G. S. Chirikjian. Kinematics of a metamorphic robotic system. In *IEEE International Conference on Robotics and Automation (ICRA)*, pages 449–455, 1994.

20. A. L. Christensen, R. O'Grady, and M. Dorigo. Morphology control in a multirobot system. *IEEE Robotics & Automation Magazine*, pages 18–25, 2007.

21. M. B. Cohn and C.-J. Kim. Self-assembling electrical networks: An application of micromachining technology. In *International Conference on Solid-State Sensors and Actuators*, pages 490–493, 1991.

22. O. Cugat, J. Delamare, and G. Reyne. Magnetic micro-actuators and systems (MAGMAS). *IEEE Trans. Magnetics*, 39(5):3607–3612, 2003.

23. E. D. Demaine, S. Hohenberger, and D. Liben-Nowell. Tetris is hard, even to approximate. Technical report, Cornell University Library arXiv.org, 2002.

24. C. Detweiler, M. Vona, K. Kotay, and D. Rus. Hierarchical control for self-assembling mobile trusses with passive and active links. In *IEEE International Conference on Robotics and Automation (ICRA)*, pages 1483–1490, 2006.

25. B. R. Donald, C. G. Levey, and I. Paprotny. An untethered, electrostatic, globally controllable mems micro-robot. *Microelectromechanical Systems*, 15:1–15, 2006.

26. K. E. Drexler. *Nanosystems*. John Wiley & Sons, Inc., 1992.

27. R. Dreyfus, M. L. Roper, M. Fermigier, H. A. Stone, and J. Bibette. Microscopic artificial swimmers. *Nature*, 437:862–865, 2005.

28. A. Eschenmoser and M. V. Kisakürek. Chemistry and origin of life. *Helvetica Chimica Acta*, 79:1249–1259, 1996.

29. K. Fujibayashi, S. Murata, K. Sugawara, and M. Yamamura. Self-organizing formation algorithm for active elements. *Forma*, 18:83–95, 2003.

30. T. Fukuda and Y. Kawauch. Cellular robotic system (CEBOT) as one of the realizations of self-organizing intelligent universal manipulator. In *IEEE International Conference on Robotics and Automation (ICRA)*, pages 662–667, 1990.

31. E. P. Furlani. *Permanent Magnet and Electromechanical Devices*. Academic Press, San Diego, CA, 2001.

32. D. Gendreau, M. Gauthier, D. Heriban, and P. Lutz. Modular architecture of the microfactories for automatic micro-assembly. *Robotics and Computer-Integrated Manufacturing*, 2010.

33. D. T. Gillespie. A general method for numerically simulating the stochastic time evolution of coupled chemical reactions. *Computational Physics*, 22:403–434, 1976.

34. D. T. Gillespie. Exact stochastic simulation of coupled chemical reactions. *Physical Chemistry*, 81:2340–2361, 1977.

35. D. T. Gillespie. Stochastic simulation of chemical kinetics. *Annual Review of Physical Chemistry*, 58:35–55, 2007.

36. D. H. Gracias, J. Tien, T. L. Breen, C. Hsu, and G. M. Whitesides. Forming electrical networks in three dimensions by self-assembly. *Science*, 289:1170–1172, 2000.

37. S. Griffith. *Growing Machines*. PhD thesis, MIT, 2004.

38. S. Griffith, D. Goldwater, and J. Jacobson. Robotics: Self-replication from random parts. *Nature*, 437:636, 2005.

39. R. Gross and M. Dorigo. Self-assembly at the macroscopic scale. *Proceedings of the IEEE*, 96:1490–1508, 2008.

40. B. A. Grzybowski, M. Radkowski, C. J. Campbell, J. N. Lee, and G. M. Whitesides. Self-assembling fluidic machines. *Applied physics letters*, 84:1798–1800, 2004.

41. B. A. Grzybowski, H. A. Stone, and G. M. Whitesides. Dynamic self-assembly of magnetized, millimetre-sized objects rotating at a liquid-air interface. *Nature*, 405:1033, 2000.

42. B. A. Grzybowski, A. Winkleman, J. A. Wiles, Y. Brumer, and G. M. Whitesides. Electrostatic self-assembly of macroscopic crystals using contact electrification. *Nature Materials*, 2:241–245, 2003.

43. K. Harada, E. Susilo, A. Menciassi, and P. Dario. Wireless reconfigurable modules for robotic endoluminal surgery. In *IEEE International Conference on Robotics and Automation (ICRA)*, pages 2880–2885, 2009.

44. R. Hayakawa, K. Itou, Y. Kimura, and K. Okano. *Hiheikoukeino Dynamics Nyumon*. BAIHUKAN, 2006.

45. T. Honda, K. I. Arai, and K. Ishiyama. Micro swimming mechanijsms propelled by external magnetic fields. *IEEE Transactions on Magnetics*, 32:5085–5087, 1996.

46. K. Hosokawa, I. Shimoyama, and H. Miura. Dynamics of self-assembling systems: Analogy with chemical kinetics. *Artificial Life*, 1(4):413–427, 1994.

47. K. Hosokawa, I. Shimoyama, and H. Miura. 2-d micro-self-assembly using the surface tension of water. *Sensors and Actuators A*, 57:117–125, 1996.

48. A. Ishiguro, M. Shimizu, and T. Kawakatsu. A modular robot that exhibits amoebic locomotion. *Robotics and Autonomous Systems*, 54:641–650, 2006.

49. K. Ishiyama, K. I. Arai, M. Sendoh, and A. Yamazaki. Spiral-type micromachine for medical applications. In *International Symposium on Micromechatronics and Human Science*, 2000.

50. H.-H. J. Pattern in plant cell walls: morphogenesis in miniature. *Proc. R. Instn Gt Br.*, 45:335–352, 1972.

51. H. O. Jacobs, A. R. Tao, A. Schwartz, D. H. Gracias, and G. M. Whitesides. Fabrication of a cylindrical display by patterned assembly. *Science*, 296:323–325, 2002.

52. J. L. T. Jeremy M. Berg (Autor), Lubert Stryer (Autor). *Biochemie*. Spektrum, Hidelberg, Berlin, 2003.

53. M. W. Jorgensen, E. H. Ostergaard, and H. H. Lund. Modular ATRON: Modules for a self-reconfigurable robot. In *IEEE/RSJ International Conference on Intelligent Robots and Systems (IROS)*, pages 2068–2073, 2004.

54. E. Klavins. Programmable self-assembly. *IEEE Control System Magazine*, 27:43–56, 2007.

55. R. Kometani and S. Matsui. Artificial nano “t4 bacteriophage” was fabricated by fib-cvd on si surface. size of the artificial nano “t4 bacteriophage” is about ten times as large as the real virus. it is made of diamond-like carbon.

56. B. Korzeniewski. Cybernetic formulation of the definition of life. *Journal of Theoretical Biology*, 209:275–286, 2001.

57. K. Kotay, D. Rus, M. Vona, and C. McGray. The self-reconfiguring robotic molecule. In *IEEE/RSJ International Conference on Intelligent Robots and Systems (IROS)*, pages 424–431, 1998.

58. C. G. Langton. Self-reproduction in cellular automata. *Physica D: Nonlinear Phenomena*, 10(1-2):135–144, 1984.

59. P. G. Leiman, S. Kanamaru, V. V. Mesyanzhinov, F. Arisaka, and M. G. Rossmann. Structure and morphogenesis of bacteriophage T4. *Cellular and Molecular Life Sciences*, 60:2356–2370, 2003.

60. T. Leong, Z. Gu, T. Koh, and D. H. Gracias. Spatially controlled chemistry using remotely guided nanoliter scale containers. *Journal of American Chemical Society*, 128:11336–11337, 2006.

61. C. Mao, T. H. LaBean, J. H. Reif, and N. C. Seeman. Logical computation using algorithmic self-assembly. *Nature*, 407:493–496, 2000.

62. C. Mao, V. R. Thalladi, D. B. Wolfe, S. Whitesides, and G. M. Whitesides. Dissections: Self-assembled aggregates that spontaneously reconfigure their structures when their environment changes. *J. Am. Chem. Soc*, 124(49):14508 –14509, 2002.

63. M. Mastrangeli, S. Abbasi, C. Varel, C. V. Hoof, J.-P. Celis, and K. F. B ohringer. Self-assembly from milli- to nanoscales: methods and applications. *Journal of Micromechanics and Microengineering*, 19:1–37, 2009.

64. L. Matthey, S. Berman, and V. Kumar. Stochastic strategies for a swarm robotic assembly system. In *IEEE International Conference on Robotics and Automation (ICRA)*, pages 1751–1756, 2009.

65. G. Mermoud, J. Brugger, and A. Martinoli. Towards multi-level modeling of self-assembling intelligent micro-systems. In *International Conference on Autonomous Agents and Multiagent Systems (AAMAS)*, pages 89–96, 2009.

66. S. Miyashita, F. Casanova, M. Lungarella, and R. Pfeifer. Peltier-based freeze-thaw connector for waterborne self-assembly systems. In *IEEE/RSJ International Conference on Intelligent Robots and Systems (IROS)*, pages 1325–1330, Nice, France, September 2008.

67. S. Miyashita, M. Göldi, C. Audretsch, R. Füchslin, and R. Pfeifer. The problems toward sub-millimeter scale self-assembling robots. In *Workshop on Bio-Inspired Self-Organizing Robotic Systems in 2010 IEEE International Conference on Robotics and Automation (ICRA)*, Anchorage, Alaska, May 2010.

68. S. Miyashita, M. Hadorn, and P. E. Hotz. Water floating self-assembling agents. In *KES Symposium on Agent and Multi-Agent Systems (KES-AMSTA)*, Wroclaw, Poland, May 2007.

69. S. Miyashita, M. Kessler, and M. Lungarella. How morphology affects self-assembly in a stochastic modular robot. In *IEEE International Conference on Robotics and Automation (ICRA)*, pages 3533–3538, Pasadena, USA, May 2008.

70. S. Miyashita, Z. Nagy, B. J. Nelson, and R. Pfeifer. The influence of shape on parallel self-assembly. *Entropy*, 11:643–666, 2009.

71. R. Moeckel, C. Jaquier, K. Drapel, A. Upegui, and A. Ijspeert. Yamor and bluemove - an autonomous modular robot with bluetooth interface for exploring adaptive locomotion. In *International Conference on Climbing and Walking Robots*, pages 685–692, 2005.

72. F. Mondada, L. M. Gambardella, D. Floreano, S. Nolfi, J.-L. Deneubourg, and M. Dorigo. The cooperation of swarm-bots. *IEEE Robotics & Automation Magazine*, 12:21–28, 2005.

73. MorphologicalComputation. `http://en.wikipedia.org/wiki/Morphological_computation_(robotics)`.

74. T. Motokawa. *Time of an elephant, time of a mouse.* CHUO-KORON-SHINSHA, INC., 1992.

75. S. Murata and H. Kurokawa. Self-reconfigurable robots. *IEEE Robotics & Automation Magazine*, pages 71–78, 2007.

76. S. Murata, H. Kurokawa, and S. Kokaji. Self-assembling machine. In *IEEE International Conference on Robotics and Automation (ICRA)*, pages 441–448, 1994.

77. S. Murata, H. Kurokawa, E. Yoshida, K. Tomita, and S. Kokaji. A 3-D self-reconfigurable structure. In *IEEE International Conference on Robotics and Automation (ICRA)*, pages 432–439, 1998.

78. S. Murata, K. Tomita, E. Yoshida, H. Kurokawa, and S. Kokaji. Self-reconfigurable robot. In *International Conference on Intelligent Autonomous Systems (IAS)*, pages 911–917, 1999.

79. Z. Nagy, S. Miyashita, S. Muntwyler, A. K. Cherukuri, J. J. Abbott, R. Pfeifer, and B. J. Nelson. Morphology detection for magnetically self-assembled modular robots. In *IEEE/RSJ International Conference on Intelligent Robots and Systems (IROS)*, pages 5281–5286, St. Louis, USA, October 2009.

80. Z. Nagy, R. Oung, J. J. Abbott, and B. J. Nelson. Experimental investigation of magnetic self-assembly for swallowable modular robots. In *IEEE/RSJ International Conference on Intelligent Robots and Systems (IROS)*, pages 1915–1920, 2008.

81. K. Nakano, S. Uchihashi, N. Umemoto, and H. Nakagama. An approach to evolutional system. In *First IEEE Conference on Evolutionary Computation*, pages 781 – 786, 1994.

82. N. Napp, S. Burden, and E. Klavins. The statistical dynamics of programmed self-assembly. In *IEEE International Conference on Robotics and Automation (ICRA)*, pages 1469–1476, 2006.

83. S. Park, J.-H. Lim, S.-W. Chung, and C. A. Mirkin. Self-assembly of mesoscopic metal-polymer amphiphiles. *Science*, 303:348–351, 2004.

84. C. Pawashe, S. Floyd, and M. Sitti. Magnetic mobile micro-robots. In *7ème Journées Nationales de la Recherche en Robotique*, 2009.

85. J. A. Pelesko. *SELF ASSEMBLY*. Chapman & Hall/CRC, 2007.

86. L. S. Penrose. Mechanics of self-reproduction. *Annals of Human Genetics*, 23:59–72, 1958.

87. L. S. Penrose. Self-reproducing machines. *Scientific American*, 200-6:105–114, 1959.

88. R. Pfeifer and C. Scheier. *Understanding Intelligence*. The MIT Press, 2001.

89. E. M. Purcell. Life at low reynolds number. *American Journal of Physics*, 45:3–11, 1977.

90. C. W. Reynolds. Flocks, herds, and schools: A distributed behavioral model. *Computer Graphics*, 21:25–34, 1987.

91. P. W. K. Rothemund. Using lateral capillary forces to compute by self-assembly. *PNAS*, 97:984–989, 2000.

92. P. W. K. Rothemund. Folding DNA to create nanoscale shapes and patterns. *Nature*, 440(7082):297–302, 2006.

93. D. Rus and M. Vona. Crystalline robots: Self-reconfiguration with compressible unit modules. *Autonomous Robots*, 10(1):107–124, 2001.

94. K. Saitou. Conformational switching in self-assembling mechanical systems. *IEEE Transactions on Robotics and Automation*, 15:510–520, 1999.

95. K. Saitou and M. J. Jakiela. Automated optimal design of mechanical conformational switches. *Artificial Life*, 2:129–156, 1995.

96. K. Saitou and M. J. Jakiela. Subassembly generation via mechanical conformational switches. *Artificial Life*, 2:377–416, 1995.

97. K. Saitou, D.-A. Wang, and S. J. Wou. Externally resonated linear microvibromotor for microassembly. *Journal of Microelectromechanical Systems*, 9:336–346, 2000.

98. B. Salemi, M. Moll, and W.-M. Shen. Superbot: A deployable, multifunctional, and modular self-reconfigurable robotic system. In *IEEE/RSJ International Conference on Intelligent Robots and Systems (IROS)*, 2006.

99. E. Schrodinger. *What is Life?: With Mind and Matter and Autobiographical Sketches*. Cambridge University Press, 1944.

100. N. C. Seeman. DNA in a material world. *Nature*, 421:427–430, 2003.

101. W. M. Shih, J. D. Quispe, and G. F. Joyce. A 1.7-kilobase single-stranded DNA that folds into a nanoscale octahedron. *Nature*, 427:618–621, 2004.

102. M. Shimizu, A. Ishiguro, and T. Kawakatsu. A modular robot that exploits a spontaneous connectivity control mechanism. In *IEEE International Conference on Robotics and Automation (ICRA)*, pages 2658–2663, 2005.

103. M. Sitti. Voyage of the microrobots. *Nature*, 458:1121–1122, 2009.

104. A. Snezhko, M. Belkin, I. S. Aranson, and W.-K. Kwok. Self-assembled magnetic surface swimmers. *Physical Leview Letters*, 102:118103–1–118103–4, 2009.

105. snowcrystal. `http://www.snowcrystals.com`.

106. J. Stambaugh, D. P. Lathrop, E. Ott, and W. Losert. Pattern formation in a monolayer of magnetic spheres. *Pysical Leview E*, 68:026207–1–026207–5, 2003.

107. K. Stoy, A. Lyder, R. F. M. Garcia, and D. Christensen. Hierarchical robots. In *IROS Workshop on Self-Reconfigurable Modular Robots*, 2007.

108. H. Takana. *Seimei to hukuzatsukei (In Japanese)*. BAIHUKAN, 2002.

109. Y. Terada and S. Murata. Automatic assembly system for a large-scale modular structure. In *IEEE/RSJ International Conference on Intelligent Robots and Systems (IROS)*, volume 3, pages 2349–2355, 2004.

110. The California NanoSystems Institute University of California Los Angeles Science Outreach Program. Self-assembly experiment: Teacher manual. `http://voh.chem.ucla.edu/\\classes/Self-assembly/pdf/Self-Assembly\%20T%eacher\%20Manual-v2.doc`, 2006.

111. Tjep. `http://www.tjep.com`.

112. K. Tomita, H. Kurokawa, and S. Murata. Graph automata: natural expression of self-reproduction. *Physica D*, 171:197–2210, 2002.

113. D. Tsutsumi and S. Murata. Multistate part for mesoscale self-assembly. In *SICE Annual Conference*, pages 1–6, 2007.

114. J. v. Neumann. *Theory of Self-reproducing Automata*. Univ. of Illinois Press, 1966.

115. J. F. V. Vincent, O. A. Bogatyreva, N. R. Bogatyrev, A. Bowyer, and A.-K. Pahl. Biomimetics: its practice and theory. *Interface*, 3:471–482, 2006.

116. K. Vollmers, D. R. Frutiger, B. E. Kratochvil, and B. J. Nelson. Wireless resonant magnetic microactuator for untethered mobile microrobots. *Applied physics letters*, 92:144103–1–144103–3, 2008.

117. B. L. Walle, M. Gauthier, and N. Chaillet. Dynamic modelling of a submerged freeze microgripper using a thermal network. In *International Conference Advanced Intelligent Mechatronics*, 2007.

118. D. B. Weibel, P. Garstecki, D. Ryan, W. R. DiLuzio, M. Mayer, J. E. Seto, and G. M. Whitesides. Microoxen: Microorganisms to move microscale loads. *PNAS*, 102(34):11963–11967, 2005.

119. P. White, K. Kopanski, and H. Lipson. Stochastic self-reconfigurable cellular robotics. In *IEEE International Conference on Robotics and Automation (ICRA)*, pages 2888–2893, 2004.

120. P. White, V. Zykov, J. Bongard, and H. Lipson. Three dimensional stochastic reconfiguration of modular robots. In *International Conference on Robotics Science and Systems (RSS)*, pages 161–168, 2005.

121. G. M. Whitesides. The 'right' size in nanobiotechnology. *Nature*, 21(10):1161–1165, 2003.

122. G. M. Whitesides and B. Grzybowski. Self-assembly at all scales. *Science*, 295:2418–2421, 2002.

123. E. Winfree, F. Liu, L. A. Wenzler, and N. C. Seeman. Design and self-assembly of two-dimensional DNA crystals. *Nature*, 394(6693):539 – 544, 1998.

124. D. B. Wolfe, A. Snead, C. Mao, N. B. Bowden, and G. M. Whitesides. Mesoscale self-assembly: Capillary interactions when positive and negitive menisci have similar amplitudes. *Langmuir*, 19(6):2206–2214, 2003.

125. M. Yamaki, J. Higo, and K. Nagayama. Size-dependent separation of colloidal particles in two-dimensional convective self-assembly. *American Chemical Society*, 11:2975–2978, 1995.

126. M. Yim. New locomotion gaits. In *IEEE International Conference on Robotics and Automation (ICRA)*, pages 2508–2514, 1994.

127. M. Yim, W.-M. Shen, B. Salemi, D. Rus, M. Moll, H. Lipson, E. Klavins, and G. S. Chrikjian. Modular self-reconfigurable robot systems. *IEEE Robotics & Automation Magazine*, pages 43–50, 2007.

128. H. Yokoi, T. Nagai, T. Ishida, M. Fujii, and T. Iida. *Morpho-functional Machines: The New Species: Designing Embodied Intelligence*. Springer, 2003.

129. T. Yokoyama, S. Yokoyama, T. Kamikado, Y. Okuno, and S. Mashiko. Selective assembly on a surface of supramolecular aggregates with controlled size and shape. *Nature*, 413:619–621, 2001.

130. A. Zlotnick. Theoretical aspects of virus capsid assembly. *Molecular Recognition*, 18(6):479–490, 2005.

131. V. Zykov, E. Mutilinaios, B. Adams, and H. Lipson. Self-reproducing machines. *Nature*, 435(7039):163–164, 2005.